1980

Detection of metal ions in flow-analyzers by reverse pulse amperometry without interference from dissolved oxygen

Paul Maitoza
Iowa State University

MAITOZA, PAUL

DETECTION OF METAL IONS IN FLOW-ANALYZERS BY REVERSE PULSE AMPEROMETRY WITHOUT INTERFERENCE FROM DISSOLVED OXYGEN

Iowa State University PH.D. 1980

Detection of metal ions in flow-analyzers by reverse pulse amperometry without interference from dissolved oxygen

by

Paul Maitoza

A Dissertation Submitted to the
Graduate Faculty in Partial Fulfillment of the
Requirements for the Degree of
DOCTOR OF PHILOSOPHY

Department: Chemistry
Major: Analytical Chemistry

Approved:

Signature was redacted for privacy.

In Charge of Major Work

Signature was redacted for privacy.

For the Major Department

Signature was redacted for privacy.

For the Graduate College

Iowa State University
Ames, Iowa

1980

TABLE OF CONTENTS

		Page
	LIST OF ACRONYMS	x
	LIST OF SYMBOLS	xii
I.	INTRODUCTION	1
II.	LITERATURE REVIEW	7
	A. Methods for Trace Metal Analysis	7
	1. Atomic spectroscopy	7
	2. Neutron activation analysis (NAA)	10
	3. Mass spectrometry	10
	4. X-ray fluorescence (XRF)	11
	5. Gas chromatography (GC)	11
	6. Electroanalytical techniques	12
	B. Polarographic Detectors for Flow-Analyzers	16
	1. Historical	16
	2. Interference from dissolved oxygen	19
	C. Separations of Metal Ions by Ion-exchange Liquid Chromatography	22
	D. Reverse Pulse Polarography	25
III.	PRINCIPLES OF REVERSE PULSE AMPEROMETRY	29
	A. Introduction	29
	B. Theory	35
	1. RPP for the reaction $M^{+m} + ne \rightleftharpoons M(Hg)$	35
	2. RPA for the reaction $M^{+m} + ne \rightleftharpoons M(Hg)$	42
	3. Flow rate dependence of EC detectors	50
	4. Dependence of response of RPA on the nature of the metal redox couple	53
	C. Experimental	57
	1. Instrumentation	57
	2. Chemicals	69
	3. Procedures	69

D. Results and Discussion 70

1. Agreement between theory and experiment for RPP 70
2. Discrimination against electrochemical interference from dissolved oxygen by RPA 77
3. Evaluation of the interferences of dissolved oxygen and hydrogen peroxide 85
4. Selectivity of RPA 88
5. Study of response of RPA for selected metal ions 91
6. Expected interferences in RPA 96

IV. EVALUATION OF THE THIN-FILM MERCURY ELECTRODE, HANGING MERCURY-DROP ELECTRODE AND STATIC DROPPING MERCURY ELECTRODE AS INDICATING ELECTRODES FOR REVERSE PULSE AMPEROMETRY 100

A. Introduction 100

B. Experimental 101

1. Instrumentation 101
2. Chemicals 107
3. Procedure 107

C. Results and Discussion 108

1. Dependence of peak shape on the Hg indicating electrode 108
2. Dependence of peak area on pulse period 112
3. Dependence of peak area and peak height on flow rate 117
4. Precision studies for Pb(II) by FIA 138
5. Calibration curves for Pb(II) by FIA 145
6. Compatibility with cation-exchange liquid chromatography 159
7. Conclusions 171

V. DETERMINATION OF Pb IN ORCHARD LEAVES BY REVERSE PULSE AMPEROMETRY 172

A. Introduction 172

B. Experimental 174

1. Instrumentation 174
2. Chemicals 174
3. Procedures 175

C. Results and Discussion 176

1. Preliminary investigations for the analysis of the orchard leaves 176
2. Determination of Pb by the method of standard addition 181
3. Conclusions 188

VI. SUMMARY 189

VII. SUGGESTIONS FOR FUTURE RESEARCH 191

VIII. BIBLIOGRAPHY 194

IX. ACKNOWLEDGEMENTS 200

LIST OF TABLES

		Page
Table II-1.	Comparison of detection limits for the determination of Pb by various analytical techniques	16
Table III-1.	Agreement between theory and experiment for RPP and the reaction $M^{+m} + ne \rightleftharpoons M(Hg)$	74
Table III-2.	Comparison of $\delta_{Pb(Hg)}$ with the electrode radius, R_{Hg}	76
Table III-3.	Solubility of metals in mercury (34)	92
Table IV-1.	Relationship between Q and t_i for the TFME, HMDE and SDME	113
Table IV-2.	Dependence of I_p on V_f for the TFME	118
Table IV-3.	Dependence of I_p on V_f for the HMDE	121
Table IV-4.	Dependence of I_p on V_f for the SDME	124
Table IV-5.	Dependence of Q on V_f for the TFME	127
Table IV-6.	Dependence of Q on V_f for the HMDE	130
Table IV-7.	Dependence of Q on V_f for the SDME	133
Table IV-8.	Slopes of log-log plots for I_p and Q versus V_f for the TFME, HMDE and SDME	136
Table IV-9.	Relative standard deviation of values for I_p for the detection of Pb(II) by FIA	140
Table IV-10.	Values of I_p observed with the TFME for successive injections of Pb(II)	143
Table IV-11.	Calibration curve for Pb(II) by FIA with the TFME	146
Table IV-12.	Calibration curve for Pb(II) by FIA with the HMDE	149
Table IV-13.	Calibration curve for Pb(II) by FIA with the SDME	152

Table V-1. Constituents present in the orchard leaves 173

Table V-2. Determination of Pb in the orchard leaves by the method of standard addition 185

LIST OF FIGURES

		Page
Figure III-1.	Potential-time waveforms for NPP, RPP and RPA	31
Figure III-2.	Representation of current-time response to the pulsed-potential waveform of RPA	34
Figure III-3.	Concentration profiles for the reaction $M^{+m} + ne \rightleftharpoons M(Hg)$ observed for the detection of M^{+m} by RPP	39
Figure III-4.	Concentration profiles for the reaction $M^{+m} + ne \rightleftharpoons M(Hg)$ under the conditions of RPA	46
Figure III-5.	Concentration profiles for the study of $M^{+m} + ne \rightleftharpoons M(Hg)$ by RPA	56
Figure III-6.	Concentration profiles for the study of $M^{+m} + ne \rightleftharpoons M^{+m-n}$ by RPA	59
Figure III-7.	Cross-sectional diagram of Model 303 Static Mercury Drop Electrode	62
Figure III-8.	LC adapter assembly for the Model 310 Polarographic LC Detector	66
Figure III-9.	Ion-exchange chromatograph	68
Figure III-10.	Reverse pulse polarograms for Pb(II) as a function of pulse period	72
Figure III-11.	Normal pulse polarograms	79
Figure III-12.	Reverse pulse polarograms	81
Figure III-13.	Comparison of response for NPA and RPA	84
Figure III-14.	Effect of H_2O_2 on response for Pb(II) by RPP	87
Figure III-15.	Reverse pulse polarograms for a solution of Cu(II), Pb(II) and Zn(II)	90
Figure III-16.	Study of the detection of selected metal ions by RPA	95

Figure III-17.	Reverse pulse polarogram for Ni(II)	98
Figure IV-1.	Cross-sectional diagram of the EC detector with the TFME	103
Figure IV-2.	Flow-analyzer used with the TFME	106
Figure IV-3.	Dependence of peak shape on the Hg indicating electrode	111
Figure IV-4.	Q versus t_i for the TFME, HMDE and SDME	115
Figure IV-5.	Log I_p versus log V_f for the TFME	120
Figure IV-6.	Log I_p versus log V_f for the HMDE	123
Figure IV-7.	Log I_p versus log V_f for the SDME	126
Figure IV-8.	Log Q versus log V_f for the TFME	129
Figure IV-9.	Log Q versus log V_f for the HMDE	132
Figure IV-10.	Log Q versus log V_f for the SDME	135
Figure IV-11.	Peaks observed for 20 successive injections of 15 μM Pb(II) detected with the SDME	142
Figure IV-12.	Calibration curve for Pb(II) with the TFME	148
Figure IV-13.	Calibration curve for Pb(II) with the HMDE	151
Figure IV-14.	Calibration curve for Pb(II) with the SDME	154
Figure IV-15.	Background noise observed with the HMDE and SDME	158
Figure IV-16.	Chromatographic separation of Tl(I), Cd(II) and Pb(II) with detection by the TFME	163
Figure IV-17.	Chromatographic separation of Tl(I), Cd(II) and Pb(II) with detection by the SDME	165
Figure IV-18.	Chromatographic separation of Cu(II), Zn(II), Pb(II) and Cd(II) with detection by the HMDE	168
Figure IV-19.	Chromatographic separation of Cu(II), Zn(II), Pb(II) and Cd(II) with detection by the SDME	170

Figure V-1. Analysis of the orchard leaves with the SDME 178

Figure V-2. Determination of the blank with the HMDE 180

Figure V-3. Determination of Pb in the orchard leaves by RPA with the HMDE and the method of standard addition 184

Figure V-4. Q versus μg Pb added for the determination of Pb in the orchard leaves 187

LIST OF ACRONYMS

AC	Alternating current
AES-ICP	Atomic emission spectroscopy with an inductively-coupled plasma
ASV	Anodic stripping voltammetry
CELC	Cation-exchange liquid chromatography
CIMS	Chemical ionization mass spectrometry
DC	Direct current
DME	Dropping mercury electrode
DPASV	Differential pulse anodic stripping voltammetry
DPP	Differential pulse polarography
EC	Electrochemical
EPA	Environmental Protection Agency
FAA	Flame atomic absorption spectroscopy
FIA	Flow injection analysis
GC	Gas chromatography
GCTE	Glassy carbon tubular electrode
HMDE	Hanging mercury-drop electrode
HPLC	High performance liquid chromatography
LC	Liquid chromatography
NAA	Neutron activation analysis
NBS	National Bureau of Standards
NFAA	Nonflame atomic absorption spectroscopy
NPA	Normal pulse amperometry
NPP	Normal pulse polarography

RDME	Rapidly dropping mercury electrode
RPA	Reverse pulse amperometry
RPP	Reverse pulse polarography
SCE	Saturated calomel electrode
SDME	"Static" dropping mercury electrode
SMDE	Static Mercury-Drop Electrode
SSCE	Silver/silver chloride electrode
SSMS	Spark source mass spectrometry
TFME	Thin-film mercury electrode
XRF	X-ray fluorescence spectroscopy

LIST OF SYMBOLS

A	Electrode area
C	Concentration
C^b	Concentration in bulk solution
C^o	Concentration at electrode surface
D	Diffusion coefficient
E	Potential
E_f	Final potential
E_i	Initial potential
E^o	Standard reduction potential
$E_{1/2}$	Polarographic half-wave potential
ΔE	Pulse height
F	Faraday constant
I	Current
I_{dep}	Deposition current
I_p	Peak current
I_{ss}	Steady-state current
I_{strip}	Stripping current
k	Constant
k'	Constant
ℓ	Film thickness
m,n	Number of electrons
N	Number of moles
Q	Peak area

R	Electrode radius
T	Pulse period
t_i	Time electrode is at E_i
t_p	Pulse width
t_s	Current sampling time
V_f	Volume flow rate
W	Atomic weight
X	Distance from electrode surface
α	Exponent of V_f for I_{ss}
β	Exponent of V_f for I_p
δ	Thickness of diffusion layer
ρ	Density
σ_{rel}	Relative standard deviation
τ	Drop lifetime

I. INTRODUCTION

Environmental awareness heightened to such a degree about ten years ago that the government of the United States established the Environmental Protection Agency (EPA) to regulate all sources of environmental contamination, particularly that from industry. The EPA was created in response to the effects of many pollutants on human health because it seemed then (and still does) that, all too commonly, a chemical or an industrial product previously considered to be "harmless", which has been introduced to the environment, turns out to be a serious health hazard, either toxic or carcinogenic, over the test of time. One particular group of such pollutants is the metals.

Industry is the principal source of the contamination of the environment with metals, specifically, due to the production of steel, batteries, pigments, catalysts, etc. (1). The sites of these large scale operations emit metals directly to air and water, which indirectly contaminate the land and, eventually, our food. The air and water are contaminated by vapors or metal-containing particulates and by waste effluents. The smaller particulates, <10 μm, can remain airborne for considerable periods of time and can be transported over long distances (2). In time, vapors and particulates pollute the land as a result of rainfall or the natural deposition of the particulates. The disposal of untreated, waste effluents into lakes, rivers and streams also causes a far-ranging problem of pollution of our waters. The exposure of flora and fauna to these abnormal levels of metal contamination produces the final health hazard since man is at the top of the food chain.

The intake of a given metal may result in several effects on the human body. At sufficiently low levels of intake, the body may pass the pollutant with no harmful effect. Or, the metal may produce a hormetic effect on a general body function, such as growth (3). Conversely, at low levels of intake, some metals can accumulate in a specific organ in the body to ultimately produce a condition of toxicity (1). At relatively higher concentrations, some metals are known to be essential micronutrients for human health (4,5), with As being the most recently discovered micronutrient in 1975 (5). Briefly, some other essential micronutrients are Ni, V, Cr, Zn and Fe. Inadequate intake of these essential metals produces symptoms of deficiency. Finally, at elevated levels of exposure to metals, acute poisoning can result to cause numerous complications, and possibly death. For example, the effects of inorganic Pb poisoning include encephalophthy, colic, anemia, changes in bone marrow, peripheral neuritis, tremor, and premature loss of teeth (1). Several metals have been shown to be carcinogenic to humans; of note are Cr, as $CaCrO_4$ in the particulate form, and Ni in any particulate form. These species increase the risk of cancer along the entire respiratory tract. The compound Ni_3S_2, in the particulate form, is the most potent carcinogen of any metal compound which has been investigated, as discussed by Sunderman (6).

Understandably, there is great concern about the presence of unnatural levels of metals in the environment and the consequential effects on human health and welfare. It is essential that governmental agencies institute stringent controls on the content of metals in our

food, land, air and water. A prerequisite for such controls are methods of trace metal analysis which fulfill the ideal requirements for specificity, precision, sensitivity, accuracy and suitability for quality control and automation (5). A relatively large number of techniques are available for trace metal analysis, but few meet all of the requirements. Typically, one out of several possible methods considered is chosen which best applies to the analytical problem at hand. This dissertation introduces an additional, alternate method for trace metal analysis.

The objective of the work presented in this dissertation was to develop an electroanalytical method utilizing a flow-analyzer for the detection of metal ions at trace levels of concentration. The use of a flow-analyzer ensures a method which can be readily automated for routine analysis and a method which is applicable with flow-injection analysis (FIA) or liquid chromatography (LC). For those situations where a chromatographic column is not necessary, FIA provides a relatively inexpensive means of analysis because of the general simplicity of the apparatus and procedure, and the high sample throughput (7,8). Otherwise, LC can furnish the required selectivity. The choice of FIA or LC is made, therefore, dependent on the complexity of the sample.

The selection of an appropriate electrochemical (EC) detector for the flow-analyzer is based on the material and the geometry of the indicating electrode. Indicating electrodes for most EC detectors are C (e.g., pyrolytic graphite, glassy carbon or carbon paste), Pt, Au, or Hg. C, Pt, and Au are frequently applied as indicating electrodes for anodic detection; whereas, Hg is, by far, the most popular indicating

electrode for cathodic detection, particularly for metal ions. Thus, Hg was the electrode material of choice for the research reported in this dissertation.

Indicating electrodes of Hg can have various geometries, e.g., pool, drop or film. The Hg drop can be applied as a stationary electrode, i.e., the hanging mercury-drop electrode (HMDE), or as a periodically dropping electrode with a renewable and reproducible surface, e.g., the dropping mercury electrode (DME). A Static Mercury Drop Electrode (SMDE) is commercially available which can be operated either as a HMDE or as a DME. Kissinger, in a review of EC detectors for LC (9), made the following comment on the application of the DME to LC during a discussion on the physical stability of an EC detector.

> "... Mechanically awkward devices such as the dropping mercury electrode will try the patience of the most stalwart chromatographer...."

The SMDE seems to offer the necessary convenience for the application of a DME to a fluid stream. The Hg-film electrode can be produced by electrodeposition of a thin film of Hg on any one of numerous solid electrode surfaces including Pt, Au and C. Hence, the geometry of the film is essentially defined by the geometry of the solid substrate. In this research, a Hg-film on a glassy carbon tubular electrode and the SMDE were investigated as the indicating electrodes for an EC detector.

An EC detector in a flow-analyzer is commonly applied under condition of constant potential with amperometric detection. The cathodic detection of metal ions with a Hg indicating electrode in this manner results in a serious problem. Dissolved oxygen is electroactive

on Hg at potentials $\leq$ 0 V versus the saturated calomel electrode (SCE). Unless the concentration of dissolved oxygen in the fluid stream and in the sample solution is lowered to an undetectable level, all current measurements will have a faradaic contribution due to the reduction of dissolved oxygen. This problem has drastically hindered the use of a Hg indicating electrode for routine applications in FIA and LC. The typical approach used as a solution to this problem has been to deaerate all analytical solutions, and to employ a flow-analyzer constructed of stainless-steel tubing and other components which are impermeable to oxygen (10). In many cases, the presence of dissolved oxygen determines the detection limit for cathodic detection. Flow-analyzers constructed of Teflon tubing and other plastic components are useless because oxygen readily permeates these materials. Needless to say, the approach of deaeration is quite inconvenient.

The major contribution of this research has been the development of an electroanalytical technique, called "reverse pulse amperometry" (RPA), which is capable of monitoring a fluid stream for metal ions using a Hg indicating electrode without the requirement of deaeration. The technique is based on the application of an unsymmetrical, pulsed-potential waveform with a large negative, initial potential for the reduction of the metal ion, followed by a positive potential pulse for the oxidation of the reduction product. The analytical signal is measured only during the anodic pulse at a potential where dissolved oxygen is not reduced. The time for one cycle of the waveform is short ($\leq$ 2 sec) so as to efficiently monitor the fluid stream for metal ions.

RPA has been shown to detect metal ions which form a metal-amalgam upon reduction, as well as metal ions which are reduced to a metal ion of a lower oxidation state which is soluble in the solution phase. RPA was applied in FIA and cation-exchange liquid chromatography (CELC). When RPA is used in conjunction with CELC, metal ions can be selectively and routinely detected at trace levels with good precision and accuracy. This method was demonstrated for the determination of Pb in NBS Standard Reference Material 1571 (orchard leaves).

II. LITERATURE REVIEW

Some analytical techniques for the determination of metals at trace levels are briefly reviewed. The purpose of this review is to compare the important analytical parameters which ultimately define the utility of a given technique. The inclusion of the electroanalytical technique also helps to illustrate the fundamental contributions these techniques have made to the development of RPA.

The focus of this dissertation is the development of RPA as an electroanalytical technique which is free of interference from dissolved oxygen when applied with a polarographic detector in LC. Hence, the remaining major topics of this review are polarographic detectors for flow-analyzers, separations of metal ions by ion-exchange liquid chromatography and reverse pulse polarography.

A. Methods for Trace Metal Analysis

The methods reviewed are atomic spectroscopy, neutron activation analysis, mass spectrometry, X-ray fluorescence and gas chromatography. A comparison of the detection limits for Pb is given in Table II-1 for the techniques considered in this review, and for several of the electroanalytical techniques considered later.

1. Atomic spectroscopy

a. Flame atomic absorption spectroscopy (FAA) This method is most commonly used for the determination of metals individually, because a separate light source is recommended for each metal of interest.

Typically, the useful analytical range for a given metal is only one order of magnitude in concentration at the part-per-million level (11). Matrix effects determine the practical applications of FAA and can usually be controlled through the proper selection of the flame conditions and the media. The method can be automated for the routine determination of trace metals.

b. Nonflame atomic absorption spectroscopy (NFAA) Like FAA, NFAA can also be automated for cost effectiveness, but is yet restricted to the determination of individual metals (12,13,14). NFAA requires more steps than FAA, e.g., the steps of drying, decomposition and furnace burnout. On the other hand, the use of a furnace with low volume significantly improves the sensitivity compared to FAA in which the sample atoms are diluted with a flame of relatively high volume. Sampling error adds to poorer precision relative to FAA. Matrix effects hinder the effectiveness of the steps of decomposition, atomization and clean-up. Both atomic absorption methods are applicable to a relatively high percentage of the metals listed in the periodic table.

c. Atomic emission spectroscopy with an inductively-coupled plasma (AES-ICP) This is perhaps the most impressive technique for the analysis of trace elements because of high sensitivity, wide linear dynamic range and freedom from interelement effects. The high temperature of the argon plasma and the absence of the combustion processes in the plasma eliminate the interference effects observed in the atomic absorption methods. Commercial instruments are now available for the simultaneous determination of more than 50 elements at a rate greater

than 40 samples per hour. Major, minor and trace constituents can readily be determined with high precision and accuracy (15,16,17). AES-ICP has also been used for powdered samples. The major limitations of this technique are the high costs of the instrumental package and its maintenance, and the high level of expertise required for operation of the instrument.

2. Neutron activation analysis (NAA)

NAA is capable of the simultaneous determination of many metals at trace levels with excellent sensitivity, and with good accuracy and precision. Through the use of semiconductor detectors and multichannel analyzers, the analysis is nondestructive and has sufficient resolution for multielemental determinations (14,18). The disadvantages of NAA include the expensive facilities and equipment, lower sample throughput and the safety problems associated with the use of radiation (19).

3. Mass spectrometry

a. Spark source mass spectrometry (SSMS) This technique is applicable to virtually all of the elements in the periodic table with a sensitivity which is large and reasonably uniform. SSMS is subject to limited effects by the matrix of the sample (14,20). SSMS has practical applications for the analysis of isotopes and solid samples such as coal or fly ash. However, precision is on the order of 20% at the part-per-million level when photographic plates are used for detection. The requirement of a high vacuum in the sample chamber results in a low sample throughput.

b. Chemical ionization mass spectrometry (CIMS) The chelation of many metal ions with fluorinated β-diketones produces thermally stable and volatile organometallic compounds. Aqueous solutions of these compounds are readily extracted into an organic phase and can be injected directly into the chemical ionization source. Mass spectra are simple and the area under the ion-current peak is directly proportional to concentration of the metal over several orders of magnitude with high sensitivity (21). The technique is useful for approximately 25 metals including most of the rare earth metals, but has yet to become popular (14).

4. X-ray fluorescence (XRF)

XRF is rapid and nondestructive. The technique is applicable to the simultaneous determination of most metals and requires little or no sample preparation. Concentrations of metals at the part-per-million level can be routinely determined, but the accuracy and precision of the method are defined by severe dependence on matrix effects. Standards of high quality are required for calibration (22). Instruments for analysis by XRF are expensive.

5. Gas chromatography (GC)

The use of GC for trace metal analysis also involves the chelation of metal ions with β-diketones and the same disadvantages are observed as mentioned for the CIMS method. Fluorinated β-diketones are used here to provide the increased sensitivity available with electron capture detection (23).

6. Electroanalytical techniques

RPA utilizes a pulsed-potential waveform applied at an EC detector with an indicating electrode of Hg. Both processes of reduction and oxidation at the Hg electrode are utilized in the analytical method. Therefore, several techniques involving Hg electrodes and pulsed-potential waveforms are presented and discussed as introductory material prior to the discussion of RPA. These are direct current (DC) polarography, normal pulse polarography, differential pulse polarography, anodic stripping voltammetry, differential pulse anodic stripping voltammetry and pulsed-potential methods used with EC detectors.

a. DC polarography Conventional DC polarography is the monitoring of the faradaic current at a DME as the applied potential is scanned in a linear manner with time (24). The response observed for the presence of an electroactive compound is a wave with a current plateau of a height which is directly proportional to the concentration of the electroactive compound. The half-wave potential, $E_{1/2}$, is characteristic of a given metal ion and is numerically close in value to the standard reduction potential of the half-reaction occurring at the electrode. Residual or charging current is produced by the potential scan and the growth of the Hg drop because of the change in the charge at the surface of the drop. At low levels of concentration of analyte, e.g., $\sim 10^{-5}$ M, the charging current severely interferes with the measurement of the faradaic current.

b. Normal pulse polarography (NPP) In NPP, the potential is "scanned" by way of steps or pulses of potential which successively increase in amplitude from an initial potential (25). The initial potential is chosen where the electrochemical reaction does not occur and the applied potential is pulsed into the region of the conventional polarographic wave. The pulse is typically instituted during the last 50 msec of the lifetime of each Hg drop. The current is monitored as a function of the pulses of applied potential. The experimental result is a wave.

NPP takes advantage of the difference in the rates of decay of the faradaic and the charging current. In response to a potential pulse of constant amplitude, the charging current typically decays to an insignificant value in less than 40 msec while the faradaic current decays as a function of $t^{-1/2}$. By delaying until the end of the pulse, a current measurement is made which significantly discriminates against charging current. However, this procedure does not lessen the charging current contributed by the changing electrode area. Nonetheless, the sensitivity of NPP is approximately 7X that of conventional polarography.

NPP is particularly useful for the determination of anions which form slightly dissociated compounds with Hg(I,II) (26,27).

c. Differential pulse polarography (DPP) DPP goes one step beyond NPP by utilizing potential pulses of small amplitude (5-100 mV) superimposed on a ramp of linear potential (25,28,29,30,31). As in NPP, the initial potential is chosen where no reaction occurs and is "scanned" toward the region of electroactivity of the analyte(s). There is one

pulse per drop during the last 50 msec of the lifetime of the Hg drop. The current is measured twice during each drop, just prior to the pulse and at the end of the pulse. The difference of these current measurements is recorded as a function of applied potential. This difference measurement effectively discriminates against charging current from both the potential scan and the growth of the Hg drop. The recorded signal is a peak which enables DPP to quantitatively distinguish between metal ions with $E_{1/2}$ values as low as 50 mV. The other polarographic methods discussed are able to distinguish between metal ions with $E_{1/2}$ values of 200 mV or more; therefore, DPP provides an improvement in resolution. DPP is 5-10X more sensitive than NPP and approaches the sensitivity available with linear sweep anodic stripping voltammetry.

DPP has practical applications in the determination of toxic heavy metals (32) and drugs in biological fluids (33).

d. Anodic stripping voltammetry (ASV) ASV employs a two-step procedure (34,35,36,37). The first step is the reduction or electrodeposition of the metal ion onto/into the indicating electrode, which is ordinarily Hg, by maintaining a constant potential for a known time period. The second step is the oxidation or stripping of the metal analyte from the electrode by a scan of linear potential in the positive direction. A current peak is observed on the plot of current versus potential, and the height or area of this peak is directly proportional to the concentration and deposition time. The advantage of ASV over most other electroanalytical techniques results from the electrodeposition step which concentrates the analyte from a solution cell of high volume

onto/into an electrode of low volume. The sensitivity is easily increased by increasing the deposition time or by increasing the rate of convection of the analytical solution to the electrode surface during the deposition step. Ultimately, the sensitivity is limited by the contribution of charging current caused by the sweep of linear potential.

The geometry of the electrode affects the response of ASV. An indicating electrode of relatively high volume decreases the sensitivity and broadens the current peaks due to the requirement of diffusion of the metal to the electrode surface during the stripping step. For this reason, the use of a thin-film mercury electrode (TFME) offers increased sensitivity over the HMDE (36,38). The TFME, however, demands more attention during use because of substrate effects. Substrates such as wax-impregnated graphite, pyrolytic graphite and glassy carbon introduce extraordinarily high charging current and signal artifacts unless the proper procedures of electrode cleaning, polishing and pre-treatment are used (39,40,41). At times, a new film must be prepared after each analysis.

ASV has been routinely applied in the analysis of fresh water, seawater, blood and urine for trace metals such as Cu, Zn, Cd, Cr, Ni and Pb. ASV has the capability of providing information on oxidation states and complexation (37,42,43).

e. Differential pulse anodic stripping voltammetry (DPASV)

DPASV combines the advantages of ASV with DPP. The two-step procedure of DPASV is identical to that of ASV except that the second step is the application of an anodic scan with the waveform for differential pulse

voltammetry rather than a linear sweep (44,45,46,47,48). The excellent sensitivity of DPASV has made this technique popular for the same applications as previously mentioned for ASV and DPP (49,50,51).

f. Pulsed-potential methods used with EC detectors The use of normal pulse and differential pulse methods for the amperometric monitoring of fluid streams for electroactive analytes has been studied by various workers (52,53,54,55). Advantages of the pulsed mode of detection can include the maintenance of electrode activity, a decreased dependence of the detector response on the flow rate of the fluid stream and increased analytical sensitivity. Kissinger (9) has discussed several approaches utilizing pulsed-potential waveforms in a review of EC detectors in LC. Rapid-scan square wave polarography at a DME has also been used in conjunction with LC to obtain voltammetry characterization for each chromatographic peak (56).

B. Polarographic Detectors for Flow-Analyzers

1. Historical

The first application of a DME as a polarographic detector in LC was for the determination of proteins containing the functional groups cysteine or cystine (57). The detector body was a cuvette made of Perspex which had several holes drilled in it to serve as the inlet and outlet ports, and to receive the reference electrode and the DME. The system was capable of amperometrically detecting proteins at concentrations as low as about 0.001%. Kemula used a similar approach, calling it "chromato-polarography", for the detection of Ni in Co salts (58).

Table II-1. Comparison of detection limits for the determination of Pb by various analytical techniques

Technique	Detection limit (reference)
FAA	15 ng mL^{-1} (36)
NFAA	0.002 ng mL^{-1} (14)
AES-ICP	0.008 µg mL^{-1} (14)
NAA	10^{-6} - 10^{-7} g (14)
SSMS	0.3 ng (14)
XRF	0.3 ng (14)
DPP	20 ng mL^{-1} (44)
ASV (HMDE)	2.5 ng mL^{-1} (44)
DPASV (HMDE)	0.01 ng mL^{-1} (44)

Lewis and Overton constructed a dual polarographic system to automatically and continuously monitor flowing or stationary solutions for metal ions (59). Wilson and Smith determined the maximum linear flow rate at horizontal and vertical DMEs prior to the onset of irregular dropping (60). For example, for the upward flow of fluid onto a DME mounted in a vertical position, the maximum linear flow rate possible without affecting the functioning of the DME was determined to be 0.66 cm sec^{-1}. This is a good illustration of the mechanical sensitivity of the DME to convection.

Mann used a polarographic cell to detect the ion-exchange elution of electroactive ions from a macro-column (61), as did Tustanowskii (62).

Rebertus, Capell and Bond (63), and Blaedel and Todd (64), used the DME to monitor step-wise, ion-exchange separations. Rebertus et al. observed the anion-exchange separations of 2-mg quantities of Ni(II), Co(II), Mn(II) and Cu(II). Blaedel and Todd observed the cation-exchange separation of Cd(II), Cu(II) and Pb(II), and the anion-exchange separation of fumaric and valeic acids. Both groups of authors used a method of continuous deaeration located in the fluid stream just before the DME assembly.

Blaedel and Strohl continued to improve the design of the flow-through, polarographic detector by decreasing the dead volume (65,66). This improvement decreased the residence time of the solution within the detector and improved the response time.

An alternate arrangement of the polarographic detector is the horizontal DME, first designed by Hartmann and Budan (67), which makes

it possible to construct a polarographic cell with a drop time of less than 1 sec and a dead volume of less than 1 μL (10). Mairanovskii, Barashkova and Vol'kenshtein used such an electrode to study the bromo-derivatives of thiophene (68). Scarano, Bonicelli and Forina applied this rapid dropping mercury electrode (RDME) to fluid streams with high sensitivity, even in the presence of a high background current, due to the very low oscillations and very low noise in the signal (69). Others used the RDME to detect nitropyridine derivatives as separated by ion-exchange or reverse-phase liquid chromatography (70). Michel and Zatka most recently combined the RDME with high performance liquid chromatography (HPLC) with interesting results (10). The RDME, when used in the amperometric mode, had an optimum drop time of 50 - 60 msec with detection limits in the 4 - 5 ng range for p-nitrophenol and nitrobenzene. The precision was also good, and there was a region of response which was dependent solely on the diffusion process and, therefore, independent of flow rate. The major limitation was that the optimum flow rate was only 0.6 mL min^{-1}, which seriously hindered its application to HPLC.

Recent applications of the polarographic detector to HPLC use the conventional vertical design of the DME with great success. The pesticides parathion, methyl parathion and p-nitrophenol were separated within 5 min by reverse-phase liquid chromatography and detected at concentrations of 10^{-8} mole L^{-1} (71). The average linear dynamic range of the detector covered 4 orders of magnitude and the precision was very good. The use of drop times of 1 sec yielded well-defined

chromatographic peaks. Stillman and Ma observed similar results also for parathion and methyl parathion with a detector design originated by Blaedel and Strohl (72). Improvements were made by decreasing the dead volume of the detector to 2-5 μL and by using a conically-ground capillary tip for an increase in the effective surface area of the electrode (73).

2. Interference from dissolved oxygen

Dissolved oxygen is reduced at a Hg electrode in two steps. The first step is the reduction of oxygen to hydrogen peroxide (Equations II-1 and II-2). The second step is the reduction of hydrogen peroxide

$$O_2 + 2H^+ + 2e \rightleftharpoons H_2O_2 \quad \text{(acid media)} \qquad \text{(II-1)}$$

$$O_2 + 2H_2O + 2e \rightleftharpoons H_2O_2 + 2OH^- \quad \text{(neutral or alkaline media)} \qquad \text{(II-2)}$$

to water or hydroxide (Equations II-3 and II-4). The $E_{1/2}$ for the first step is -0.05 V versus SCE and for the second step is

$$H_2O_2 + 2H^+ + 2e \rightleftharpoons 2H_2O \quad \text{(acid media)} \qquad \text{(II-3)}$$

$$H_2O_2 + 2e \rightleftharpoons 2OH^- \quad \text{(neutral or alkaline media)} \qquad \text{(II-4)}$$

-0.5 to -1.3 V versus SCE, depending on the pH. For the analysis of those species with $E_{1/2}$ more negative than 0 V versus SCE, it is necessary to lower the concentration of dissolved oxygen to an undetectable level, otherwise a background contribution to the analytical current will be observed.

Interferences other than the background contribution of current will also be observed if dissolved oxygen is not removed (74). The production of hydrogen peroxide by the first step in the reduction can affect other electroactive species by serving as either an oxidizing or reducing agent. Also, changes in the pH at the surface of the electrode because of both reduction steps can cause the precipitation of heavy metal ions at the electrode surface. This can be obviated through the use of a buffered supporting electrolyte. The advantages of removing dissolved oxygen are obvious.

The decision to remove dissolved oxygen from the analytical solution is made by considering the problem at hand and the polarographic method to be used. When the solution contains an analyte of concentration considerably greater than that of dissolved oxygen, the removal of dissolved oxygen may be unnecessary regardless of the polarographic method used. However, at analyte concentrations of approximately 10^{-4} M or less, the removal of dissolved oxygen will be required when the determination is performed by DC polarography, NPP or DPP (75).

This is not the case when alternating current (AC) polarography is used, particularly with high frequency and phase-sensitive detection. Metal ions can be determined down to 5×10^{-7} M without the removal of dissolved oxygen with this AC method. This is accomplished by taking advantage of the irreversible character of the electrochemical reduction of dissolved oxygen. The AC polarographic methods are not sensitive to irreversible electrode processes and, therefore, discriminate against the electrode process of oxygen. However, this also limits the

application of the technique to the determination of analytes with electrode processes which are reversible (75).

Dissolved oxygen has been removed from polarographic cells with reducing agents, such as ascorbic acid (76) and sodium sulfite (77,78), with enzymes such as glucose oxidase (79), or most commonly by purging the solution with a pure, inert gas such as nitrogen or helium. In fluid streams, nitrogen-activated glass nebulizers have been used (80). The following excerpt is presented (10) as an example of the lengths some workers have gone through to remove dissolved oxygen from a fluid stream.

> "... Two deaeration systems were used. With the Haskel pump, bubbling with pure nitrogen was used; the eluant (sic) was first filtered through a glass frit; through the same filter plate, nitrogen (99.999%) presaturated with the solution in a wash bottle, was then introduced for 1 hr. Vacuum was then applied for 10 min and the solution was transferred to the pump reservoir by gentle nitrogen pressure. A slow stream of nitrogen was kept flowing over the surface of the solution in the reservoir. The whole system was built of glass with ground ball joints.
>
> With the Altex pump, deaeration was done by boiling. The metallic inlet tubing of the pump with filter was introduced through the central neck into a three-neck round-bottom flask and sealed with a rubber stopper. One of the side necks was equipped with a reflux cooler, and the other with a thermometer. This system is much simpler; there are no solvent losses and the vacuum application is unnecessary. The boiling liquid can be pumped directly, as it cools sufficiently in the inlet line (30 cm) before entering the pump.
>
> The injected samples were deaerated directly in the syringe...."

All of these approaches for eliminating interference from dissolved oxygen have major disadvantages for routine electroanalysis in fluid

streams. The reducing agents mentioned have limited, useful pH ranges. Ascorbic acid is useful for the removal of dissolved oxygen over a range of pH 3.5-8.5. Sodium sulfite has a more limited range, pH 6-9, and its function is inhibited by the organic compounds of alcohols, glycols and aldehydes. Glucose oxidase is slow in its reaction and useful only in a buffered solution of pH 5-8.5. Nitrogen-activated glass nebulizers introduce significant dead volume and are, therefore, incompatible with requirements for high resolution in HPLC. The purging of all solutions is inconvenient, time-consuming, expensive in the case of helium, and virtually useless if the flow-analyzer is constructed from Teflon tubing which is readily permeated by oxygen. The latter problem, in particular, led to the development of RPA.

C. Separations of Metal Ions by Ion-exchange Liquid Chromatography

Although the EC detector is specific for electroactive species, it still applies to a large number of analytes; therefore, separations are required upstream from the detector. EC detectors are limited in application to those chromatographic methods which have mobile phases of high conductivity. Hence, analysis of complex mixtures is best made with ion-exchange LC.

The separation of metal ions by ion exchange was initially performed with gravity-flow columns and step-wise elutions using concentrated solutions of acids such as HCl (81,82), $HClO_4$ (83), HNO_3 (84) and H_2SO_4 (84). Organic acids such as tartaric acid were also studied in this manner

(85,86). These methods of separation are quite slow and not compatible with techniques for routine, automatic detection.

Seymour, Sickafoose and Fritz developed a forced-flow liquid chromatograph made of Teflon and various plastics which could withstand the corrosive eluents needed for the separation of metal ions with ion-exchange resins of full capacity (87). These authors determined Fe in several matrices by the stepwise elution of Fe(III) from various interferences. The Fe(III) was detected by the UV absorbance of its chloro-complex. The metal ions of Cd, Zn, Fe, Pb, Cu, Co and Mn were separated and detected in a similar fashion using the mixed aqueous-organic eluents of HCl-acetone (88,89), HCl-propanol (90) and HCl-dimethylformamide (90). The ion-exchange resins used were macro-reticular and were shown to provide rapid exchange rates in these mixed solvents. The disadvantages of these methods were the step-wise elution procedure, which requires operator attention, and the changing baseline between steps.

Fritz and Story (91,92), and Lieser (93), synthesized cation-exchange resins of low capacity as compared to the commercially available resins of full capacity. Synthesis was accomplished by the partial- or surface-sulfonation of macroporous, polystyrene resins with a high degree of cross-linkage. Although some differences were observed in the selectivities of the low- and full-capacity resins, the low capacity resins have the advantage of requiring lower acid or salt concentrations for the elution of strongly retained cations. Improvements in the kinetics of the exchange were also suggested. These

initial studies of ion-exchange resins of low capacity were followed by the development of the method of ion chromatography by Small, Stevens and Bauman (94).

A unique approach to the ion-exchange separation of metal ions was introduced by Yamabe (95). He showed that the metal ions in the lanthanide and transition metal series, respectively, could be separated by using a mixed-bed column of anion- and cation-exchange resins. The eluents used were solutions of chelating agents such a lactic acid and tartaric acid. The retention times observed were dependent on the stability constants of the complexes, the pH of the mobile phase, the mixing ratio of the ion-exchange resins and the ethanol content of the eluent. In the separation of the metal ions of Cu, Zn, Co, Cd, Pb and Mn, the elution order can also be changed by varying the mixing ratio of the cation/anion exchange bed (96). Yamabe and Hayashi applied this technique to the separation of the ions of the alkaline earth series (97). The use of the mixed ligands, lactic acid and sodium acetate, resulted in an enhancement of the effect of the mixed resin ratio on the order of elution for Fe(III) (98). The addition of a low percentage of ethanol to the eluent significantly improved the separation (99). Because of the additional analytical variables, this method has many practical applications to the separations of metal ions.

The cation-exchange separations of metal ions by HPLC have been accomplished aided by the availability of commercial resins with very small particle sizes and good mechanical strength (100,101,102). With a sodium tartrate-sodium chloride eluent, which is pH controlled, a

baseline separation of the ions of Cu, Zn, Ni, Pb, Co and Cd was achieved within 7 min. Using a similar approach and a resin with a particle size of 5-8 μm, these metal ions were still well-separated within 2 minutes (100)! The detector was a coulometric detector of the sandwich-type with an indicating electrode of carbon cloth.

D. Reverse Pulse Polarography

The only literature directly pertinent to RPA is that of reverse pulse polarography (RPP). RPA is discussed in detail and compared to RPP in Section III.A in this dissertation. Hence, only the literature of RPP is presented here.

The first description in the literature of a voltammetric method resembling RPP was by Kalousek (103) and Kalousek and Ralek (104). He studied the reversibility of electrode processes such as the electroreductions of K(I), Pb(II), Zn(II), Bi(III) and IO_3^- in selected media. The pulsed-potential waveform used was essentially that of RPP except that the potential was also changing linearly during the pulse. However, the results were a good indication of the reversible nature of the electrode process at a DME. He found, for instance, that Zn(II) proceeds reversibly in noncomplexing, acid media, but irreversibly, in ammoniacal media. Kambara provided some mathematical equations to fit the polarograms observed by Kambara (105).

Oldham and Parry introduced "scan-reversal pulse polarography" which, like the method described by Kalousek, yielded information pertaining to the reversible and irreversible behavior of the reaction

of a given redox couple (106). The current measured by this technique represents the difference between currents measured after and before pulse application. Unlike the Kalousek method, there is no potential scan during the application of the pulse. Mathematical expressions to describe the polarographic response and discern between reversible and irreversible processes were presented and shown to agree with experimental results. For example, the ratio of limiting currents for the cathodic and anodic scans of this method are predicted by the approximately 7, for a totally irreversible reoxidation of the reduction product, and 1, for a reversible reoxidation. Experimental values were 5.7 for the irreversible CrO_4^{-2} reduction and 1.03 for the reversible Fe(III) reduction.

Opekar and Stulik (107) applied the Kalousek method to anodic stripping analysis. An instrument to generate the necessary pulsed-potential waveform, called the "Kalousek commutator", was constructed with modern electronic circuitry. The method was tested for the anodic stripping analysis of Pb(II) using both the HMDE and the TFME. Excellent analytical results were obtained and a detection limit of about 10^{-9} M for Pb(II) was observed with a 2 min electrolysis for the TFME.

The determination of hydroxide ions by NPP with scan reversal was done by Kirowa-Eisner and Osteryoung (108). They found that hydroxide ions could be directly determined in the concentration range of 0.6-400 μM at the DME or TFME with this method due to the cleaning of the electrode during the initial potential. Without the cleaning step,

the Hg electrodes became easily inactivated. This system was also found suitable for amperometric, acid-base titrations with coulometric generation of the titrant.

NPP with an anodic scan, i.e., RPP, was used to study the irreversible Zn(II)-Zn(0) reaction at a DME in NH_3 buffer and in concentrated NaOH solutions (109). In concentrated NaOH solutions, a minimum was observed at the head of the anodic wave as well as a general anodic shift in the wave due to the irreversible oxidation of Zn. The minimum was observed to disappear at concentrations higher than 0.5 M NaOH, and the disappearance was explained by the formation of the soluble oxidation product, $Zn(OH)_4^{-2}$. At low concentrations of NaOH, $Zn(OH)_2$ is deposited on the Hg surface to limit the rate of further Zn dissolution. An anodic shift in the wave for the Zn oxidation was detected in the NH_3 buffer, but no minimum was observed because Zn(II) forms soluble Zn(II)-ammine complexes.

Osteryoung and Kirowa-Eisner proposed the use of RPP for applications to the characterization of reversibility, the identification and quantitative determination of products of an electrode reaction and the study of reactions poorly separated from solvent or electrode decomposition (110). RPP characterizes the electrochemical behaviour of the product of a reaction on a time scale of msec. This had been shown by Saito and Himeno (109) and mentioned by Kalousek in his original paper (103). The identification and quantitative determination of products of electrochemical reactions was illustrated by Kirowa-Eisner and Osteryoung (110). Kirowa-Eisner and Osteryoung studied the

reductions of organic molecules on Hg which are poorly separated from the hydrogen evolution in aqueous solutions. Stoichiometries of reaction and reversibility studies were demonstrated for the reduction of halogenated-pyridine compounds such as 2,3-dichloropyridine. The feature of RPP which makes it useful for detection of products of electrode reactions was exploited in the research described in this dissertation for the detection of metal ions without interference from dissolved oxygen.

III. PRINCIPLES OF REVERSE PULSE AMPEROMETRY

A. Introduction

RPA is best described by first explaining the technique of RPP through a comparison with NPP as applied for cathodic reactions. The potential-time waveforms for NPP and RPP are shown in Figure III-1 by Curves A and B, respectively. In NPP, the initial potential, E_i, has a value positive of the $E_{1/2}$ for the cathodic wave; the applied potential is "scanned" by way of regular increases in the amplitude, ΔE, of the negative potential pulses of short duration, t_p, which are added to E_i at regular time intervals, T. For application of NPP at a DME, the lifetime of each Hg drop, τ, corresponds to the period, T. In RPP, E_i is chosen at a value negative of $E_{1/2}$, in the potential region where the cathodic reaction is controlled by mass transport, and the potential is "scanned" by way of increasingly positive pulses. In both techniques, the faradaic current is measured at the end of each pulse when the charging current resulting from the application of ΔE has decayed to an insignificant value.

The potential-time waveform for RPA is illustrated in Figure III-1 by Curve C and is simply one segment of the waveform for RPP which is applied repeatedly without changing E_i or ΔE. The initial potential is chosen at a value for the mass transport-limited reduction of the analyte; and a large, constant value of ΔE is applied such that the final potential, $E_f = E_i + \Delta E$, is at a value for the oxidation of the product of the initial reaction at E_i. In the case of many metal ions,

Figure III-1. Potential-time waveforms for NPP, RPP and RPA

Curves: (A) normal pulse polarography

(B) reverse pulse polarography

(C) reverse pulse amperometry

E_i - initial potential

E_F - final potential

ΔE - pulse height

T - pulse period

t_p - pulse width

t_i - time period at E_i

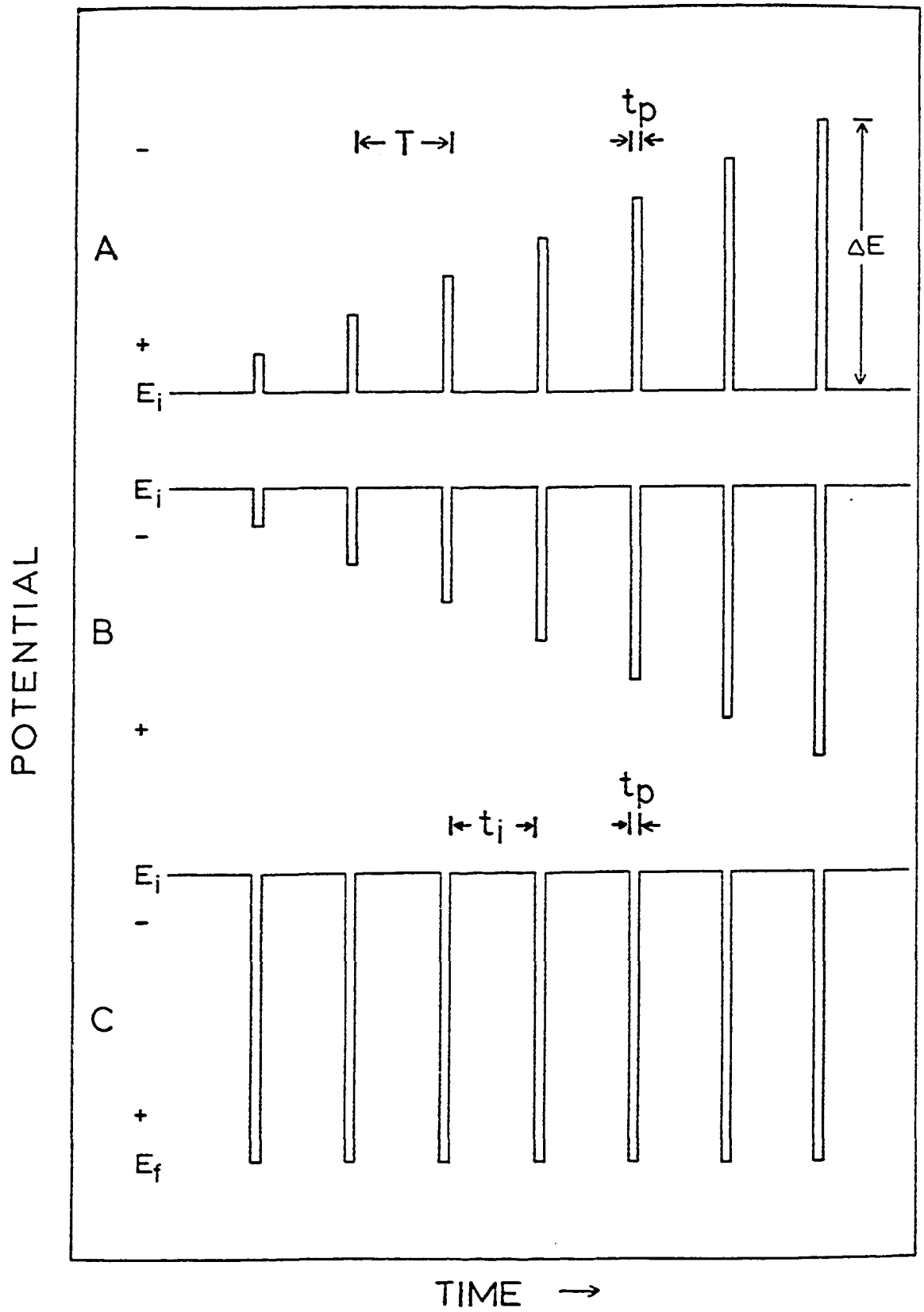
POTENTIAL
A
B
C
T
t_p
t_i
ΔE
E_i
E_f
+
-
TIME

a metal-amalgam is formed at E_i, e.g., Pb(II) + 2e $\rightleftharpoons$ Pb(Hg). This process is analogous to the accumulation process in voltammetric stripping analysis. For those metal ions reduced to a lower oxidation state which is soluble in the solution, e.g., Fe(III) + e $\rightleftharpoons$ Fe(II), the product of the reduction accumulates in the diffusion layer at the electrode-solution interface. In either case, oxidation of the product of the initial reaction occurs at E_f and the faradaic current for the oxidation is measured at the conclusion of the pulse period, t_p. As described here for the DME, the process of cathodic accumulation and anodic detection occurs once for each drop. With proper selection of E_f, there is no contribution to the analytical signal from the direct reaction of dissolved oxygen at the electrode.

A representation of the current-time response to the pulsed-potential waveform of RPA is given in Figure III-2 which is drawn to scale for T = 1 sec and t_p = 57 msec. Figure III-2 describes the response for a reaction which produces a metal-amalgam. The dashed lines represent the electrode response in the absence of analyte, i.e., the current due to the re-establishment of the charge at the electrode surface following a potential pulse (the charging current). Note that the charging current decays virtually to zero in less than 40 msec. The solid line is the total current, i.e., the sum of the faradaic and charging currents. The positive or cathodic current which flows while the electrode is at E_i is due to the reduction or deposition process. The current caused by the reduction of dissolved oxygen is not shown, but this current would interfere if the current was measured in this

Figure III-2. Representation of current-time response to the pulsed-potential waveform of RPA

t_s - time during which the current is sampled

Scale - T = 1 sec

t_p = 57 msec

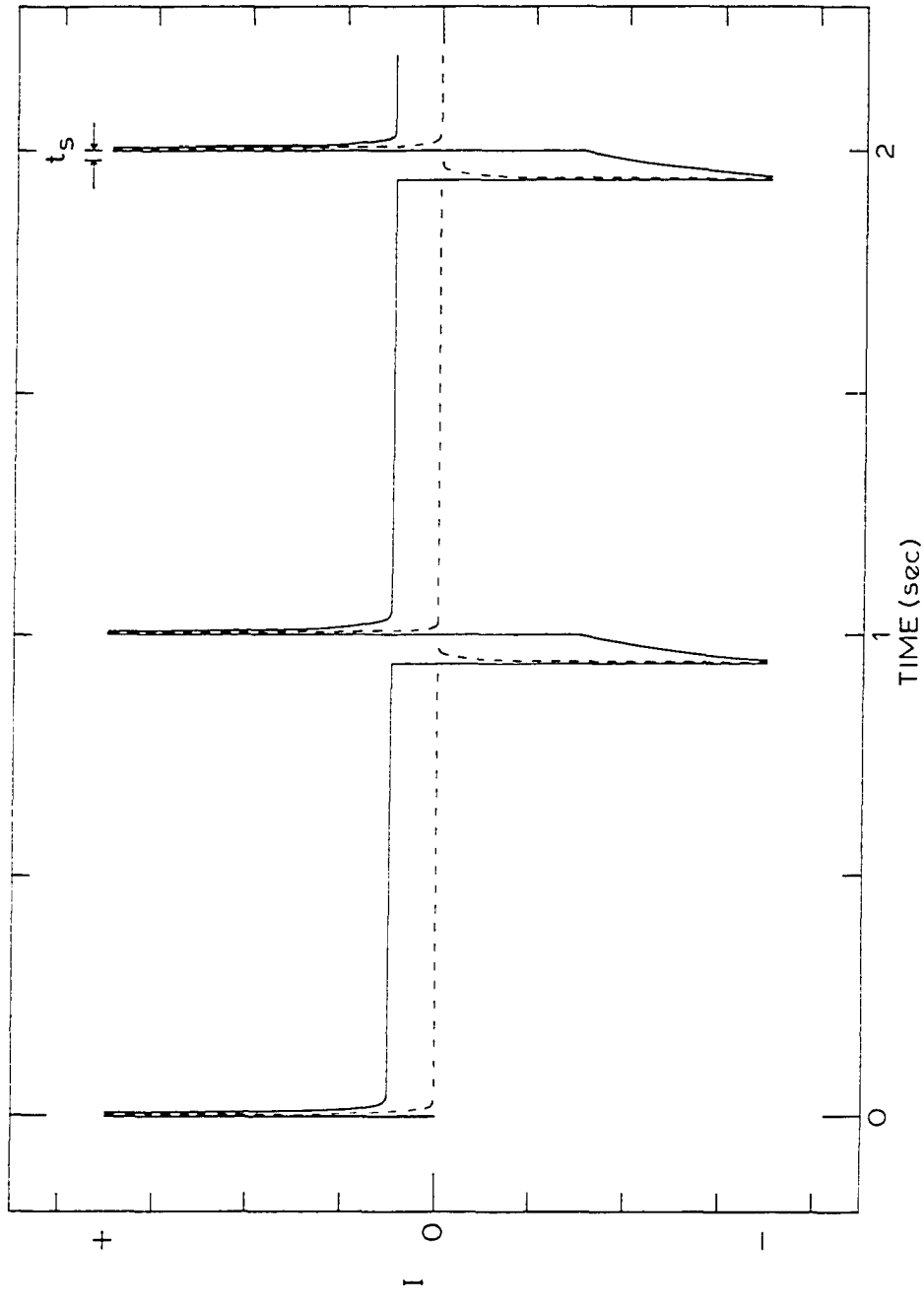
t_s
+
0
−
I
0
1
2
TIME (sec)

region. The negative or anodic current is observed at E_f for the oxidation or stripping of the product of the initial reaction at the Hg electrode. The total anodic current is sampled near the end of t_p where there is little contribution from the charging current. The anodic current provides a more sensitive analytical measurement in comparison to the cathodic current for RPA, as will be explained later.

B. Theory

1. RPP for the reaction $M^{+m} + ne \rightleftharpoons M(Hg)$

A rigorous derivation of the mathematical description of the electrochemical response of a Hg-drop electrode in a fluid stream under the constraints of RPA would be very difficult. This difficulty would result from the lack of a rigorous, closed-form description of the hydrodynamics of this situation. Derivations of polarographic response have been produced in the literature for Hg-drop electrodes in unstirred solutions; however, these are not expected to have direct application for the fluid stream. Osteryoung and Kirowa-Eisner (110) have recently reviewed the derivation for RPP at the DME in unstirred solutions for the case where the product of the initial reaction at E_i is soluble in the solution phase. A similar derivation is given here for the deposition of a metal at E_i which is soluble in the Hg drop. Whereas this derivation would be applicable to the case of a stirred solution, i.e., the fluid stream, only for low rates of convection and small T and t_p, the derivation provides useful insight into the mechanism of the electrochemical response.

Consider the reduction step for a redox couple which forms a metal-amalgam, i.e., $M^{+m} + ne \rightleftharpoons M(Hg)$; here, m = n. The limiting cathodic current for this step is defined by Equation III-1, which is an empirical equation applicable for all electrode geometries and all forms of stirring.

$$I_{dep} = n_R F A D_{M^{+m}} \left(\frac{C_{M^{+m}}^{b} - C_{M^{+m}}^{o}}{\delta} \right) \qquad \text{(III-1)}$$

In Equation III-1,

I_{dep} = limiting current for the reduction or deposition (mA);

n_R = number of electrons for the reduction (equiv mol^{-1});

F = Faraday constant (coul $equiv^{-1}$);

A = electrode surface area (cm^2);

$D_{M^{+m}}$ = diffusion coefficient for the metal ion in solution ($cm^2\ sec^{-1}$);

$C_{M^{+m}}^{b}$ = concentration of metal ions in the solution bulk ($mol\ L^{-1}$);

$C_{M^{+m}}^{o}$ = concentration of metal ions at the electrode surface ($mol\ L^{-1}$);

δ = thickness of diffusion layer (cm).

For a planar electrode in an unstirred solution, the thickness of the diffusion layer for M^{+m} in the solution phase is given by Equation III-2.

$$\delta = (\pi D_{M^{+m}} t_i)^{1/2} \qquad \text{(III-2)}$$

In this equation, t_i is the period for the reduction during one cycle of the waveform (sec). Substitution for δ in Equation III-1 produces Equation III-3 because $C_{M^{+m}}^{o}$ is zero for a reduction process with a

$$I_{dep} = \frac{n_R F A D_{M^{+m}}^{1/2} C_{M^{+m}}^{b}}{\pi^{1/2} t_i^{1/2}} \qquad \text{(III-3)}$$

high rate of electron transfer. Therefore, I_{dep} is the measurement of the cathodic or deposition current at the end of the deposition period, t_i.

At any instant during the deposition, there is a balance of fluxes at the electrode surface which can be mathematically written as Equation III-4. The so-called "Nernstian approximation" can now be applied for the evaluation of the concentration gradients. According to this approximation, $\partial C/\partial x$ is assumed constant over the distance adjacent to the electrode surface where diffusion occurs, $x \leq \delta$ (Figure III-3). Hence, Equation III-4 can be written as Equation III-5 where distances on both sides of the electrode surface are taken as positive.

$$D_{M^{+m}} \left[\frac{\partial C_{M^{+m}}}{\partial x}\right]_{x=0} = - D_{M(Hg)} \left[\frac{\partial C_{M(Hg)}}{\partial x}\right]_{x=0} \qquad \text{(III-4)}$$

$$D_{M^{+m}} \left[\frac{C_{M^{+m}}^{b} - C_{M^{+m}}^{o}}{\delta_{soln}}\right] = - D_{M(Hg)} \left[\frac{C_{M(Hg)}^{b} - C_{M(Hg)}^{o}}{\delta_{Hg}}\right] \qquad \text{(III-5)}$$

This balance of fluxes is pictorially illustrated in Figure III-3A by the concentration profiles for M^{+m} and M(Hg) in the solution phase and Hg phase, respectively. $C_{M(Hg)}^{b}$, the concentration of the metal-amalgam at the inner boundary of the diffusion layer in the Hg drop, is equal to zero. $C_{M^{+m}}^{o}$ is also zero. For a diffusion-controlled reduction in the absence of any stirring, $\delta_{Hg} = \delta_{soln}$. The result of substituting these

Figure III-3. Concentration profiles for the reaction $M^{+m} + ne \rightleftharpoons M(Hg)$ observed for the detection of M^{+m} by RPP

C - concentration

X - distance

σ_t - diffusional layer thickness at time t

A) For reduction or deposition, $E - E_i$

t - time elapsed since application of E_i

$t_2 > t_1$

B) For oxidation or stripping, $E - E_F$

t' - time elapsed since application of E_f following the establishment of the corresponding profiles at E_i

$t'_2 > t'_1$

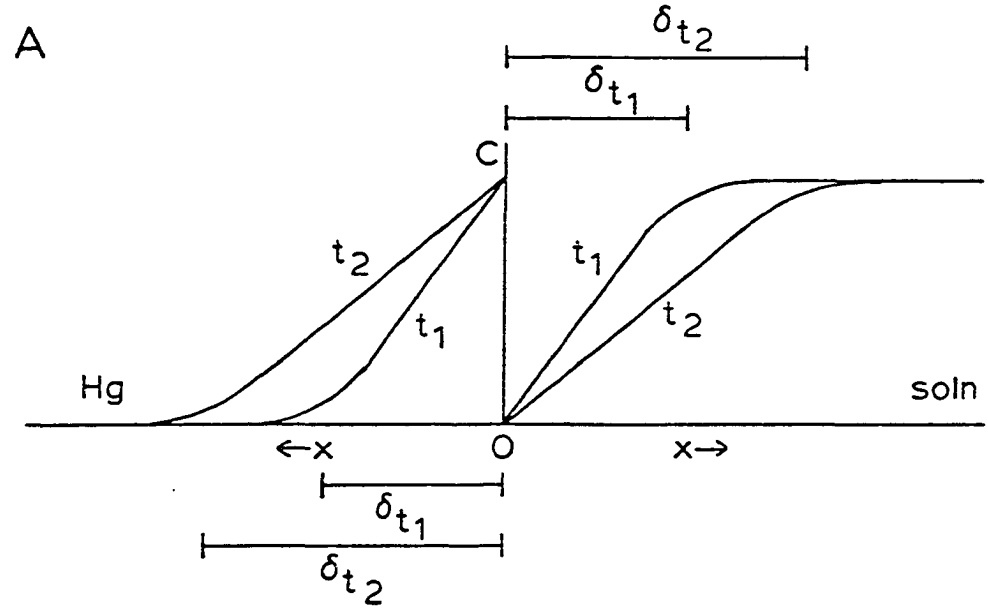
A
δ_{t_2}
δ_{t_1}
C
t_2
t_1
t_1
t_2
Hg
soln
←x
O
x→
δ_{t_1}
δ_{t_2}

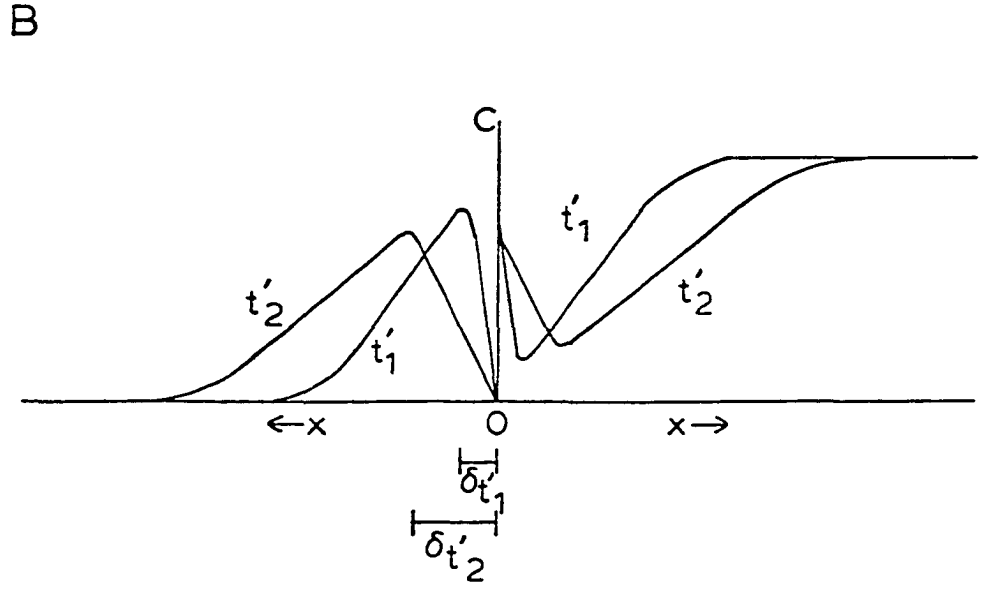
B
C
t'_1
t'_2
t'_2
t'_1
←x
O
x→
$\delta_{t'_1}$
$\delta_{t'_2}$

equalities into Equation III-5 produces Equation III-6. Equation III-6

$$C_{M^{+m}}{}^{b} = \frac{D_{M(Hg)}}{D_{M^{+m}}} C_{M(Hg)}{}^{o} \qquad \text{(III-6)}$$

can be substituted into Equation III-3 to yield Equation III-7.

$$I_{dep} = \frac{n_R F A D_{M(Hg)}{}^{1/2} C_{M(Hg)}{}^{o}}{\pi^{1/2} t_i{}^{1/2}} \qquad \text{(III-7)}$$

The concentration profile for the oxidation process is shown in Figure III-3B. An expression for I_{strip} can be derived in a way analogous to that for Equation III-7 with the following result.

$$- I_{strip} = \frac{n_0 F A D_{M(Hg)}{}^{1/2} C_{M(Hg)}{}^{o}}{\pi^{1/2} t_p{}^{1/2}} \qquad \text{(III-8)}$$

In this equation,

I_{strip} = limiting current for the oxidation or stripping, i.e., the current for the reverse pulse (mA);

n_0 = number of electrons in the oxidation (equiv mol^{-1});

t_p = time period prior to the measurement of the anodic current (sec).

All other parameters have the usual electrochemical significance. I_{strip} is the measurement of the stripping current since it represents the anodic current due to the stripping of metal from the Hg electrode at time t_p.

The relationship between the stripping current and the deposition current for RPP is evaluated by taking the ratio. The final result is Equation III-9,

$$- \frac{I_{strip}}{I_{dep}} = \left(\frac{t_i}{t_p}\right)^{1/2} \qquad \text{(III-9)}$$

when $n_R = n_O$. Equation III-9 is the same as that given by Osteryoung and Kirowa-Eisner (110) for the reaction $M^{+m} + ne \rightleftharpoons M^{+m-n}$ under diffusion-controlled conditions.

Several assumptions have been made in this mathematical derivation; however, the result provides important information which can be visualized using the concentration profiles in Figure III-3. During the reduction, a transfer of analyte from the solution to the electrode is predicted. This transfer distributes the analyte in the electrode at a concentration no higher than the bulk concentration of the metal ion in solution, for $D_{M^{+m}} = D_{M(Hg)}$, and in a diffusion layer which grows with the deposition time, t_i. The distribution of M(Hg) in the diffusion layer as a result of deposition is nonuniform, i.e., $C_{M(Hg)}$ in the diffusion layer decreases as x increases. During the oxidation, the analyte in the Hg near the electrode surface is oxidized. For small t_p, the quantity of analyte oxidized is only a small fraction of that in the electrode. The current response, therefore, is a function of the surface concentration of the analyte and, thereby, the bulk concentration of analyte in the solution, i.e., $C_{M(Hg)}^{o} = C_{M^{+m}}^{b}$. The concentration profile, Figure III-3A, illustrates the equality of the

concentration of metal-amalgam at the electrode surface to the bulk concentration of metal ion in solution just prior to the anodic pulse. Therefore, the measurement of the current due to the anodic pulse yields a signal which represents the bulk concentration of analyte in the solution.

The derivation of Equation III-9 was based on the assumption that $C_{M(Hg)}^{o}$ at the conclusion of the deposition period adequately expresses the value of $C_{M(Hg)}$ corresponding to the boundary of the diffusion layer in the Hg drop at $t = t_p$. This is referred to as the "assumption of uniform distribution". This assumption is valid only for short pulse times, t_p, and long deposition times, t_i, and, thus, for small ratios of t_p/t_i, i.e., $t_p < 0.001\ t_i$. In a rigorous mathematical treatment for a double-potential step method for planar electrodes, Schwarz and Shain (111) have accounted for the effect of a nonuniform distribution. The correction of Schwarz and Shain produced the following equation. This equation also applies to the reaction, $M^{+m} + ne \rightleftharpoons M^{+m-n}$, for

$$-\frac{I_{strip}}{I_{dep}} = \left[\left(\frac{t_i}{t_p}\right)^{1/2} - 1\right] \qquad \text{(III-10)}$$

studies by RPP.

2. RPA for the reaction $M^{+m} + ne \rightleftharpoons M(Hg)$

In Section III.B.1, mathematical equations were developed for RPP as applied with unstirred solutions for the reaction $M^{+m} + ne \rightleftharpoons M(Hg)$. It was mentioned that the mathematical derivations would be applicable to the case of stirred solutions, i.e., the fluid stream, only for low

rates of convection and small values of t_i and t_p. In this section, a simple and approximate theory is developed with an approach similar to that taken in Section III.B.1 to predict the response of a Hg electrode, under conditions of RPA, in the fluid stream of a flow-analyzer. Equations are presented relating peak height, I_p, and peak area, Q, to the deposition period, t_i, flow rate, V_f, and the number of moles of metal ion injected, N. A key assumption in this theoretical development is that the equation of diffusion which is written for a planar Hg electrode (e.g., TFME) is also applicable for a spherical Hg electrode (e.g., Hg-drop electrode). This approximation is good provided the distance over which diffusion occurs, δ_{Hg}, is small relative to the radius of the spherical electrode (34).

For the cathodic reaction of a metal ion at a Hg electrode, according to $M^{+m} + ne = M(Hg)$, where M(Hg) signifies that the reduced form is soluble in the Hg electrode, a balance of fluxes can be written as given by Equations III-4 and III-5. To a good approximation, $D_{M^{+m}} = D_{M(Hg)}$. Recall, C^b for M^{+m} and M(Hg) in Equation III-5 represent the bulk concentrations of the designated species in the bulk of the solution and bulk of Hg, respectively; i.e., $C = C^b$ when $x = \delta$. When pure Hg is used for the electrode, $C_{M(Hg)}{}^b = 0$. C^o for M^{+m} and M(Hg) represent the corresponding concentrations measured at the interface of the solution with the electrode, i.e., at $x = 0$. When the deposition process is occurring at a rate limited by mass transport, $C_{M^{+m}}{}^o = 0$. Hence, Equation III-5 can be written as Equation III-11. The thickness

$$\frac{C_{M^{+m}}^{b}}{\delta_{M^{+m}}} = \frac{C_{M(Hg)}^{o}}{\delta_{M(Hg)}} \qquad \text{(III-11)}$$

of the diffusion layer, δ, in the absence of convection is given by Equation III-2 and applies to both the solution and Hg phases. As discussed in Section III.B.1, $\delta_{M(Hg)} = \delta_{M^{+m}}$ for the case where $D_{M(Hg)} = D_{M^{+m}}$, and, as a result, $C_{M(Hg)}^{o} = C_{M^{+m}}^{b}$. For the application of interest here where the Hg electrode is positioned in a fluid stream, the value of $\delta_{M^{+m}}$ is influenced by the flow rate. An exact equation for $\delta_{M^{+m}}$ has not been derived for the electrode geometries used in this research because the vectors describing fluid velocity at the electrode surfaces have not been described. In general, the limiting value of $\delta_{M^{+m}}$ will decrease with increases in flow rate. The value of $\delta_{M(Hg)}$ will still be given by Equation III-2 because motion of the fluid stream is not expected to induce motion of M(Hg) within the Hg electrode. Hence $C_{M(Hg)}^{o}$ is given by Equation III-12.

$$C_{M(Hg)}^{o} = C_{M^{+m}}^{b} \left[\frac{\delta_{M(Hg)}}{\delta_{M^{+m}}}\right] \qquad \text{(III-12)}$$

For very small t, $\delta_{M^{+m}}$ will be relatively unaffected by flow rate and $\delta_{M^{+m}} = \delta_{M(Hg)}$. For $t \gg 0$, $\delta_{M^{+m}}$ will be independent of t. The value of t for the transition between these two conditions is not known but is expected to be considerably less than 1 sec. The concentration profiles for M^{+m} and M(Hg) are represented in Figure III-4A for two values of t with $t_2 > t_1 \gg 0$. Note that the profile for M^{+m} is

Figure III-4. Concentration profiles for the reaction $M^{+m} + ne \rightleftharpoons M(Hg)$ under the conditions of RPA

C - concentration

X - distance

A) for reduction or deposition, $E - E_i$

t - time elapsed after application of E_i

δ - diffusional layer thickness at time t

B) for oxidation or stripping, $E - E_f$

t´ - time elapsed since application of E_f following the establishment of the corresponding profiles at E_i

δ - diffusional layer thickness at time t_p

A

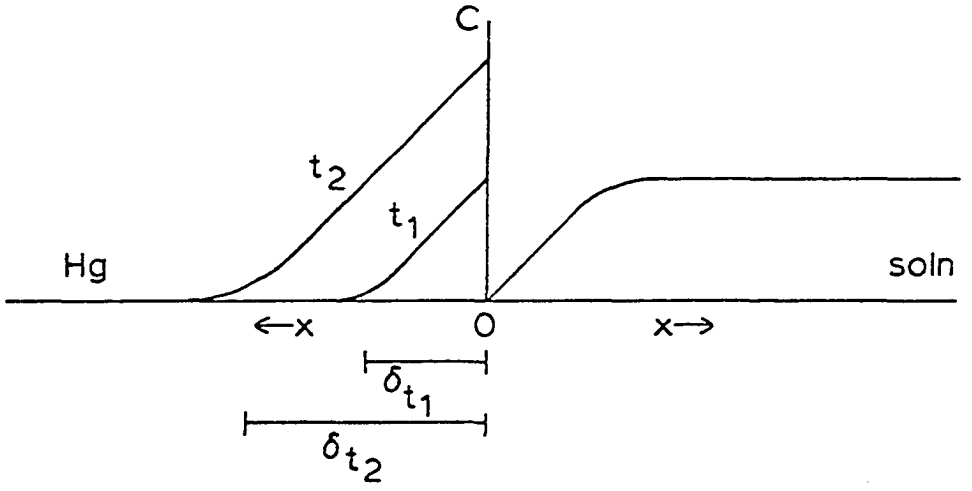

B

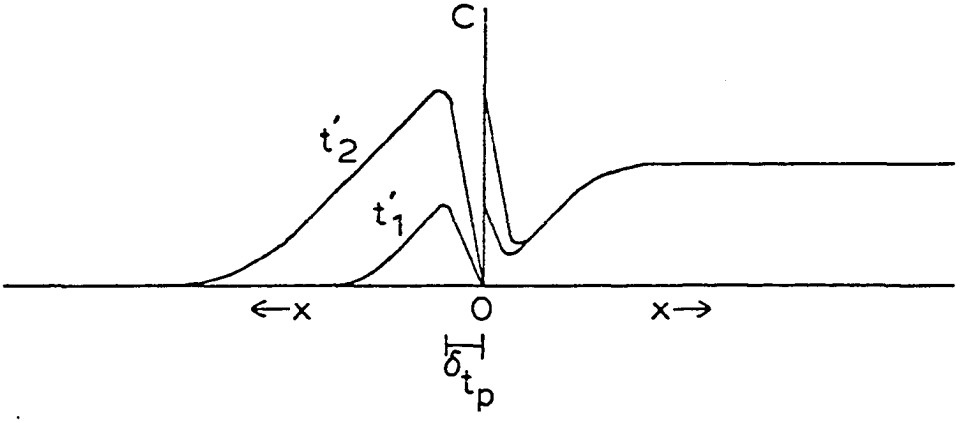

independent of t. Note further that $(\partial C_{M(Hg)}/\partial x)_{x=0} = (\partial C_{M^{+m}}/\partial x)_{x=0}$, (see Equation III-4).

The total number of moles, N, deposited during a deposition time of t_i is evaluated by integrating $C_{M(Hg)}$ over the volume of the Hg electrode as given by Equation III-13. The equality dV = Adx, applied

$$N = \int C_{M(Hg)}\, dx$$
$$= A \int C_{M(Hg)}\, dx \qquad \text{(III-13)}$$

in Equation III-13, is strictly accurate only for a planar electrode, but is a reasonable approximation for a spherical electrode when $\delta_{M(Hg)}$ is much less than the radius of the spherical electrode. Since the total mass of M(Hg) is considered to be contained within the volume $A \cdot \delta_{M(Hg)}$, Equation III-13 can be written as Equation III-14.

$$N = A \int_0^{\delta_{M(Hg)}} C_{M(Hg)}\, dx \qquad \text{(III-14)}$$

The concentration profile is assumed here to be linear within the region $x < \delta_{M(Hg)}$ (see Figure III-4A), and $C_{M(Hg)}$ is given by Equation (III-15).

$$C_{M(Hg)} = C_{M(Hg)}^{o} \left[\frac{\delta_{M(Hg)} - x}{\delta_{M(Hg)}}\right] \qquad \text{(III-15)}$$

Equations III-14 and III-15 are combined and evaluated to yield Equation III-16.

$$N = \frac{A\, C_{M(Hg)}^{o}\, \delta_{M(Hg)}}{2} \qquad \text{(III-16)}$$

Substituting for $\delta_{M(Hg)}$ in Equation III-16 based on Equation III-2, $C_{M(Hg)}^{o}$ is evaluated as a function of time for the deposition.

$$C_{M(Hg)}^{o} = \frac{2N}{A\,\pi^{1/2}\,D_{M(Hg)}^{1/2}\,t_i^{1/2}} \qquad \text{(III-17)}$$

The number of moles of metal deposited is evaluated approximately from the steady-state electrode current for deposition, I_{ss}, by applying Faraday's law.

$$N = \frac{I_{ss}\,t_i}{n\,F} \qquad \text{(III-18)}$$

Equations III-17 and III-18 are combined to give $C_{M(Hg)}^{o}$ as a function of t_i.

$$C_{M(Hg)}^{o} = \frac{2\,I_{ss}\,t_i^{1/2}}{n\,F\,A\,\pi^{1/2}\,D_{M(Hg)}^{1/2}} \qquad \text{(III-19)}$$

The value of I_{ss} is given by Equation III-20 and this definition is

$$I_{ss} = \frac{n\,F\,A\,D_{M^{+m}}\,C_{M^{+m}}^{b}}{\delta_{M^{+m}}} \qquad \text{(III-20)}$$

combined with Equation III-19 to give $C_{M(Hg)}^{o}$ as a function of t_i and $C_{M^{+m}}^{b}$. As before, $D_{M^{+m}} = D_{M(Hg)}$.

$$C_{M(Hg)}^{o} = \frac{2\,D_{M^{+m}}^{1/2}\,t_i^{1/2}\,C_{M^{+m}}^{b}}{\delta_{M^{+m}}\,\pi^{1/2}} \qquad \text{(III-21)}$$

Next, we consider the anodic stripping process which commences immediately upon the conclusion of the deposition. The anodic current is measured at the end of a short anodic pulse, t_p. It will be assumed that $t_p << t_i$ so that the concentration profile for M(Hg), which exists at the conclusion of t_i, is maintained throughout t_p. For the PAR 174A Polarographic Analyzer, used in the RPA mode, t_p = 57 msec. Furthermore, because $t_p << t_i$, the value of $C_{M(Hg)}$ at the end of t_p is assumed to adequately represent the bulk boundary condition for the evaluation of the diffusion-limited stripping current. The concentration profiles at the end of t_p are illustrated in Figure III-4B. The value of I_{strip} is given by Equation III-22.

$$I_{strip} = \frac{n\ F\ A\ D_{M(Hg)}^{1/2}\ C_{M(Hg)}^{o}}{\pi^{1/2}\ t_p^{1/2}} \qquad \text{(III-22)}$$

Equations III-21 and III-22 are combined to predict I_{strip} as a function of t_p, t_i and $C_{M^{+m}}^{b}$.

$$I_{strip} = \frac{2\ n\ F\ A\ D_{M(Hg)}\ t_i^{1/2}\ C_{M^{+m}}^{b}}{\pi\ \delta_{M^{+m}}\ t_p^{1/2}} \qquad \text{(III-23)}$$

Equation III-23 predicts the value of I_{strip} for a single pulse cycle at a Hg electrode which contains no M(Hg) prior to application of the pulsed-potential waveform. In the case of the SDME, the electrode is renewed prior to the start of each pulse cycle in compliance with this assumption. The HMDE and TFME are not renewed, and the M(Hg) not stripped for one pulse cycle is carried over into

succeeding pulse cycles. Ultimately, all of the M(Hg) will be stripped from the electrodes; however, this will occur only after the value of $C_{M^{+m}}^{b}$ in the fluid stream has dropped to zero so no additional metal is deposited during the deposition periods of the pulse cycles. Hence, significant tailing is expected for the detection peaks obtained with the TFME and the HMDE.

Peak tailing for the TFME can be minimized by keeping the thickness of the Hg film at a minimum. The relationship between film thickness and stripping current for ASV with a linear sweep of potential has been discussed by Roe and Toni (38). As clearly described by Roe and Toni, the sensitivity of the anodic stripping signal for a TFME is larger than for a HMDE because the diffusion of the deposited metal is limited to a very small volume of Hg equal to $A \cdot \ell$, where ℓ is the thickness of the Hg film. Consequently, if the diffusion of the M(Hg) reaches a distance $x = \ell$, $C_{M(Hg)}^{o}$ for the TFME will be larger than predicted by Equation III-23.

3. Flow rate dependence of EC detectors

A general equation for the limiting steady-state current of an EC detector in the conventional amperometric mode is given by Equation III-24. In Equation III-24, k = limiting, specific, mass transfer coefficient ($cm^{1-3\alpha}\ sec^{\alpha-1}$) and α is a fraction which is dependent on electrode geometry and fluid dynamics.

$$I_{ss} = k\ n\ F\ V_f^{\alpha}\ C^{b} \qquad \text{(III-24)}$$

In practice, peak height, I_p, is commonly used as the analytical current measurement. For amperometric detectors, the peak height is given empirically by Equation III-25, where k´ is a proportionality

$$I_p = k' n F V_f^{\beta} C^b \qquad \text{(III-25)}$$

constant related to the mass transfer and dispersion coefficients and β is a fraction which is dependent on electrode geometry, fluid dynamics and dispersion. The concentration of analyte in the detector, C, is typically lower than the concentration of sample injected, C^b, because of the dispersion of the sample plug during transport from the sample loop to the detector. The dispersion of the sample plug is a function of several parameters which include flow rate, retention volume, volume of the sample loop and the chromatographic retention time. Hence, the requirements for using I_p as the analytical signal are the meticulous control of the flow rate and the precise reproduction of the effects of dispersion. V_f can be controlled for the purpose of most analyses, and the values for the retention volume, the volume of the sample loop and the chromatographic retention time are essentially constant. Nevertheless, even small changes in the curvature of the tubing, between the sample injection valve and the detector, affect the dispersion to such a degree that the precision in the values for I_p can change by several percent (112).

The equation for the peak area, Q, observed with an EC detector is given by Equation III-26. Substituting I_{ss} from Equation III-24

$$Q = \int I_{ss}\, dt \qquad \text{(III-26)}$$

into Equation III-26 yields Equation III-27. The number of moles

$$Q = k\ n\ F\ V_f^{\alpha} \int C^b\ dt \qquad \text{(III-27)}$$

of analyte injected is described by Equation III-28. Incorporating

$$\text{moles} = V_f \int C^b\ dt \qquad \text{(III-28)}$$

Equation III-28 into Equation III-27 produces the final result,

$$Q = k\ n\ F\ V_f^{\alpha-1}\ (\text{moles}) \qquad \text{(III-29)}$$

Equation III-29.

Although the peak area still depends on flow rate, P. L. Meschi and D. C. Johnson (112) of this laboratory proved that peak area is independent of dispersion for flow-analyzers commonly used in chemical analysis. More precise results are expected for peak area as compared to those for peak height for this reason. The measurement of peak area is recommended in analytical situations where the peak area can be determined conveniently.

Note that the exponents of the V_f terms have a difference of unity for the equations describing the steady-state current (Equation III-24) and the peak area (Equation III-29).

To evaluate the exponents of the V_f terms in Equation III-24, Equation III-25 and Equation III-29, the logarithms of both sides are taken to give Equation III-30, Equation III-31 and Equation III-32.

$$\log I_{ss} = \text{constant} + \alpha \log V_f \qquad \text{(III-30)}$$

$$\log I_p = \text{constant} + \beta \log V_f \qquad \text{(III-31)}$$

$$\log Q = \text{constant} + (\alpha\text{-}1) \log V_f \qquad \text{(III-32)}$$

Therefore, straight lines are anticipated for plots of log I_{ss} versus log V_f, log I_p versus log V_f and log Q versus log V_f; the slopes of these lines are α, β and α-1, respectively.

4. Dependence of response of RPA on the nature of the metal redox couple

The dependence of the sensitivity of RPA on the nature of the reduction product of the metal ion is best explained by considering the concentration profiles for both the reduction and oxidation processes as was done in Section III.B.2. The contribution of the convection process must be taken into account since RPA is applied in a fluid stream. The flow rate of the fluid stream affects the diffusion layer of M^{+m} in solution and, in turn, the diffusion layer of M(Hg) in the electrode. The concentration profiles are given in Figures III-5 and III-6. Figure III-5 gives the concentration profiles for a reaction which results in the formation of a metal amalgam, i.e., $M^{+m} + ne \rightleftharpoons M(Hg)$. At the start of the deposition period ($t < t_1$), the flux of M^{+m} to the electrode surface is controlled solely by diffusion for a very short time period. There is an equal flux of M(Hg) in the electrode during this period and the concentration of M(Hg) at the electrode surface corresponds to the concentration of M^{+m} in the bulk of solution, as is the case for the situation discussed in Section III.B.1. The diffusion layer in the solution phase rapidly reaches a thickness which is controlled by the rate of convection ($t > t_1$, shown by t_2). Hence,

the flux of M^{+m} to the electrode is large and constant. The flux of M^{+m} from the bulk solution to the electrode surface is equal to the flux of M(Hg) from the electrode surface to the center of the electrode as described by Equation III-4. Therefore, the flux of M(Hg) in the electrode is large and constant. According to Equation III-4, and assuming diffusion coefficients which are equal, the slopes of the curves describing the concentration gradients must be equal. This is illustrated in Figure III-5A by parallel concentration gradients in the solution and in the Hg. The result is an accumulation of M(Hg) ($t > t_1$) near the surface of the drop at a concentration which is larger than the bulk concentration of the metal ion in solution. This is in contrast to the situation in unstirred solutions where $C_{M(Hg)}{}^{o}$ never exceeds $C_{M^{+m}}{}^{b}$. This accumulation, in turn, produces an enhancement in the current measurement for RPA.

For those metal ions with reduction products of limited solubility in Hg, the lower response observed by RPA is explained by the concentration profiles of Figure III-5. There are two limiting cases for the deposition process. The first case is a metal which is soluble in the Hg and readily diffuses into the electrode with an increase of deposition time. This is the case considered thus far. The second case is a metal which is not soluble in Hg and forms a film on the electrode surface. A reduction product with a limited solubility in Hg, such as Sb or Ni, approaches the second case and tends to concentrate at the electrode surface. With the application of an anodic pulse of potential, there results a relatively large flux of metal ion from the electrode surface.

Figure III-5. Concentration profiles for the study of $M^{+m} + ne \rightleftharpoons M(Hg)$ by RPA

C - concentration

X - distance

A) for reduction or deposition, $E - E_i$

t - time elapsed after application of E_i

$t_2 > t_1$

$\delta_{M^{+m}}$ - diffusional layer thickness for M^{+m}

B) for oxidation or stripping, $E - E_f$

t' - time elapsed since application of E_f following the establishment of the corresponding profiles at E_i

$t_2' > t_1'$

δ_{t_p} - diffusional layer thickness at time t_p

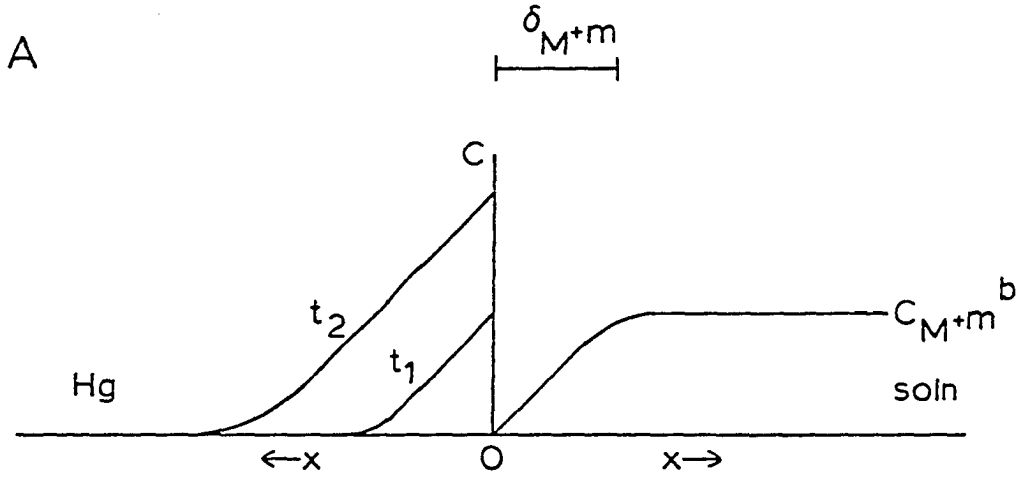
A
$\delta_{M^{+}m}$
C
t_2
t_1
$C_{M^{+}m}{}^{b}$
Hg
soln
←x
O
x→

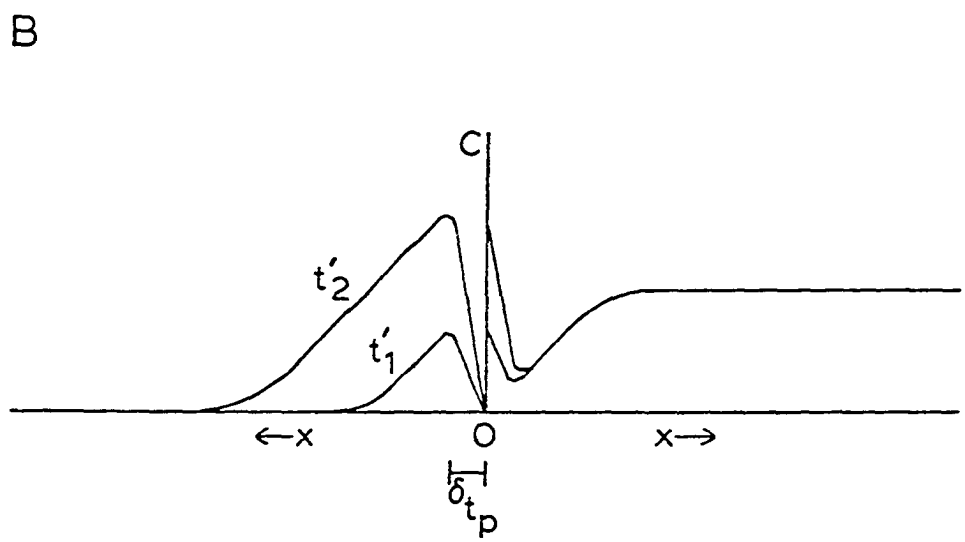
B
C
t'_2
t'_1
←x
O
x→
δ_{t_p}

A larger fraction of the deposited metal is oxidized before the current measurement for a metal of limited solubility as compared to a metal which is soluble in Hg. The result is a current measurement for RPA which is lower for a metal with a relatively low solubility in Hg.

Figure III-6 shows the concentration profiles for the reaction of $M^{+m} + ne = M^{+m-n}$; here, $m > n$. Again, for short time periods ($t < t_2$, shown by t_1), the flux of M^{+m} is controlled only by diffusion. The thickness of the diffusion layer is determined by the flow rate of the fluid stream and is rapidly established ($t = t_2$). The large flux of M^{+m} to the electrode surface yields a large flux of M^{+m-n} from the electrode surface to the boundary of the diffusion layer. Therefore, a significant amount of M^{+m-n} generated by the reduction during this period can be swept away from the diffusion layer by the fluid stream. In effect, there is no accumulation of M^{+m-n} in the diffusion layer at a concentration greater than the bulk concentration of M^{+m}; hence, no resulting enhancement in the analytical signal. The concentration of M^{+m-n} at the electrode surface, $C_{M^{+m-n}}^{o}$, is predicted to be equal to the bulk concentration of M^{+m}, $C_{M^{+m}}^{b}$. The analytical signal should therefore correspond directly to $C_{M^{+m}}^{b}$.

C. Experimental

1. Instrumentation

Polarograms were obtained with a Model 303 Static Mercury Drop Electrode (SMDE) from EG&G Princeton Applied Research, Princeton, NJ. Amperometric detection for FIA was achieved with a Model 310

Figure III-6. Concentration profiles for the study of $M^{+m} + ne \rightleftharpoons M^{+m-n}$ by RPA

C - concentration

X - distance

A) for reduction, $E - E_i$

t - time elapsed after application of E_i

$t_2 > t_1$

$\delta_{M^{+m}}$ - diffusional layer thickness for M^{+m}

B) for oxidation, $E - E_f$

t' - time elapsed since application of E_f following the establishment of the corresponding profiles at E_i

$t_2' > t_1'$

δ_{t_p} - diffusional layer thickness at time t_p

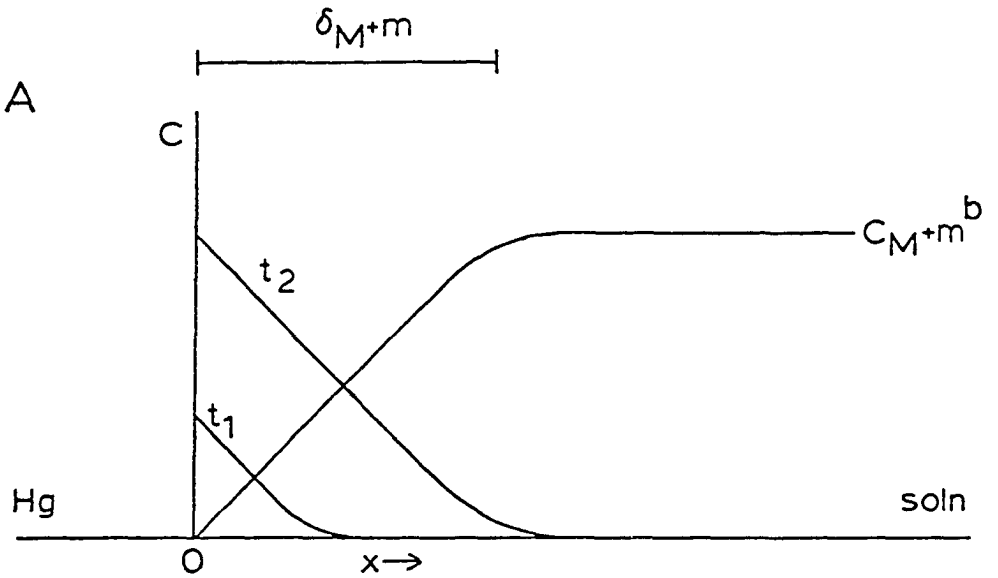
A
δ_{M+m}
C
C_{M+m}^{b}
t_2
t_1
Hg
soln
0
x→

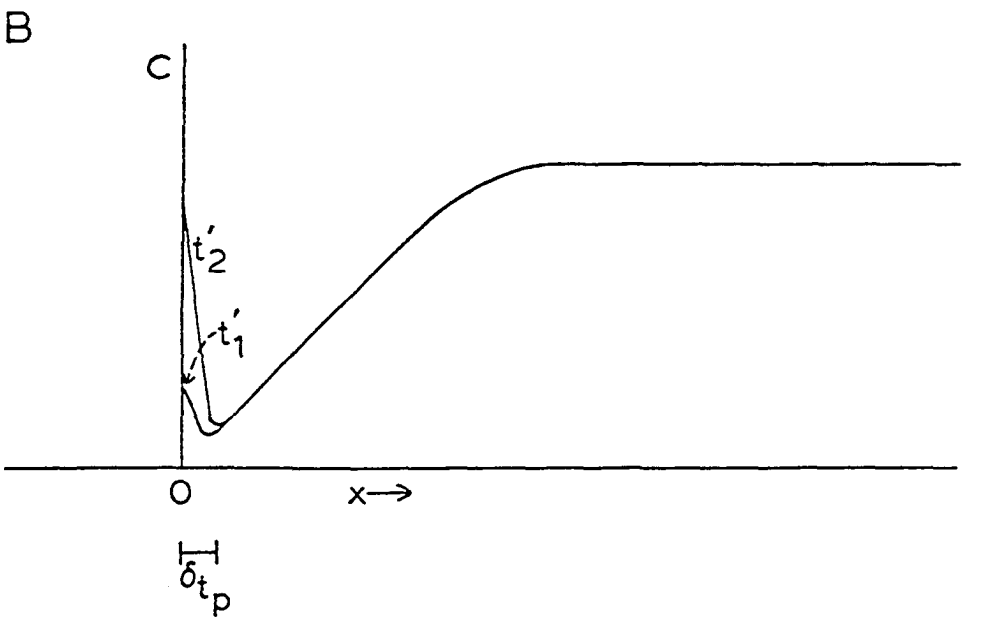
B
C
t'_2
t'_1
0
x→
δ_{t_p}

Polarographic LC Detector from EG&G Princeton Applied Research. The "small" size for the Hg drop was selected for all work. The glass capillary was cleaned and siliconized as described later.

A diagram for the Model 303 SMDE is shown in Figure III-7. The Hg for the electrode flows from the reservoir (A), shown at the top of the diagram, through a hollow, stainless-steel cylinder (the valve body, C) and finally to the capillary (M) firmly secured at the bottom of the cylinder. The Hg is allowed to flow when the valve stem (D) is raised; this occurs only for a short time period when the solenoid (B) is activated. For a small Hg drop, the solenoid effectively "raises" the valve stem for 50 msec and then "drops" the valve stem on top of the head of the capillary to stop the flow of Hg. The result is a small Hg drop that hangs at the tip of the siliconized capillary in the solution; the size of this drop does not change once the drop is completely dispensed. A drop of larger size can be delivered, but with poorer reproducibility. The small drop size is recommended for most applications; the area of the small drop is 0.96 cm^2 (113).

The Model 303 SMDE can be used in either the HMDE or the DME mode. The Model 303 SMDE used in the HMDE mode will be referred to simply as the HMDE. The Model 303 SMDE used in the DME mode will be referred to as the SDME, i.e., the "static" dropping mercury electrode. In the operation of the Model 303 SMDE as a HMDE, a single Hg drop is dispensed and used for all analytical work. The drop can be replaced at the discretion of the analyst by use of an external switch which activates the mechanical "drop-knocker" to dislodge the present drop. A new drop

Figure III-7. Cross-sectional diagram of Model 303 Static Mercury Drop Electrode

A - Hg reservoir

B - solenoid

C - valve body

D - valve stem (plunger)

E - guide bushing

F - compression spring

G - polyurethane tip

H - capillary seal

I - ferrule (bonded to capillary)

J - valve seat

K - ferrule support

L - capillary nut

M - capillary

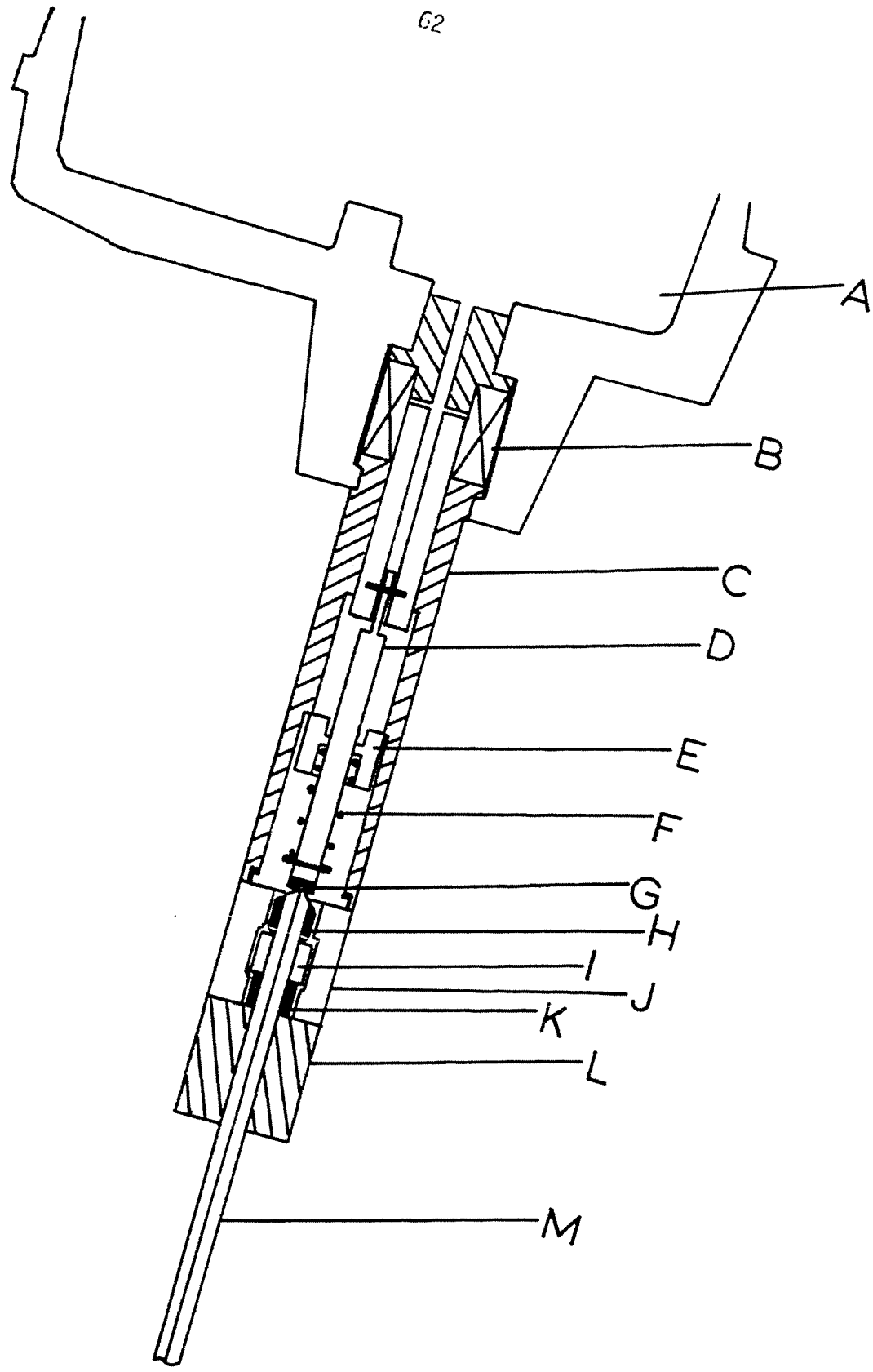
A
B
C
D
E
F
G
H
I
J
K
L
M

is then dispensed by activating a push-button switch for that purpose. In the operation of the Model 303 SMDE as a SDME, Hg drops are repeatedly dispensed, held and dislodged in a cyclic manner to mechanically approximate the function of a conventional DME.

At this point, an explanation is necessary to differentiate between the conventional DME and the SDME. For the conventional DME, Hg flows continuously through the capillary because of gravitational pull. The result is the formation of Hg drops with typical drop lifetimes of 2-6 sec. The area of each Hg drop increases with time. Therefore, when the current is measured, the electrode area is changing. The changing electrode area during the current measurement results in a contribution of a capacitive or charging component to the current which interferes at low concentration of analyte. The SDME has the advantage of the periodic delivery of Hg drops which have a reproducible and constant area, and the measurement of current is made at an electrode of constant area. Hence, current measurements can be made with the SDME for detection at lower concentration of analyte than the conventional DME.

The cell obtained from EG&G Princeton Applied Research for use with the Model 303 SMDE contains a Ag/AgCl reference electrode (SSCE) and a Pt-wire counter electrode in addition to the Hg indicating electrode. All values of electrode potential were made versus the SSCE which had a saturated solution of AgCl and KCl as the filling solution. The value for E_{SSCE} is -0.024 V versus the SCE at 25°C.

The Model 310 Polarographic LC Detector is an extended application of the Model 303 SMDE. The polarographic detector uses an assembly illustrated in Figure III-8 to connect the outlet of a chromatographic column to the tip of the capillary. This assembly is compatible for use with HPLC because of the very low dead volume introduced between the flow adapter (F) and the Hg drop (E). The effective dead volume is very low because the effluent flows continuously over the surface of the drop to prevent the waste analyte in the cell from contacting the Hg surface. The assembly stands in an open polarographic cell with an SSCE and a Pt wire counter electrode. The cell is constructed so as to allow the excess chromatographic effluent in the cell to flow into a waste container. The HMDE or SDME can be used as indicating electrodes for the polarographic detector.

Potential control and current measurement were made with a Model 174A Polarographic Analyzer from EG&G Princeton Applied Research. The instrument was operated in the PULSE mode. The potential limits for RPA were set by selecting the appropriate negative value of E_i, scanning with ΔE in the positive direction to give the desired value of E_f and setting the scan function on HOLD. All polarograms were recorded on a Model 7035 X-Y recorder from Hewlett-Packard Co., Pasadena, CA. Detection peaks for FIA were recorded on a stripchart recorder, Model SR-204, from Heath-Schlumberger Instruments, Benton Harbor, MI.

A diagram of the flow-analyzer is the same as that for the ion-exchange chromatograph given in Figure III-9, but with the ion-exchange column removed. All tubing, tube-end fittings and valves were Cheminert

Figure III-8. LC adapter assembly for the Model 310 Polarographic LC Detector

A - capillary

B - plug

C - O-rings

D - adapter body

E - Hg drop

F - flow adapter

G - gripper fitting

H - tube-end fitting

I - inlet tubing

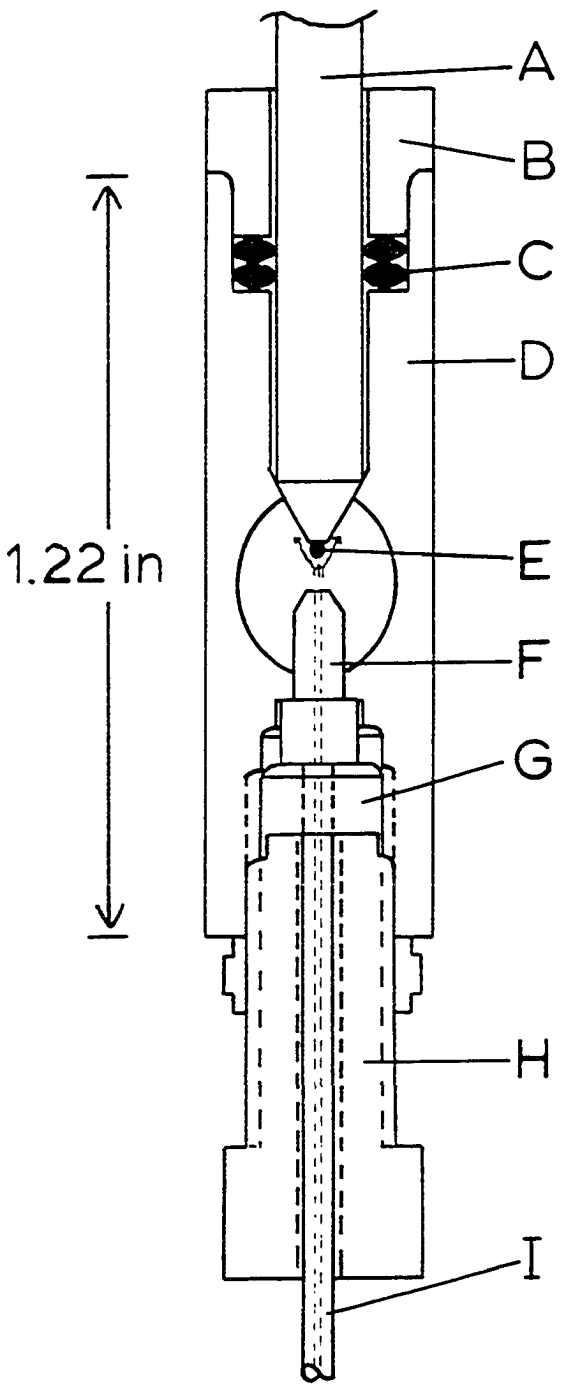
A
B
C
D
1.22 in
E
F
G
H
I

Figure III-9. Ion-exchange chromatograph

A1-A5 - eluent reservoirs

B - valve for selection of eluent

C - peristaltic pump

D - inverted T-tube

E - adjustable needle valve

F - sample injection valve

G - sample loop

H - syringe

I - sample

J - ion-exchange column

K - polarographic detector

L - pulse polarographic analyzer

M - stripchart recorder

N - bottle for collection of waste

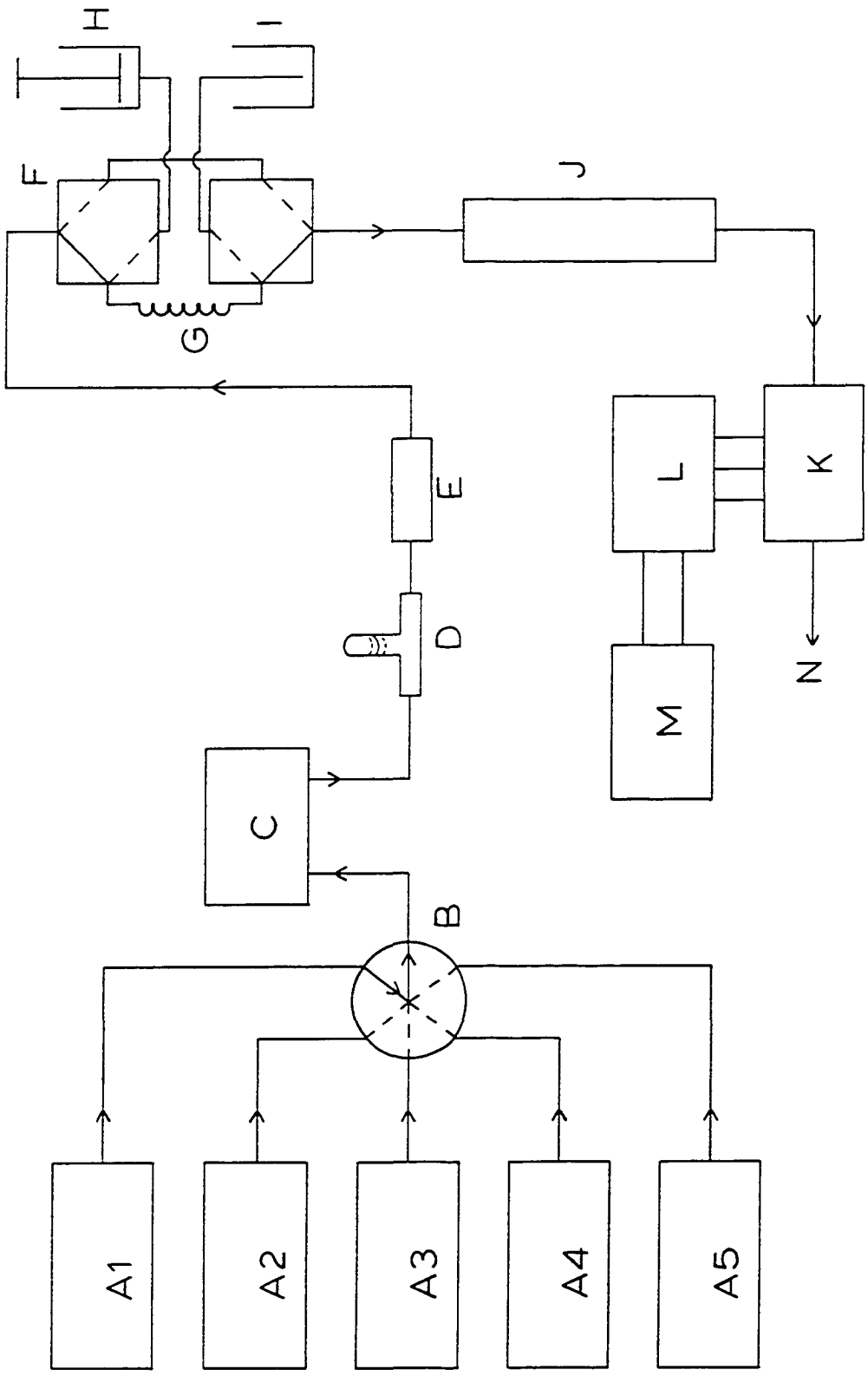
H
I
F
J
G
E
L
K
D
N
M
C
B
A1
A2
A3
A4
A5

from Laboratory Data Control, Riviera Beach, FL. Tubing (0.787-mm i.d.) was of Teflon, tube-end fittings were polypropylene and valves were from Kel-F. The sample loop of the sample injection valve had a volume of 0.206 mL. The sample loop was calibrated according to a method described by Morris (114). Pumping of the fluid stream was provided by a calibrated Gilson HP Minipuls-2 Peristaltic Pump, Gilson Medical Electronics, Inc., Middletown, WI. The peristaltic pump had a useful range of flow rate of 0.2 - 1.3 mL min^{-1} for a 0.76-mm i.d., vinyl manifold. The pulse dampener was an inverted T-tube containing a bubble of air ($\sim$0.5 mL) in series with an adjustable needle valve, for generating back pressure, which was constructed from Kel-F in the Chemistry Mechanical Shop at Iowa State University.

2. Chemicals

All chemicals were Analytical Reagent Grade from Mallinkrodt Chemical Works, St. Louis, MO, except where noted. Mercury was triply distilled by Chemistry Stores at Iowa State University. Water was demineralized prior to use after a single distillation. The glass capillary of the polarographic detector was siliconized with a 5% solution of dichlorodimethylsilane (99% purity) from Aldrich Chemical Co., Inc., Milwaukee, WI, prepared in carbon tetrachloride (Certified ACS) from Fisher Scientific Co., Fair Lawn, NJ.

3. Procedures

This worker found the siliconization of the glass capillary to be a critical step in the successful functioning of the Model 303 SMDE.

With a glass capillary which has been properly siliconized, the Model 303 SMDE performed well for longer than four months before it was necessary to re-siliconize the capillary. Mercury drops which fail to hang from the capillary tip and poor reproducibility for Hg drops of small size are tell-tale signs of the failure of the hydrophobic layer of silane at the tip and bore of the capillary.

The glass capillary was cleaned (115) by aspiration of 3 M HNO_3 for 5 min, followed by aspiration with water for 10 min. Air was briefly aspirated into the capillary. The capillary was placed in an oven at 70 °C for 1 hr, and allowed to cool in a desiccator. The tip of the capillary was submerged into a freshly prepared solution of 5% dichlorodimethylsilane for 5 min; this caused the siliconizing solution to be drawn about halfway up the bore of the tube by capillary action. Finally, air was again aspirated into the capillary for 10 min and the capillary was ready for use. When not in use, the tip of the capillary was submerged in water without detachment from the detector.

D. Results and Discussion

1. Agreement between theory and experiment for RPP

The result of the approximate mathematical description for RPP is given by Equation III-9. In order to test this equation experimentally, reverse pulse polarograms were obtained for Pb(II) in an unstirred solution as a function of the lifetime of the Hg drop, τ. These polarograms are shown in Figure III-10. The drop lifetime is related to the deposition time, t_i, according to $\tau = T = t_i + t_p$. The parameter,

Figure III-10. Reverse pulse polarograms for Pb(II) as a function of pulse period

electrode - SDME

E_i - -1.20 V versus SSCE

$\emptyset$ - 5 mV sec^{-1}

[Pb(II)] - 10^{-4} M

medium - 0.01 M HNO_3

Curves: A - T = 0.5 sec

B - T = 1 sec

C - T = 2 sec

D - T = 5 sec

E - residual, T = 2 sec

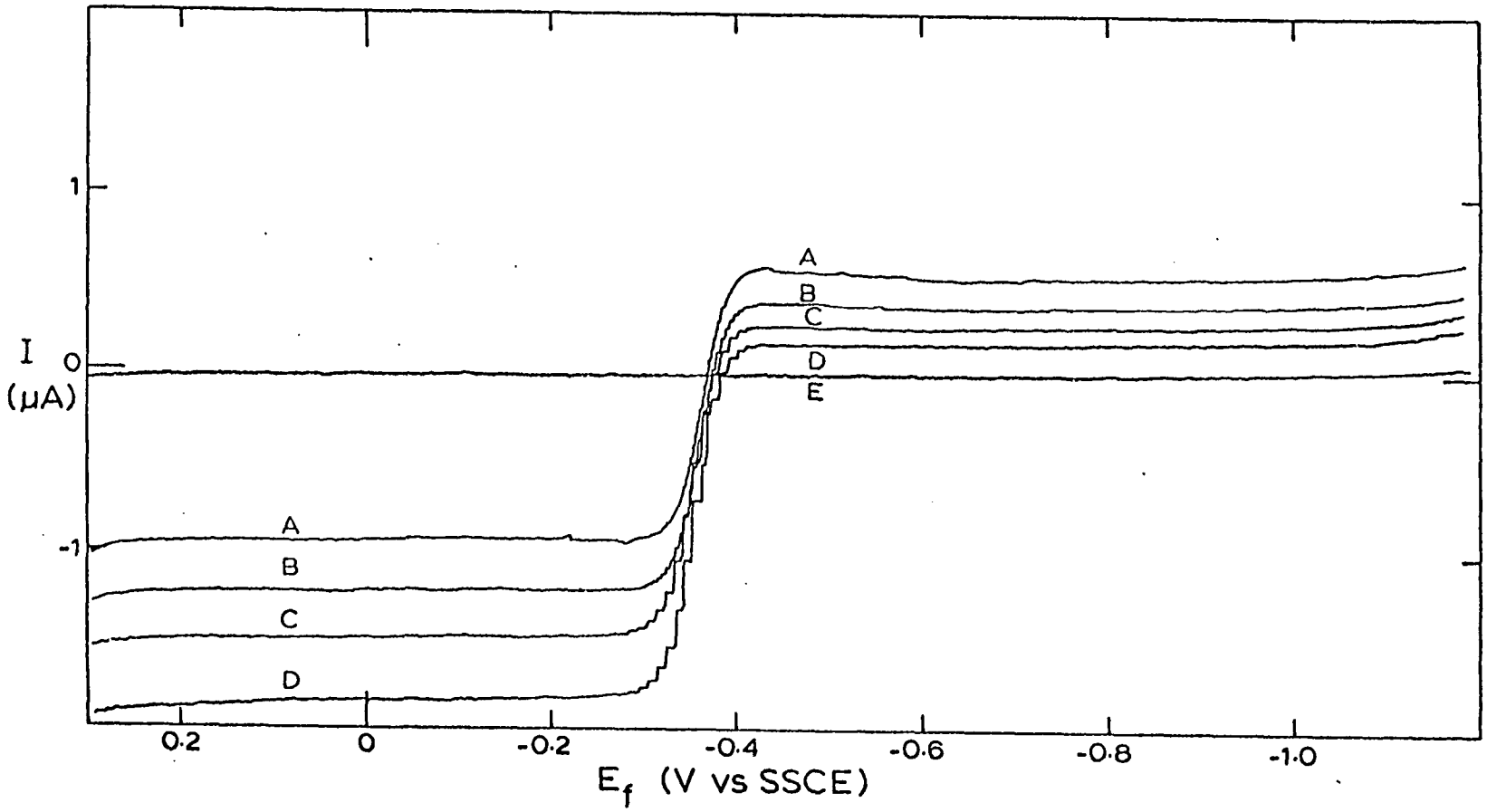
1
I 0
(μA)
-1
A
B
C
D
E
A
B
C
D
0·2
0
-0·2
-0·4
-0·6
-0·8
-1·0
E_f (V vs SSCE)

t_p, has a value of 57 msec and could not be varied with the instrument used in this research. The solution was quiescent and free of dissolved oxygen. The SDME was used. The height of the anodic wave at +0.10 V was taken as the value for $-I_{strip}$ and the height of the cathodic wave at -0.70 V was taken as the value for I_{dep}. The results are listed in Table III-1.

For T = 0.5 or 1 sec, the experimental results agree with Equation III-10 which corrects for a nonuniform distribution of M(Hg). In effect, the results illustrate that for small t_i, the current is measured after the $C_{M(Hg)}$ near the surface of the drop has decreased substantially below that corresponding to C_M+m in the bulk of solution. This is expected for short deposition periods since the diffusion layer of M(Hg) in the electrode produced by deposition is relatively thin (Table III-2), and is therefore significantly depleted before the measurement of the current. If a narrow pulse width, t_p, of 5 msec rather than 57 msec was available, to provide a current measurement soon after the application of the pulse, and used even with T = 1 sec, the result expected should agree with Equation III-9. The data for drop lifetimes greater than 2 sec show that it is no longer necessary to correct for nonuniform behaviour; for practical purposes of RPP, the M(Hg) is evenly distributed in the diffusional layer thickness in the electrode which is defined by t_p.

The relationship between the thickness of the diffusion layer for deposition and the radius of the electrode is an important concept in discussing the distribution of the M(Hg) in the Hg drop. The thickness

Table III-1. Agreement between theory and experiment for RPP and the reaction $M^{+m} + ne \rightleftharpoons M(Hg)$

T(sec)	t_i(sec)	$(t_i/t_p)^{1/2}$	$\left\lvert\left(\frac{t_i}{t_p}\right)^{1/2} - 1\right\rvert$	I_{dep}(nA)	$-I_{strip}$(nA)	$-I_{strip}/I_{dep}$
0.5	0.443	2.79	1.79	525	950	1.81
1.0	0.943	4.07	3.07	360	1230	3.42
2.0	1.943	5.84	4.84	250	1500	6.00
5.0	4.943	9.31	8.31	160	1860	11.63

of the diffusional layer for a stationary, spherical electrode in an unstirred solution is given by Equation III-33 (116).

$$\frac{1}{\delta_{Hg}} = \left[\frac{1}{(\pi\ D_{M(Hg)}\ t_i)^{1/2}} + \frac{1}{R}\right] \qquad \text{(III-33)}$$

All of the variables have been previously defined except for R, which is the electrode radius (cm). The radius of the electrode for the drop of small size delivered by the SDME is 2.8×10^{-2} cm. The thickness of the diffusion layer, $\delta_{M(Hg)}$, can be calculated as a function of t_i for the reduction of Pb(II) ($D_{Pb(Hg)} = 2 \times 10^{-5}$ cm^2 sec^{-1}) using the above equation. A comparison of $\delta_{Pb(Hg)}$ with the electrode radius for the given pulse periods is in Table III-2.

With the limitation of t_p = 57 msec, the data suggest that the thickness of the diffusion layer for the deposition process should be at least 30% of the value for the electrode radius in order to confidently make the assumption that the M(Hg) is uniformly distributed within the Hg drop. The data show that the metal is not concentrated in the electrode above the bulk concentration of metal ion in solution, because, for the drop lifetimes used, the thickness of the diffusion layer is substantially less than the radius of the electrode.

To summarize, the distribution of M(Hg) in a SDME has been studied for the technique of RPP which is performed with unstirred solutions. For the detection of Pb(II) under the constraint of t_p = 57 msec, the assumption of uniform behaviour is valid only for $T \geq 2$ sec. The

Table III-2. Comparison of $\delta_{Pb(Hg)}$ with the electrode radius, R_{Hg}

T (sec)	δ (cm x 10^3)	$\delta_{Pb(Hg)}/R_{Hg}$ [a]
0.5	4.7	0.17
1.0	6.2	0.22
2.0	7.9	0.30
5.0	11.0	0.39

[a] $R_{Hg} = 2.8 \times 10^{-2}$ cm.

Pb(Hg) is not concentrated in the Hg electrode above the bulk concentration of Pb(II) in solution for the values of T tested.

2. Discrimination against electrochemical interference from dissolved oxygen by RPA

The major advantage of RPA over amperometric detection at constant potential for detection of metal ions is the ability to discriminate against interference from dissolved oxygen. This illustrated in Figures III-11 and III-12 which contain polarograms obtained by NPP and RPP for Pb(II) in an unstirred solution in the presence and absence of dissolved oxygen.

Curve B of Figure III-11 shows the two polarographic waves characteristic of the reduction of dissolved oxygen. Figure III-11 also shows that only the cathodic wave for the electrodeposition of Pb(II) as Pb(Hg) is observed by NPP, and this wave superimposes those due to the presence of oxygen. The accurate measurement of the limiting faradaic current for low levels of Pb(II) can be made only after the removal of dissolved oxygen.

In Figure III-12, Curves C and D, RPP yields waves for both the cathodic deposition and the anodic dissolution of the Pb. Oxygen again interferes with the measurement of the cathodic wave for Pb(II), but the limiting current for the anodic wave can be measured without a background contribution from oxygen in the potential region +0.1 V - +0.3 V versus SSCE. Based on the information in Figure III-12, appropriate conditions for detection of Pb(II) by RPA would be

Figure III-11. Normal pulse polarograms

electrode - SDME

E_i - +0.30 V versus SSCE

T - 2 sec

Ø - 5 mV sec^{-1}

medium - 0.01 M H_2SO_4 / 0.05 M Na_2SO_4

Curves: A - air saturated, 10^{-4} M Pb(II)

B - air saturated

C - oxygen free, 10^{-4} M Pb(II)

D - oxygen free

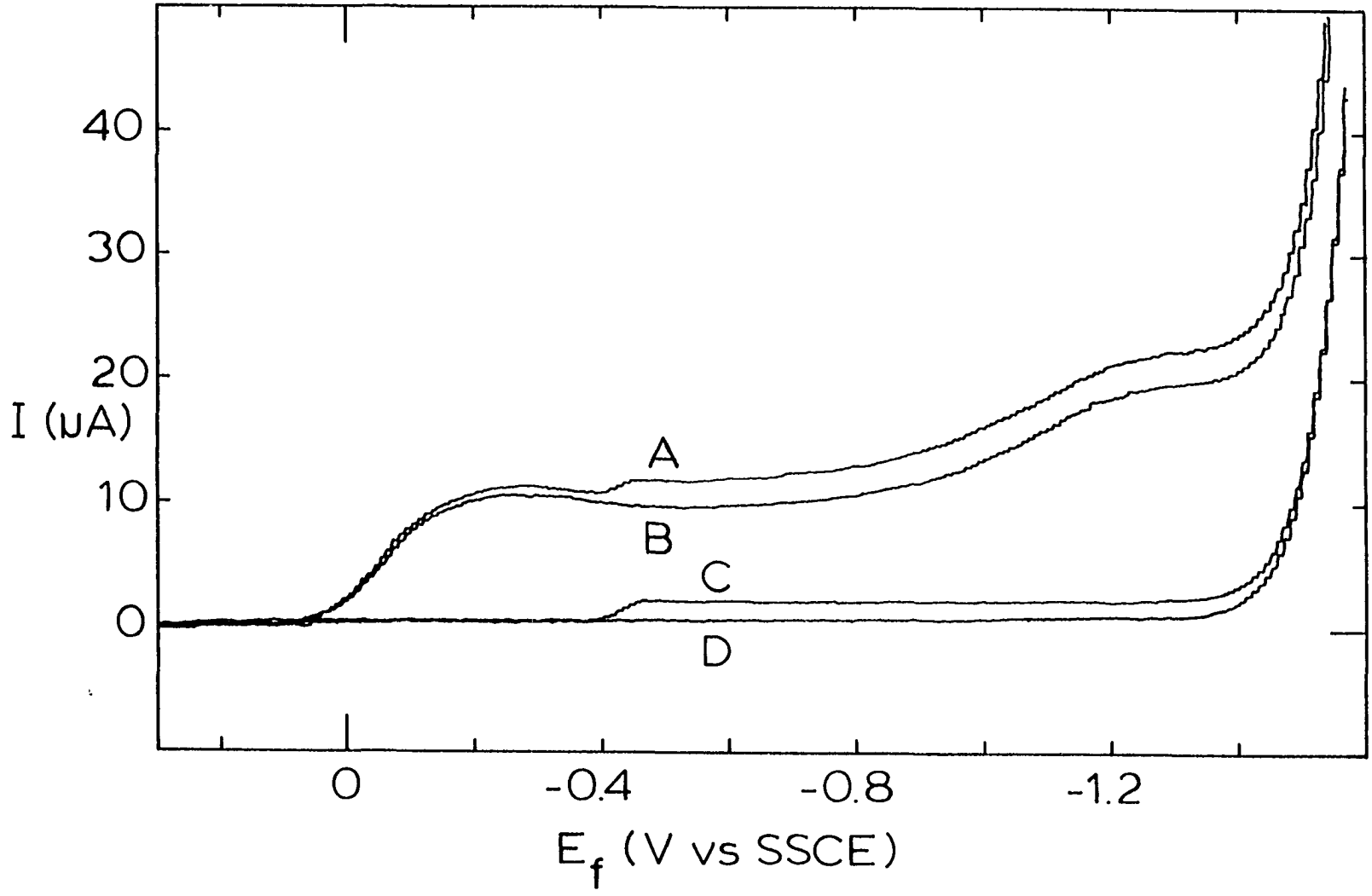
40
30
20
I (μA)
10
0
A
B
C
D
0
-0.4
-0.8
-1.2
E_f (V vs SSCE)

Figure III-12. Reverse pulse polarograms

electrode - SDME

E_i - -1.3 V versus SSCE

T - 2 sec

Ø - 5 mV sec^{-1}

medium - 0.01 M H_2SO_4/0.05 M Na_2SO_4

Curves: A - air saturated

B - oxygen free

C - air saturated, 10^{-4} M Pb(II)

D - oxygen free, 10^{-4} M Pb(II)

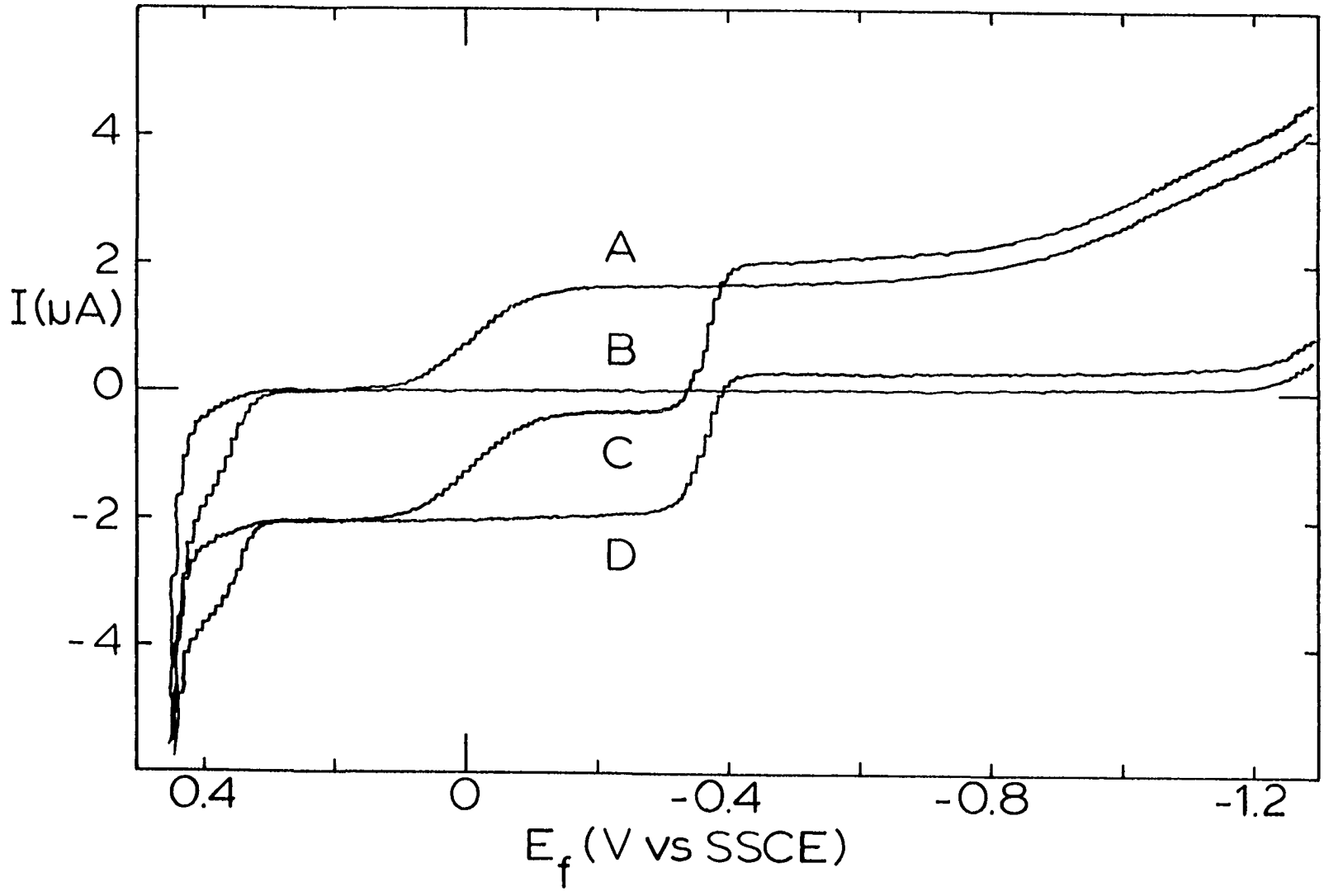
4
2
I(μA)
0
-2
-4
A
B
C
D
0.4
0
-0.4
-0.8
-1.2
E_f (V vs SSCE)

E_i = -0.5 - -1.3 V and E_f = +0.2 V. Increasing the negative value of E_i increases the number of electroactive species which can be detected simultaneously with Pb(II) by RPA. The anodic wave at +0.4 V results from Cl^- which is present in the polarographic cell by leakage of the filling solution in the SSCE.

Peaks are shown in Figure III-13 for the detection of Zn(II) by FIA without benefit of deaeration to further illustrate the advantage of RPA for eliminating interference by dissolved oxygen. The techniques of RPA and NPA are compared for the detection of Zn(II). NPA is related to NPP as RPA is related to RPP. That is, in NPA, an initial potential E_i is chosen where no cathodic reaction occurs. The final potential E_f is chosen in a region corresponding to the mass transport-limited reduction of the metal ion. The current is measured only during each cathodic pulse of potential. Curve A in Figure III-13 is the determination of 6.5 ppm Zn(II) by NPA; the sample and blank solutions contained the same concentration of supporting electrolyte as the fluid stream. Application of a large, constant offset potential in the Polarographic Analyzer was necessary to bring the signal on scale for NPA and the high uncertainty in the background current is attributed to fluctuation in the concentration of oxygen. The detection limit for NPA (signal: noise = 2) is estimated to be approximately 1 ppm Zn(II). The detection peak for Zn(II) by RPA is shown by Curve B in Figure III-13. The noise in the background current is much lower for RPA than for NPA and the detection limit is estimated to be a factor of 100X smaller.

Figure III-13. Comparison of response for NPA and RPA

FIA

T - 2 sec

RC - 0.3 sec

V_f - 1.0 mL min^{-1}

V_s - 0.206 mL

medium - 0.01 M H_2SO_4 / 0.05 M Na_2SO_4

labels - s = sample injection

b = blank injection

Curves: A - NPA; E_i = +0.20 V versus SSCE

E_f = -1.20 V versus SSCE

sample = 6.5 ppm Zn(II)

B - RPA; E_i = -1.20 V versus SSCE

E_f = +0.20 V versus SSCE

sample = 0.65 ppm Zn(II)

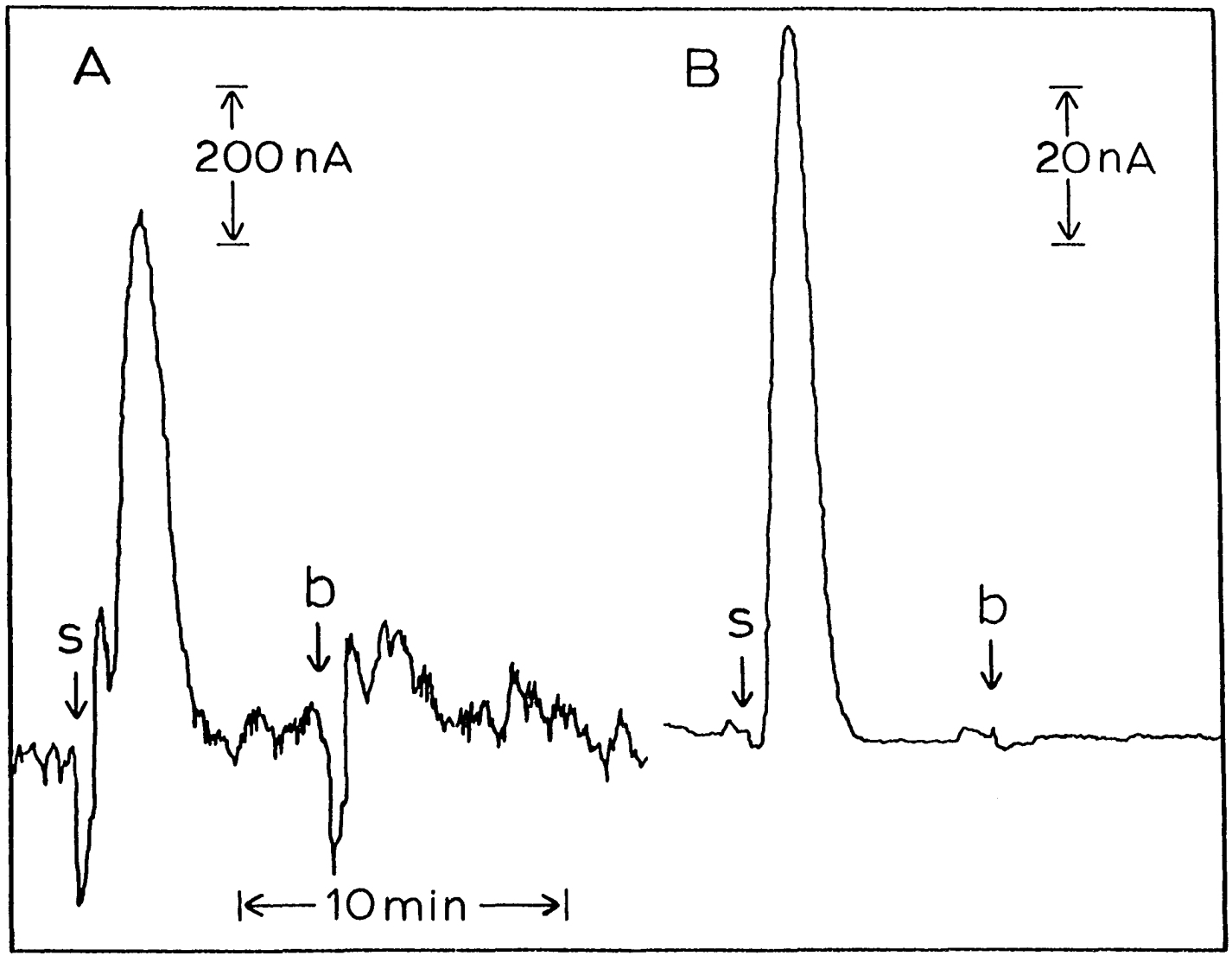
A
200 nA
s
b
10 min
B
20 nA
s
b

3. Evaluation of the interferences of dissolved oxygen and hydrogen peroxide

Indeed, there is no evidence that dissolved oxygen is a source of electrochemical or chemical interference in the detection of metal ions at a Hg electrode by RPA. Figure III-12, Curves C and D, show that the height of the anodic wave for the oxidation of Pb(Hg) is the same in air-saturated and O_2-free media when the value for E_i = -1.30 V versus SSCE. However, H_2O_2 is the product of the electrode reaction for oxygen at 0.0 V < E < -1.0 V and could possibly interfere with the detection of Pb(II) by chemical stripping of Pb(Hg) according to the reaction $2H^+ + H_2O_2 + Pb(Hg) \rightleftharpoons Pb(II) + 2H_2O$. Curve B in Figure III-14 presents the reverse pulse polarogram for Pb(II) in an unstirred, air-saturated solution with E_i = -0.60 V. The anodic plateau is equal in height to that observed for Pb(II) without dissolved oxygen present. Therefore, any H_2O_2 generated at E_i does not interfere chemically with the detection of Pb(II) at E_f.

As an additional test of the possible interference of H_2O_2, a polarogram was obtained by RPP for a deaerated solution of H_2O_2. This is given by Curve C in Figure III-14. Hydrogen peroxide did not introduce an electrochemical interference in the potential region which is positive of 0.0 V.

A reverse pulse polarogram was taken for a deaerated solution of Pb(II), to which H_2O_2 was added, to further study the possible chemical interference of H_2O_2. This polarogram is shown by Curve D of Figure III-14. Once again, there was no change in the height of the plateau

Figure III-14. Effect of H_2O_2 on response for Pb(II) by RPP

electrode - SDME

T - 2 sec

Ø - 5 mV sec^{-1}

medium - 0.01 M HNO_3

Curves: A - oxygen free, 10^{-4} M Pb(II), E_i = -1.20 V versus SSCE

B - air saturated, 10^{-4} M Pb(II), E_i = -0.60 V versus SSCE

C - oxygen free, 1 drop of 3% H_2O_2 added,
E_i = -0.80 V versus SSCE, no Pb(II) present

D - oxygen free, 10^{-4} M Pb(II), 1 drop of 3% H_2O_2 added,
E_i = -0.60 V versus SSCE

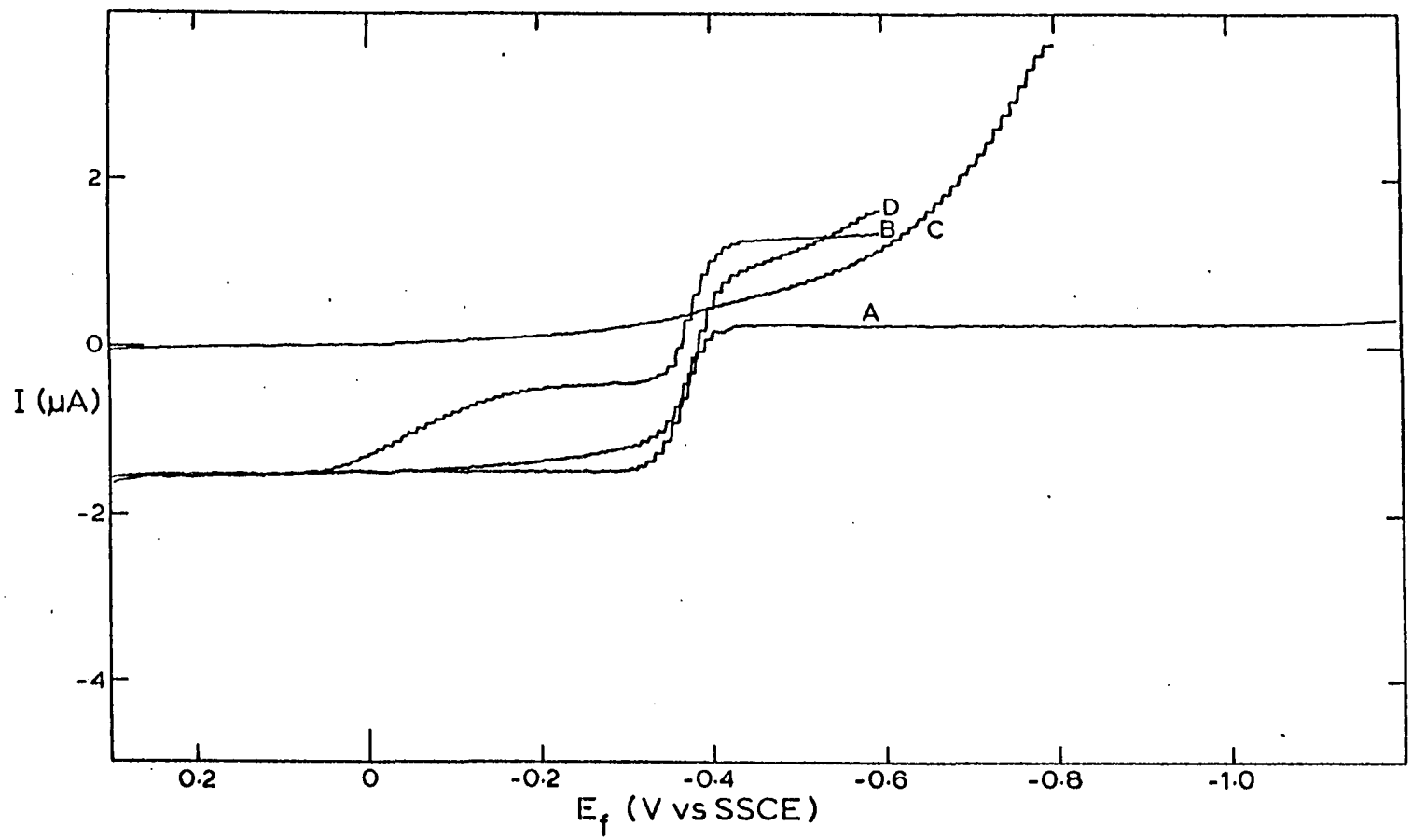
2
0
-2
-4
I (μA)
0.2
0
-0.2
-0.4
-0.6
-0.8
-1.0
E_f (V vs SSCE)
A
B
C
D

for the anodic current in the region +0.1 - +0.3 V. It was concluded that H_2O_2 does not serve as a chemical interference in the detection of Pb(II) by RPA.

4. Selectivity of RPA

A polarogram obtained by RPP is shown in Figure III-15 for a mixture of Zn(II), Pb(II) and Cu(II). The SDME was used and the solution was deaerated with nitrogen to simplify the interpretation of the polarograms. With values of E_i = -1.3 V and E_f = -1.3 V, i.e., ΔE = 0, the net current is cathodic resulting from the simultaneous electrodeposition of the three metals. With the completion of the scan, three anodic waves are observed at -1.0 V, -0.4 V and +0.05 V corresponding to Zn(II), Pb(II) and Cu(II), respectively. To assist in the interpretation of the polarogram, consider the reactions for E_f = -0.2 V. The net signal is the algebraic sum of the anodic currents for the dissolution of Zn(Hg) and Pb(Hg) and the cathodic current for the deposition of Cu(II). For E_f = +0.2 V, the signal is the result of anodic dissolution of the three metals. When attempting to increase the selectivity of RPA by judicious choice of parameters for the pulse waveform, there is little flexibility available in the choice of E_f if interference from dissolved oxygen is to be avoided. As illustrated by Figure III-15 for the mixture of Zn(II), Pb(II) and Cu(II), E_i can be chosen to be -0.2 V so that the anodic current at E_f = +0.2 V results only from detection of Cu(II). However, it is not possible under these circumstances to detect Zn(II) exclusive of Cu(II)

Figure III-15. Reverse pulse polarograms for a solution of Cu(II), Pb(II) and Zn(II)

electrode - SDME

E_i - -1.30 V versus SSCE

T - 2 sec

Ø - 5 mV sec^{-1}

medium - 0.01 M H_2SO_4 / 0.05 M Na_2SO_4

Curves: A - oxygen free

B - oxygen free and 10^{-4} M in Cu(II), Pb(II) and Zn(II)

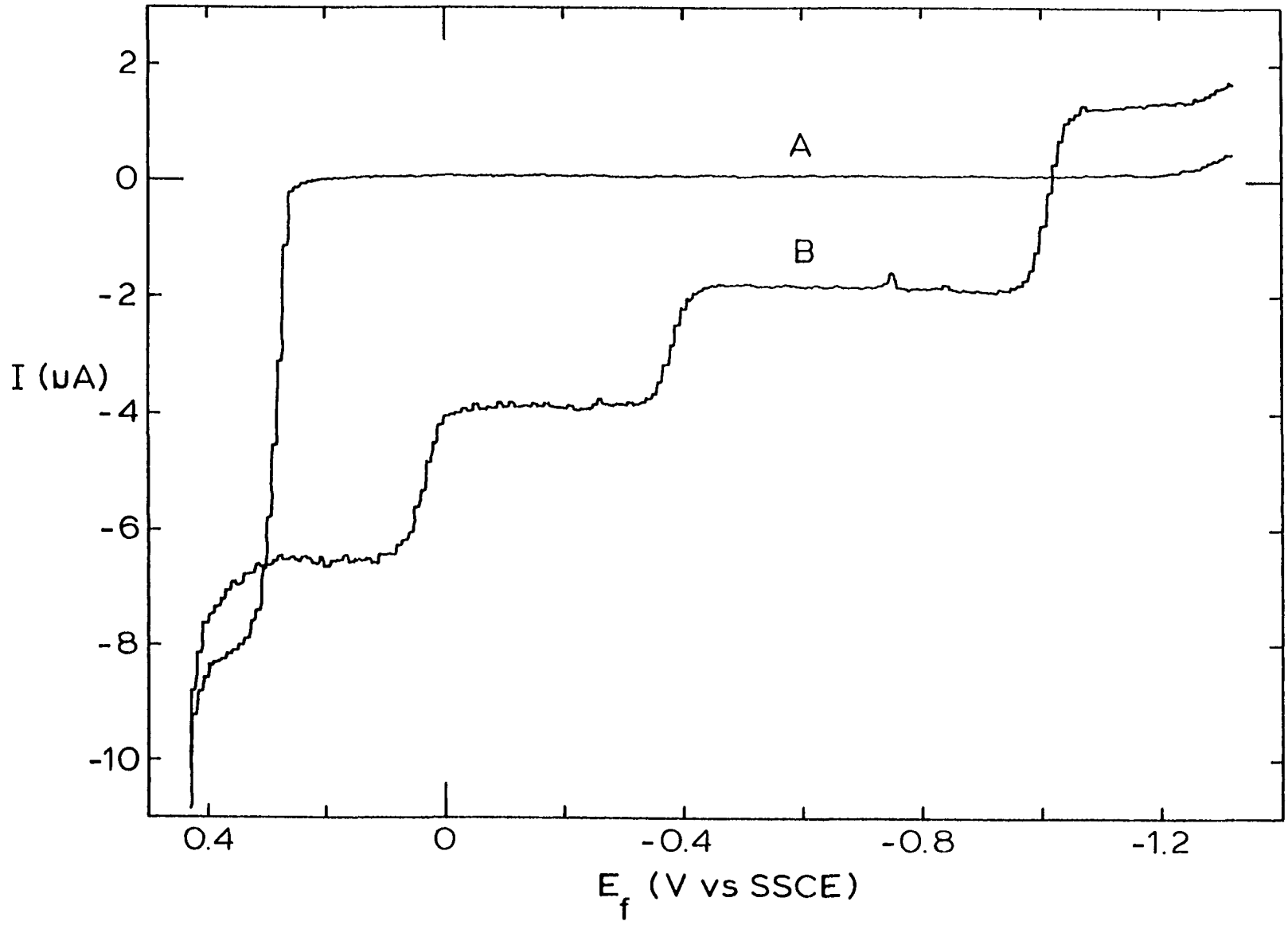
2
0
-2
-4
-6
-8
-10
I (μA)
A
B
0.4
0
-0.4
-0.8
-1.2
E_f (V vs SSCE)

and Pb(II) for E_f = +0.2 V. The choice of E_i = -1.3 V and E_f = -0.8 V for the detection of Zn(II) would be hampered by the large uncertainty in the background signal for oxygen.

5. Study of response of RPA for selected metal ions

Thus far, all of the experiments have illustrated the use of RPA for the detection of metal ions with reduction products that form metal-amalgams which are quite soluble in Hg. It was also of interest to test the ability of RPA to detect those metal ions with reduction products which are relatively insoluble in Hg as well as those metal ions with reduction products which are metal ions of a lower oxidation state which are soluble in solution.

Table III-3 lists the solubilities of metals which are commonly determined by polarographic methods. Metals of various solubilities were selected to be tested for detection by RPA. The metals chosen with a relatively high solubility in Hg were Tl, Cd, Zn, Pb and Cu; those chosen with poor solubility were Ni, Sb and Cr. The metal ions Fe(III), V(V) and Mo(VII) were also selected, because polarographic information was available which described the reduction of these metal ions to lower oxidation states (117). Reverse pulse polarograms were obtained for all of the metal ions selected and were used to determine the proper values of E_i and E_f for RPA. The supporting electrolyte used for the detection of each metal ions was that which resulted in the most favorable electrochemical behaviour for that metal ion.

Table III-3. Solubility of metals in mercury (34)

Metal	Temperature (°C)	Solubility (% w/w)	Solubility (M)
Cu	20	0.003	0.006
Ag	20	0.035	0.044
Au	20	0.131	0.0909
Zn	20	1.99	4.14
Cd	20	5.3	6.4
Al	20	0.002	0.010
Ga	22	1.13	2.20
In	20	57.0	67.5
Tl	20	42.8	28.5
Sn	20	0.6	0.69
Pb	20	1.1	0.72
Sb	20	2.9×10^{-5}	3.2×10^{-5}
Bi	20	1.1	0.72
Co	20	8×10^{-5}	1.8×10^{-4}
Ni	20	4.8×10^{-5}	1.11×10^{-4}
Cr	20	4×10^{-7} to 3.1×10^{-11}	1×10^{-6} to 8.1×10^{-11}

The peaks observed by RPA for the selected metal ions are shown in Figure III-16. The experiment involved an injection of a solution of each metal ion at a given concentration into a fluid stream containing the supporting electrolyte at the same concentration as that in the sample. Note that the concentration of metal ion was the same for all injections, but the current sensitivity was varied. For these metal ions, the range of the response by RPA is within an order of magnitude. Taking into account the relative number of electrons in each process, the sensitivity of RPA is good for metal ions which are soluble in solution in both oxidation states, better for metal ions with reduction products which have a low solubility in Hg and best for metal ions with reduction products which have a relatively high solubility in Hg. This experiment illustrates that the technique of RPA is applicable to the determination of a large number of metal ions, most of which are analytically important.

Some of the details observed in Figure III-16 deserve elaboration and comment. A peak for Cr(III) (A) failed to appear because the concentration of the supporting electrolyte in the fluid stream did not exactly match that in the sample. Nonetheless, the top of the peak can be discerned just following the shift in the baseline. The noise in the background current differs somewhat in the various media and is particularly high in the sulfate medium. This is explained by the formation of a slightly-dissociated compound of Hg(I,II) with sulfate in this region of potential, E_f = +0.10 V versus SSCE.

Figure III-16. Study of the detection of selected metal ions by RPA

electrode - SDME

T - 2 sec

RC - 0.3 sec

V_f - 1.0 mL min^{-1}

V_s - 0.206 mL

injections - 10^{-4} M M^{+m}

Peaks: A - Cr(III) in 0.05 M Na_2SO_4 ($50\ nA\ in^{-1}$)

B - Sb(III) in 0.5 M tartaric acid, pH 4.5 ($200\ nA\ in^{-1}$)

C - Fe(III) in 0.5 M tartaric acid, pH 6.00 ($50\ nA\ in^{-1}$)

D - VO_3^- in 0.1 M tartaric acid, pH 2.0 ($100\ nA\ in^{-1}$)

E - MoO_4^- in 0.1 M tartaric acid, pH 2.0 ($100\ nA\ in^{-1}$)

F - Pb(II) in 0.3 M tartaric acid/0.02 M NaCl, pH 3.30 ($500\ nA\ in^{-1}$)

G - Zn(II) in same medium as F ($500\ nA\ in^{-1}$)

H - Cu(II) in same medium as F ($500\ nA\ in^{-1}$)

I - Tl(I) in same medium as F ($500\ nA\ in^{-1}$)

J - Cd(II) in same medium as F ($500\ nA\ in^{-1}$)

K - Ni(II) in same medium as F ($100\ nA\ in^{-1}$)

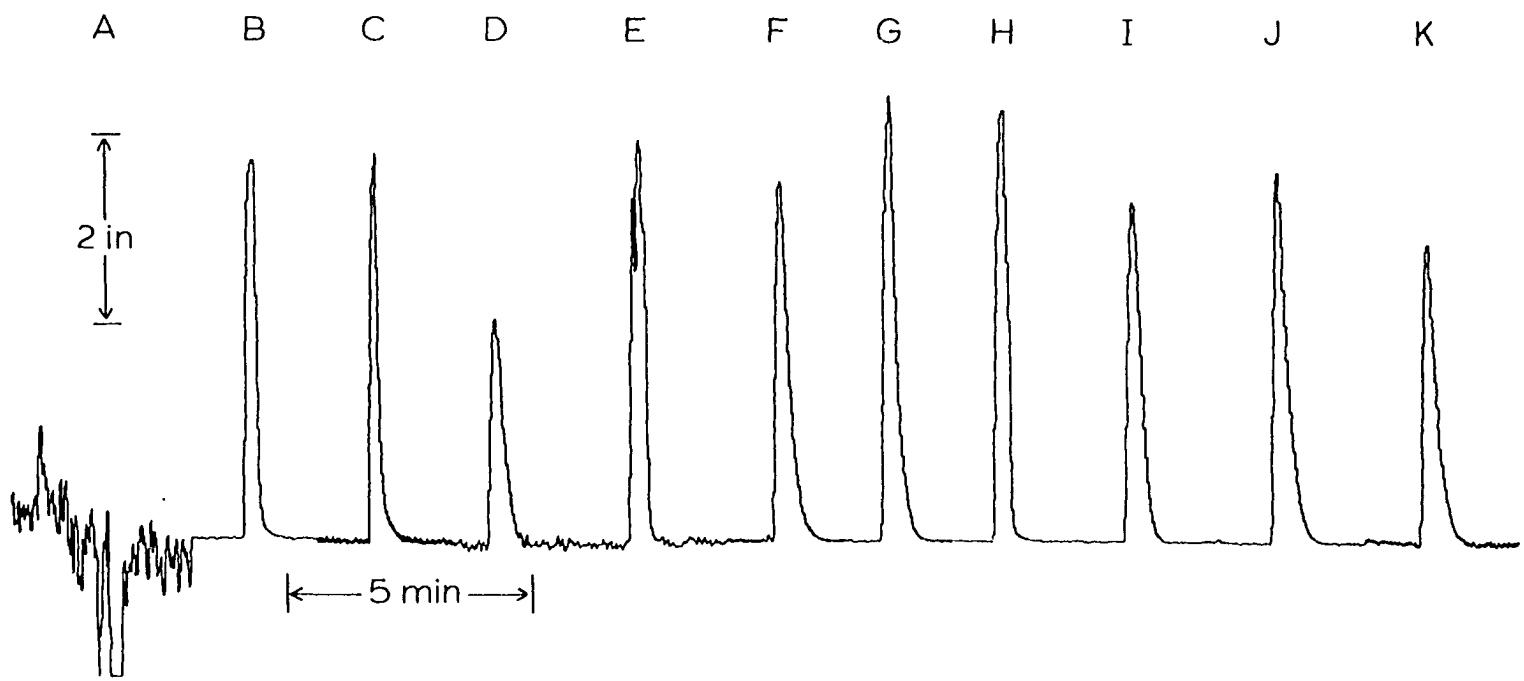
A
B
C
D
E
F
G
H
I
J
K
2 in
5 min

Another factor which influences the response of RPA for a given redox couple is the reversibility of the electrochemical reaction. Although all of the reverse pulse polarograms which were used to determine the potential values for the experiment shown in Figure III-16 are not given here, the reverse pulse polarogram for Ni(II) is shown for the purpose of this discussion.

When studied polarographically, an electrochemical reaction is said to be irreversible if the $E_{1/2}$ for the polarographic wave is significantly different from the standard reduction potential, E^o, for the redox couple. The reverse pulse polarogram obtained for Ni(II) is shown in Figure III-17. The E^o value for the half-reaction of Ni(II)/Ni(0) is -0.47 V versus SSCE (118). Thus, the reaction of Ni(II) is irreversible in this supporting electrolyte. In spite of this irreversibility, Ni(II) can be determined by RPA because values for E_i and E_f can be chosen in a region of potential where the current is directly proportional to concentration and in a region where there is no interference from dissolved oxygen.

6. Expected interferences in RPA

Interference is expected from the presence of any species which is directly electroactive at E_f; or which produces an anodic wave at E_f by forming a slightly dissociated compound with Hg(I,II), e.g., halides, OH^-, CN^-, S^{-2}, EDTA, etc. This information must be considered when selecting the supporting electrolyte for the fluid stream. For instance, the application of RPA with a Hg electrode as a detection

Figure III-17. Reverse pulse polarogram for Ni(II)

electrode - SDME

E_i - -1.30 V versus SSCE

T - 2 sec

Ø - 5 mV sec^{-1}

medium - 0.3 M tartaric acid / 0.04 M NaCl, pH 3.30

Curves: A - oxygen free

B - oxygen free, 10^{-3} M Ni(II)

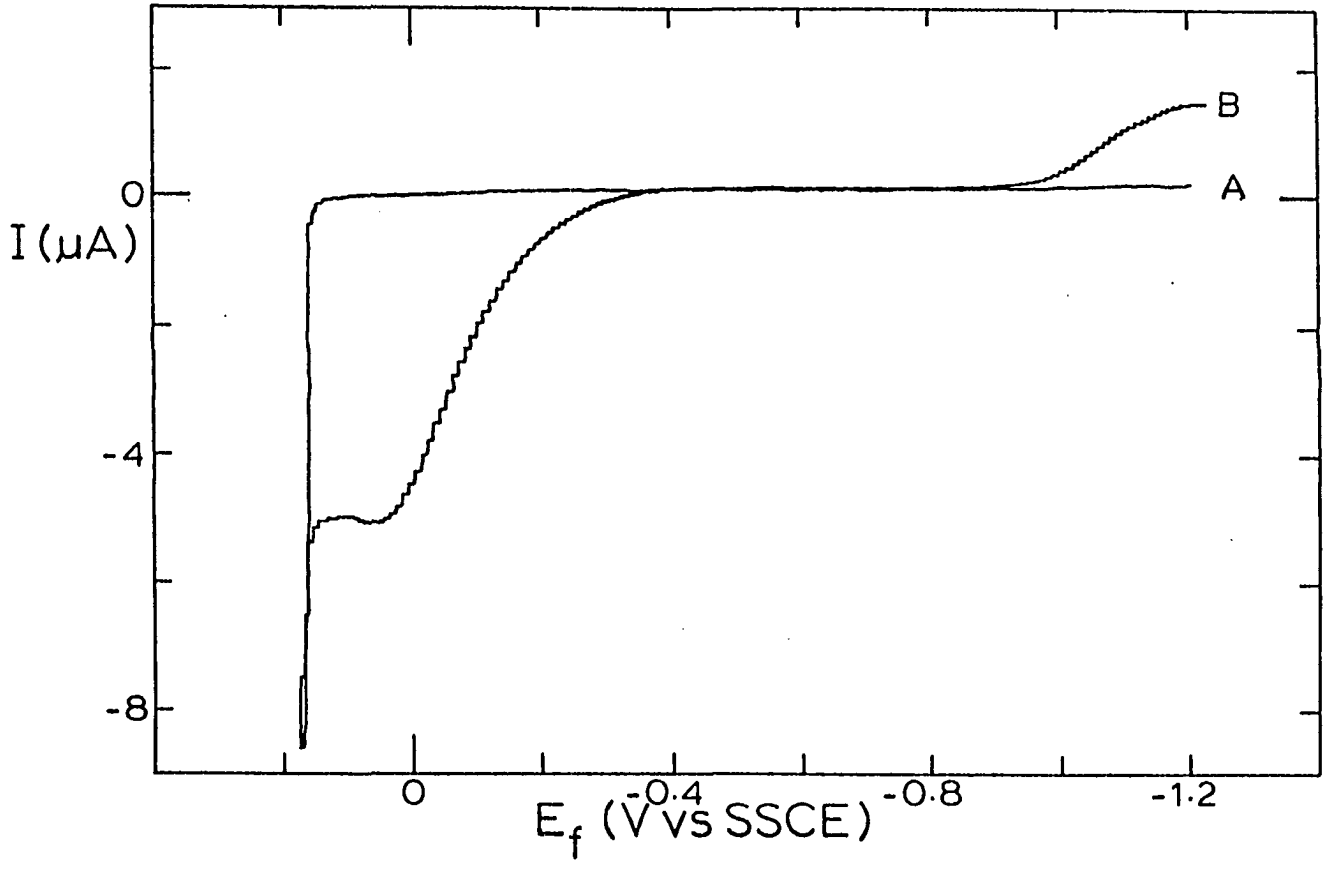
B
A
0
I (μA)
-4
-8
0
-0.4
-0.8
-1.2
E_f (V vs SSCE)

system for ion-exchange LC precludes the use of eluents which contain halides at high ionic strength.

IV. EVALUATION OF THE THIN-FILM MERCURY ELECTRODE, HANGING MERCURY-DROP ELECTRODE AND STATIC DROPPING MERCURY ELECTRODE AS INDICATING ELECTRODES FOR REVERSE PULSE AMPEROMETRY

A. Introduction

Mercury was chosen as the material for the indicating electrode in the EC detector for the detection of metal ions in a flow-analyzer. Indicating electrodes of Hg for electroanalysis can have several different geometries, e.g., pool, drop and film. Of these three geometries, the Hg-pool electrode has the largest volume relative to the surface area exposed to the solution. A stationary indicating electrode of large volume for use in RPA is undesirable because excessive diffusion of the metal into the Hg during the deposition process will result in a current response with excessive tailing. Consequently, the Hg-pool is not a suitable indicating electrode for RPA. Those Hg electrodes which are commonly applied in ASV were considered to provide the greatest promise in the application of RPA, and so the HMDE and the TFME were chosen. The SDME was also selected since it has a volume which is equal to the HMDE but with the added advantage of a renewable electrode surface.

The objective of the work described in this section was the investigation of the response of the Hg indicating electrodes for RPA in terms of those analytical parameters which have the most significance in the application of EC detectors to chemical analysis. The TFME, HMDE

and SDME were explored as indicating electrodes for RPA. The criteria used to evaluate the response of these electrodes were peak definition, dependence on pulse period, dependence on flow rate, precision, linear dynamic range, detection limit and compatibility for use with cation-exchange liquid chromatography. The results of this investigation were used as the basis for choosing the electrode to be applied in the analysis of a "real" sample.

B. Experimental

1. Instrumentation

The instrumentation used for this work was the same as that described in Section III.C.1 with the exception of the TFME and the flow-analyzer used with the TFME. The TFME and modified flow-analyzer are described here.

A cross-sectional diagram of the detector with the TFME is shown in Figure IV-1. The detector was based on a design by T. R. Lindstrom and D. C. Johnson (119) and was constructed of upper and lower parts. The upper and lower parts were screwed together and the Teflon washers (D) above and below the glassy carbon tubular electrode (GCTE) (E) were intended to confine contact of the solution to the inner cylindrical surface of the tube. The fluid stream flowed up through the inlet at the base of the detector, through the GCTE which bore a film of Au plated with Hg, into a reservoir containing an SCE (A) and a Pt-wire counter electrode (B), and out through the exit port (C) by way of aspiration. The area of the GCTE was 0.10 cm^2 and the internal volume

Figure IV-1. Cross-sectional diagram of the EC detector with the TFME

A - saturated calomel electrode

B - Pt-wire, counter electrode

C - exit port

D - Teflon washers

E - glassy carbon tubular electrode (GCTE)

F - Pt wire contact to the GCTE

G - detector body

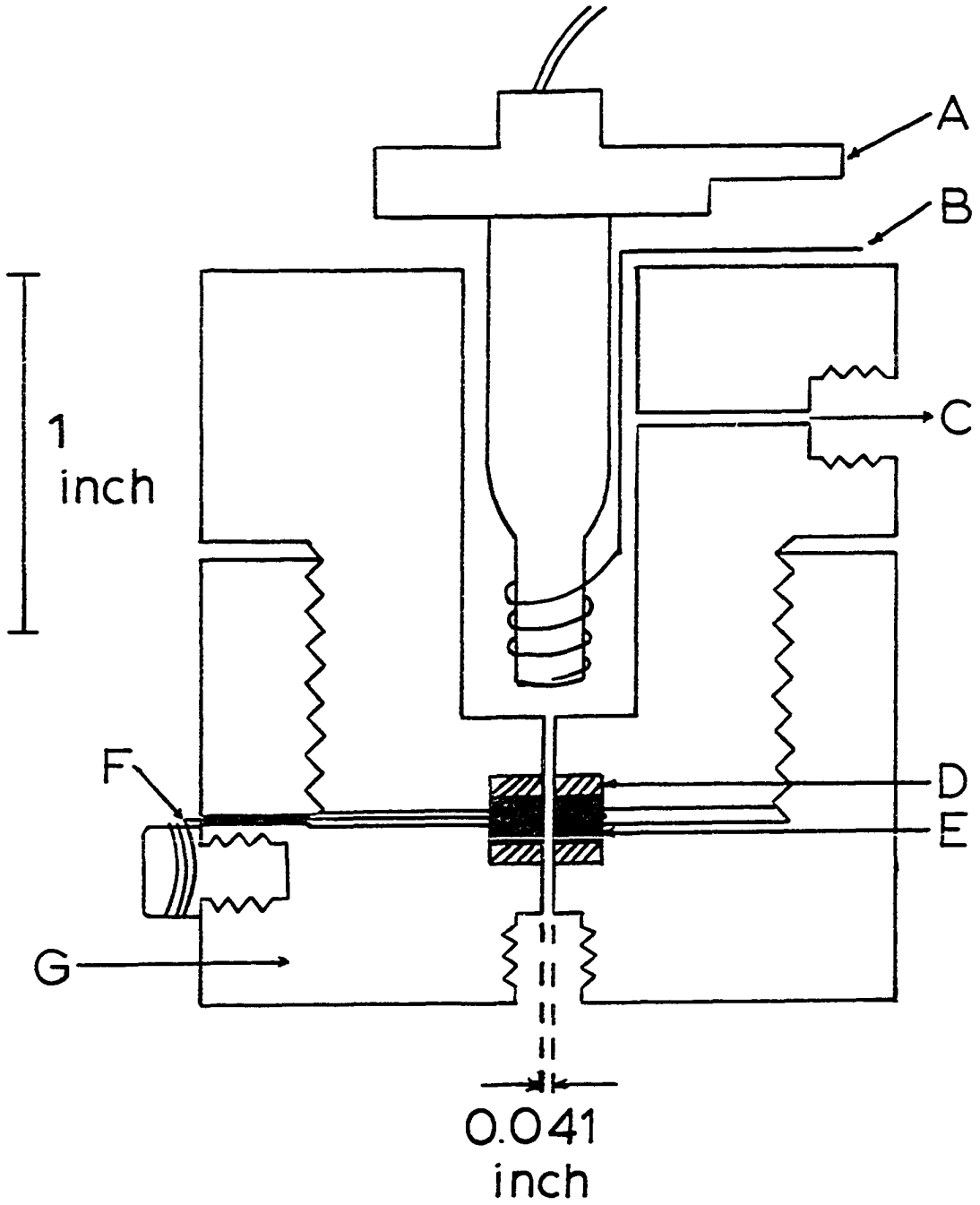
A
B
C
D
E
F
G
1
inch
0.041
inch

was 2.7 µL. The GCTE had a radius of 0.52 mm and a length of 3.17 mm. The SCE was a Model 39270 fiber-junction calomel electrode from Beckman Instruments, Inc., Fullerton, CA. The filling solution of the SCE was saturated NaCl. The body of the detector was constructed from glass-filled Teflon in the Chemistry Mechanical Shop at Iowa State University.

The flow-analyzer used with the TFME is illustrated in Figure IV-2. All of the components of this flow analyzer were the same as those shown in Figure III-9 except for the detector (L) and the by-pass system (J1, J2 and K). J1 and J2 were three-way valves also from Laboratory Data Control and K is the ion-exchange column. The by-pass system was used to easily switch the ion-exchange column into and out of the fluid stream. It was necessary to switch the ion-exchange column out of the fluid stream during the preparation and removal of the Hg-Au film on the GCTE.

The ion-exchange column (4-mm i.d. X 100 mm) was packed with low-capacity, surface-sulfonated, cation-exchange resin (45-53 µm) from Dionex Corp., Sunnyvale, CA. This column was virtually equivalent to the Dionex No. 030233 Cation-Separator Column and was used to separate Tl(I), Cd(II) and Pb(II) with an isocratic elution. Another column of the same dimensions was packed with AG 50W X-8 (37-44 µm) which is a full-capacity, cation-exchange resin from Bio-Rad Laboratories, Richmond, VA. The column packed with this resin was used to separate Cu(II), Zn(II), Pb(II) and Cd(II), also with an isocratic elution.

Figure IV-2. Flow-analyzer used with the TFME

A1-A5 - eluent reservoirs

B - valve for selection of eluent

C - peristaltic pump

D - inverted T-tube

E - adjustable needle valve

F - sample injection valve

G - sample loop

H - syringe

I - sample

J1, J2 - three-way valves

K - ion-exchange column

L - EC detector with TFME

M - pulse polarographic analyzer

N - stripchart recorder

O - bottle for collection of waste

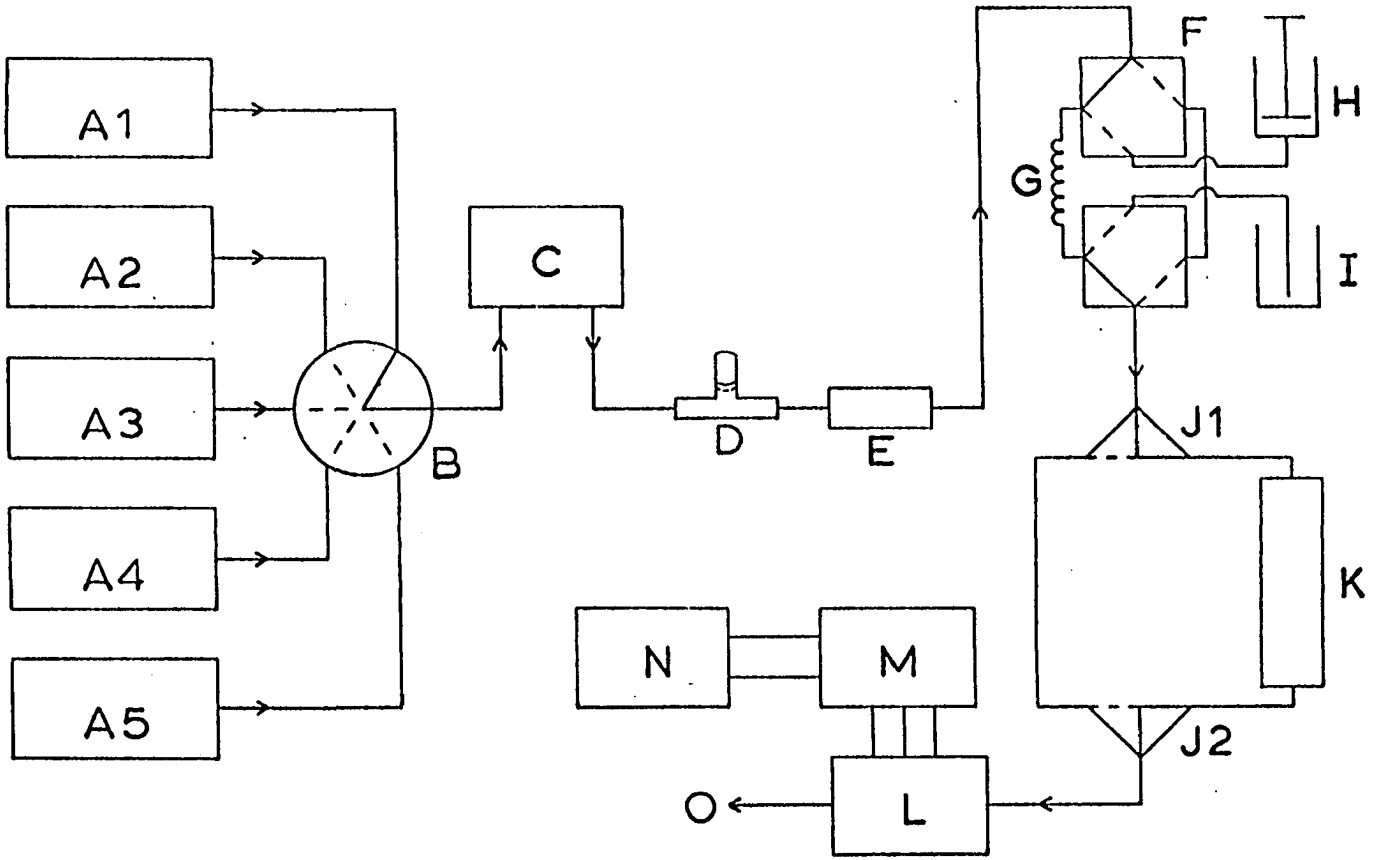
A1
A2
A3
A4
A5
B
C
D
E
F
G
H
I
J1
J2
K
L
M
N
O

2. Chemicals

All chemicals used were available as described in Section III.C.2 except for the gold chloride ($HAuCl_4 \cdot 3H_2O$) which was from Fisher Scientific Company, Fair Lawn, NJ.

3. Procedure

All peak areas were measured with a planimeter from Keufel and Esser Co., Germany.

A composite Hg-Au film on the GCTE served as the TFME for RPA. A Au film approximately 50 Å in thickness was electrochemically deposited on the surface of the glassy carbon. Next, a Hg film approximately 500 Å in thickness was electrodeposited on the Au-carbon surface. The procedure for preparation of the Hg-Au film is described below.

A solution of 0.5 M $HClO_4$ containing 0.01 M HCl was pumped through the GCTE at 1.0 mL min^{-1} for 5 min. Measurements of time were made with a stop watch. The GCTE was potentiostated at 0.0 V versus SCE (120). The current measured was assumed to be the background current for the electrodeposition of the Au. A solution of 2.4×10^{-5} M $HAuCl_4 \cdot 3H_2O$ in 0.5 M $HClO_4$/0.01 M HCl was pumped through the GCTE under identical conditions for electrodeposition of Au. The current measurement during the deposition of Au was corrected for the background and used to calculate the quantity of Au deposited The average thickness of the Au film was calculated by Equation IV-1.

$$\ell_{av} = \frac{I\ t\ W}{n\ F\ A\ \rho} \qquad \text{(IV-1)}$$

In Equation IV-1,

ℓ_{av} = average thickness of the metal film (cm);

I = average faradaic current for the deposition (A);

t = time of deposition (sec);

W = atomic weight of the metal (g g-atom^{-1});

and ρ = density of the metal (g cm^{-3}).

The other parameters have their usual significance. The average thickness of the Au film deposited for 5 min under these conditions was 50 Å.

Following the deposition of the Au film, a film of Hg was deposited. A solution of 0.1 M $HClO_4$ was used for the measurement of the background current at an applied potential of -0.2 V versus SCE. The Hg film was deposited from 1.0×10^{-3} M $Hg(NO_3)_2$ in 0.1 M $HClO_4$ for 5 min. The average thickness of the Hg film was calculated with Equation IV-1 and was approximately 500 Å.

The composite Hg-Au film was prepared at the beginning of each day and was removed at the end of the day. To remove the film, a solution of 0.5 M $HClO_4$/0.01 M HCl was pumped through the TFME at 1.0 mL min^{-1}; an electrode potential of 1.0 V versus SCE was used to anodically dissolve the film in about 10 min.

C. Results and Discussion

1. Dependence of peak shape on the Hg indicating electrode

The shape of the current peak observed by RPA is presented in Figure IV-3 for the TFME, HMDE and SDME. Peaks A, B and C show the

response to a solution of 10^{-5} M Pb(II) which was injected into the fluid stream and detected with the Hg electrodes for a pulse period T = 2 sec. Peak tailing, shown in Peaks A and B, was observed for the stationary Hg electrodes, but most remarkably for the HMDE under these conditions. This peak tailing was a result of the diffusion of the metal into the electrode during long pulse periods, i.e., long deposition times. Long pulse periods required a long time to allow the metal to diffuse back to the electrode surface during stripping. Since this diffusion of the deposited metal from the bulk of the Hg drop to the electrode surface occurred only during the anodic pulse, a large number of anodic pulses were necessary to strip all of the metal analyte from the stationary Hg electrode. The result was a peak with excessive tailing. Peak tailing was minimal in the detection of Pb(II) when using the TFME because the Hg film was very thin compared to the radius of the HMDE; and, also, the TFME had a much smaller electrode volume. Peak D in Figure IV-3 illustrates that minimal peak tailing was observed with the HMDE for a pulse period T = 0.5 sec.

Sharp, symmetrical peaks were observed by RPA with the SDME as shown by Peak C. The use of relatively long pulse periods did not cause excessive peak tailing, because each current measurement was made on a new Hg drop. The metal which diffused into the Hg drop and was not stripped during the lifetime of the Hg drop, did not contribute to the current measurement at the subsequent drop and, therefore, did not cause tailing; this metal was discarded along with the Hg drop when the drop was dislodged at the end of the period T.

Figure IV-3. Dependence of peak shape on the Hg indicating electrode

FIA

V_f - 1.0 mL min^{-1}

V_s - 0.206 mL

injections - 10^{-5} M Pb(II)

media - 0.3 M tartaric acid/0.04 M NaCl at pH 3.30

for TFME - E_i = -1.20 V versus SCE

E_f = 0.00 V versus SCE

for HMDE and SDME - E_i = -1.20 V versus SSCE

E_f = +0.10 V versus SSCE

A - TFME	B - HMDE	C - SDME	D - HMDE
T = 2 sec	T = 2 sec	T = 2 sec	T = 0.5 sec
2 μA in^{-1}	200 nA in^{-1}	50 nA in^{-1}	100 nA in^{-1}

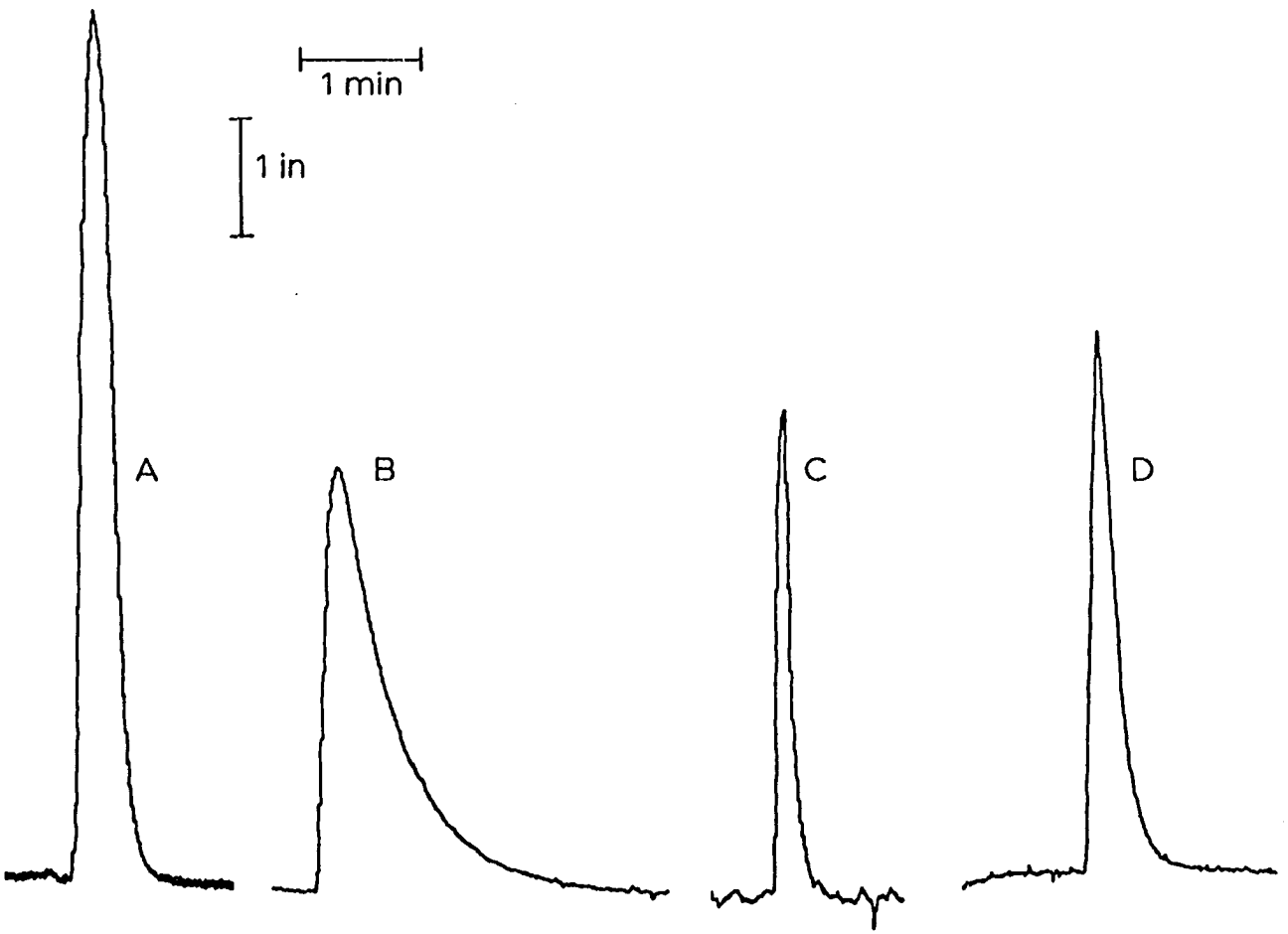
1 min
1 in
A
B
C
D

In conclusion, the value of T for use with a given Hg electrode is selected by considering the tradeoff between resolution and sensitivity. For the TFME, resolution is restricted by the frequency of the current measurements and not by peak tailing. A pulse period of 2 sec is used to maximize sensitivity and to obtain good peak definition. A pulse period of 0.5 sec results in minimal peak tailing for the HMDE while maintaining good sensitivity. Longer pulse periods for the HMDE introduce too much peak tailing for most analytical applications. A pulse period of 2 sec is recommended for the SDME to provide the highest sensitivity possible without the loss of peak definition. Pulse periods of < 2 sec will be necessary if either the TFME or the SDME were used for RPA in conjunction with HPLC in order to produce at least 10 current measurements per chromatographic peak.

2. Dependence of peak area on pulse period

In Section III.B.2, Equation III-23 was derived to develop the mathematical relationships for the response of a Hg indicating electrode under the conditions of RPA. Equation III-23 predicts that I_{strip} for RPA is directly proportional to $t_i^{1/2}$, where t_i is the deposition period in each cycle of the waveform. The value of t_i is experimentally determined by the value for T; T_i = T - 0.057 sec for the instrumentation used in this research. The relationship between peak area, Q, and deposition period, t_i, was experimentally evaluated by determining the response of the three Hg electrodes to injections of 10^{-5} M Pb(II) as a function of T. The results of these experiments are given in Table IV-1 and Figure IV-4.

Table IV-1. Relationship between Q and t_i for the TFME, HMDE and SDME

T (sec)	t_i (sec)	Q_{TFME} (μcoul)	Q_{HMDE} (μcoul)	Q_{SDME} (μcoul)
0.5	0.443	74	13.7	1.01
1.0	0.943	215	27.4	1.95
2.0	1.943	517	56.2	3.54
5.0	4.943	1460	138.0	5.74

Figure IV-4. Q versus t_i for the TFME, HMDE and SDME

FIA

V_f - 1.0 mL min^{-1}

V_s - 0.206 mL

injections - 10^{-5} M Pb(II)

media - 0.3 M tartaric acid/0.04 M NaCl at pH 3.30

• TFME

E_i = -1.20 V versus SCE

E_f = 0.00 V versus SCE

o HMDE

E_i = -1.20 V versus SSCE

E_f = +0.10 V versus SSCE

Δ SDME

E_i = -1.20 V versus SSCE

E_f = +0.10 V versus SSCE

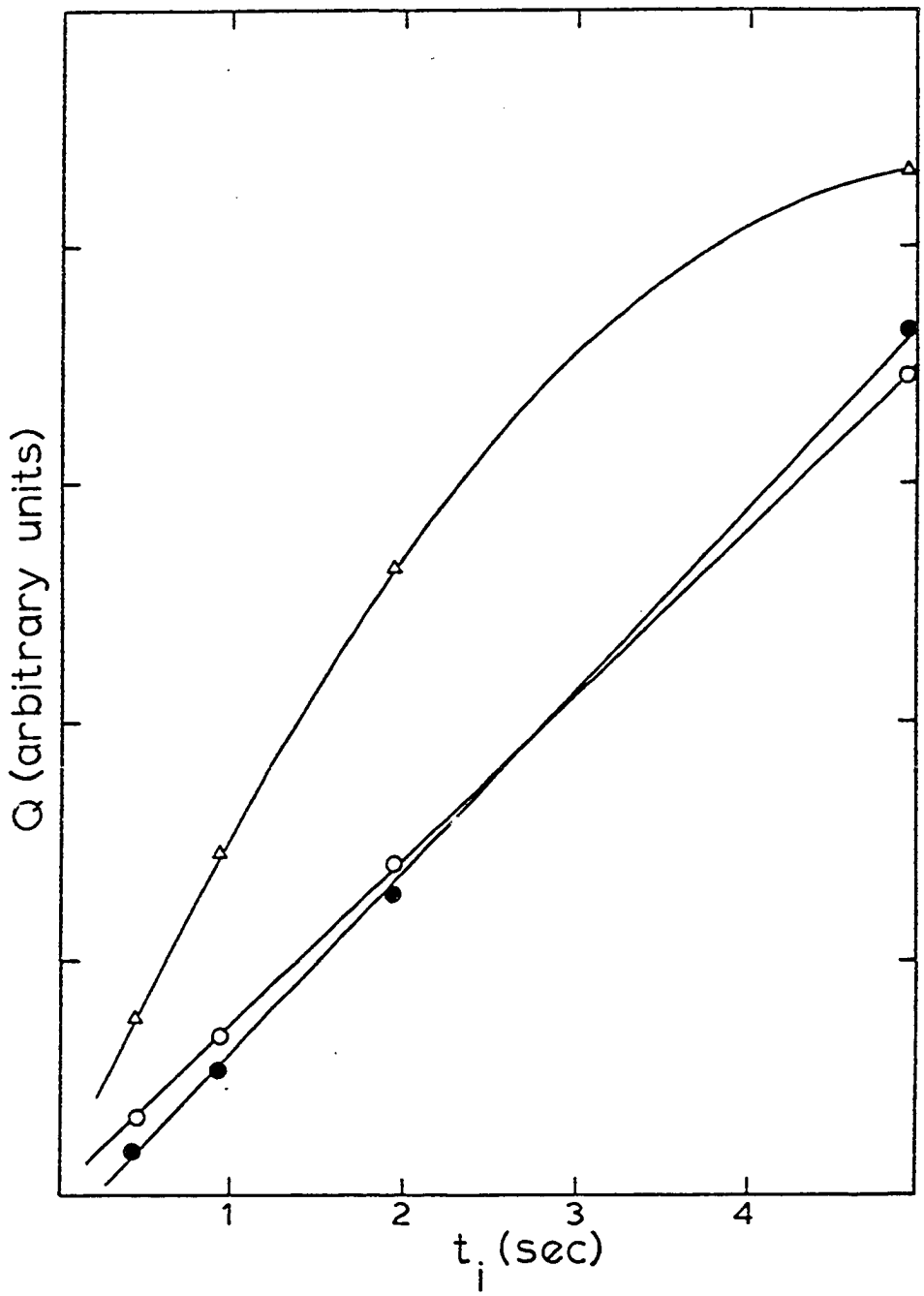
Q (arbitrary units)
1
2
3
4
t_i (sec)

For the TFME and HMDE, Q is directly proportional to t_i. These electrodes are stationary and, as reported in Section III.B.2, the metal accumulates at the surface of these electrodes to a concentration higher than that of the metal ion in solution, i.e., $C_{M(Hg)}^{o} > C_{M^{+m}}^{b}$ (essentially Equation III-12), because of the convection in the fluid stream. This accumulation occurs for virtually the entire time the sample is in contact with the electrode. For a constant flow rate, the efficiency of the deposition is constant. Hence, for consecutive injections, a reproducible fraction of metal ion will be deposited for each injection. Eventually, all of the metal which is deposited in the stationary electrode, for a single injection, is stripped from the electrode and contributes to the total signal observed for RPA. This is analogous to the linear relationship which exists between peak area and deposition time in ASV.

The relationship between Q and t_i obtained with the SDME is approximately linear for small t_i, but definitely nonlinear for $t_i \geq 2$ sec. Recall that the SDME differs from the stationary electrodes in that the SDME provides a periodic and renewable surface for RPA. Therefore, Equation III-23 can be applied since it was derived on the assumption of this experimental condition. According to Equation III-23, I_{strip} is not directly proportional to t_i, but to $t_i^{1/2}$. As discussed in Section III.B.2, the measurement of I_{strip} for the SDME corresponds to $C_{M(Hg)}^{o}$ for each new Hg drop. The measurement of peak area, Q, is a summation of these current measurements for the residence time of each injection plug of M^{+m} in the detector. Therefore, at a

constant flow rate, Q is not predicted to be directly proportional to t_i for the SDME. This is observed experimentally as shown in Figure IV-4.

3. Dependence of peak area and peak height on flow rate

Injections of a solution of Pb(II) were made in the range of flow rate 0.2 - 1.3 mL min^{-1}. The Pb(II) was detected with the TFME, HMDE and SDME to experimentally determine the flow rate dependence of the response of these electrodes by FIA. Peak heights and peak areas were measured as a function of flow rate The results are given in Tables IV-2 to IV-7. Plots of log I_p versus log V_f and log Q versus log V_f are shown in Figures IV-5 to IV-10. A summary of the values for the exponents of the flow rate terms is given in Table IV-8.

There will be no attempt here to interpret the fundamental factors which contribute to the exponent of the flow rate term for each electrode. Nonetheless, it is appropriate to comment on some observations which will ultimately affect the choice of the Hg indicating electrode to be used for analysis.

Both peak height and peak area for the TFME are severely dependent on flow rate as shown in Figures IV-5 and IV-8. Hence, the use of peak height or peak area necessitates precise control of the flow rate in the analytical application of the TFME with RPA. The nonlinear log I_p versus log V_f plot in Figure IV-5 is evidence of the complexity in the factors which determine the flow rate dependence of the TFME.

Table IV-2. Dependence of I_p on V_f for the TFME

V_f (mL min^{-1})	log (V_f x 10)	I_p (μA)	log I_p
1.30	1.11	13.6	1.134
1.20	1.08	14.3	1.155
1.10	1.04	14.6	1.166
1.00	1.00	14.9	1.73
0.90	0.95	15.7	1.196
0.80	0.90	16.2	1.210
0.70	0.85	16.8	1.225
0.60	0.78	17.2	1.236
0.50	0.70	17.8	1.250
0.40	0.60	18.4	1.265
0.30	0.48	18.6	1.271

Figure IV-5. Log I_p versus log V_f for the TFME

FIA

E_i - -1.20 V versus SCE

E_f - 0.0 V versus SCE

T - 2 sec

V_s - 0.206 mL

injections - 10^{-5} M Pb(II)

media - 0.3 M tartaric acid/0.04 M NaCl

at pH 3.30

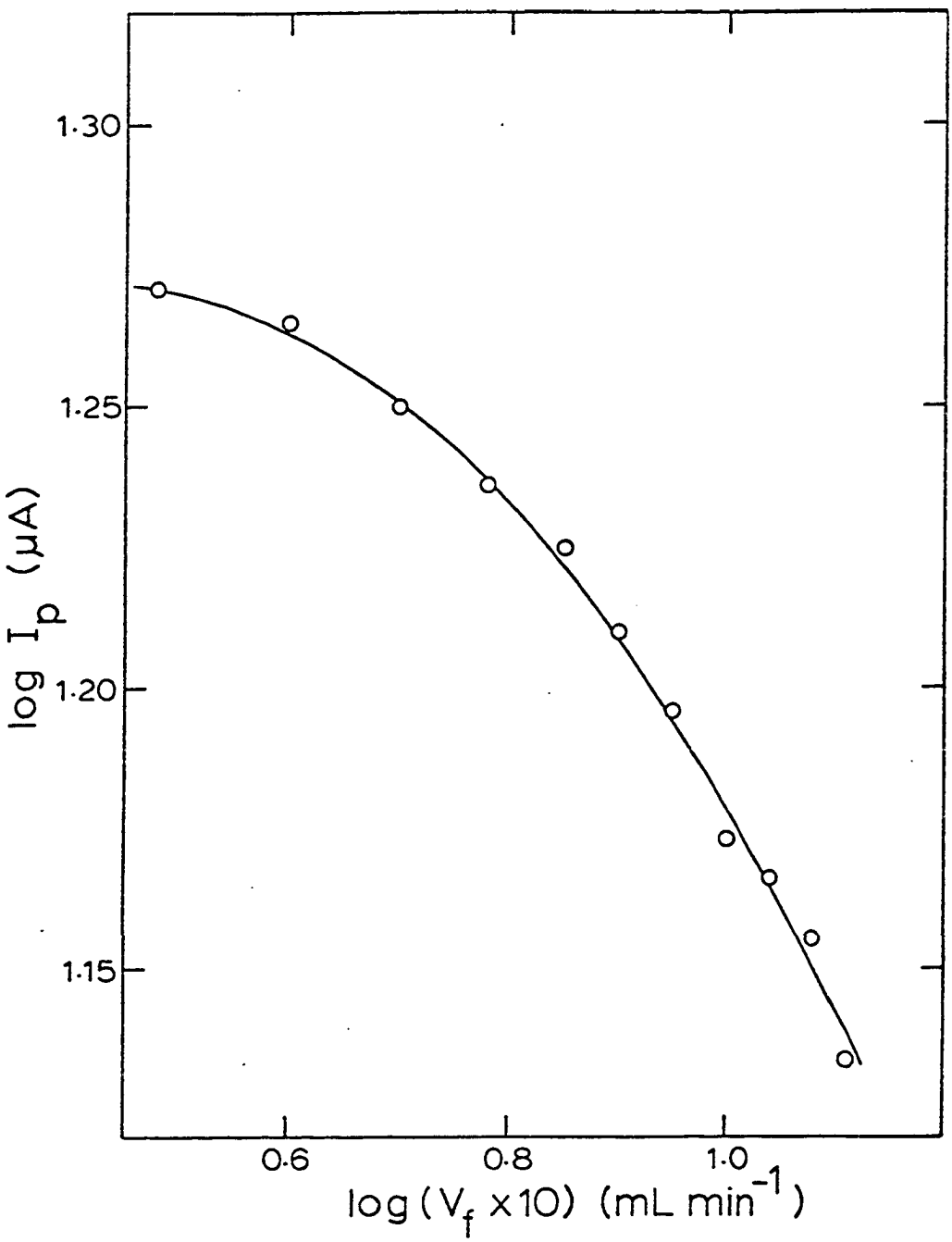
1·30
1·25
1·20
1·15
log I_p (μA)
0·6
0·8
1·0
log (V_f x10) (mL min^{-1})

Table IV-3. Dependence of I_p on V_f for the HMDE

V_f (mL min^{-1})	log (V_f x 10^2)	I_p (nA)	log I_p
1.17	2.07	452	2.655
1.12	2.05	446	2.645
1.02	2.01	428	2.632
0.92	1.96	442	2.645
0.79	1.90	438	2.641
0.71	1.85	428	2.631
0.62	1.80	432	2.636
0.52	1.72	430	2.633
0.39	1.59	424	2.628
0.29	1.46	422	2.626
0.21	1.32	444	2.648

Figure IV-6. Log I_p versus log V_f for the HMDE

FIA

E_i - -1.20 V versus SSCE

E_f - +0.10 V versus SSCE

T - 0.5 sec

V_s - 0.206 mL

injections - 10^{-5} M Pb(II)

media - 0.3 M tartaric acid/0.04 M NaCl at pH 3.30

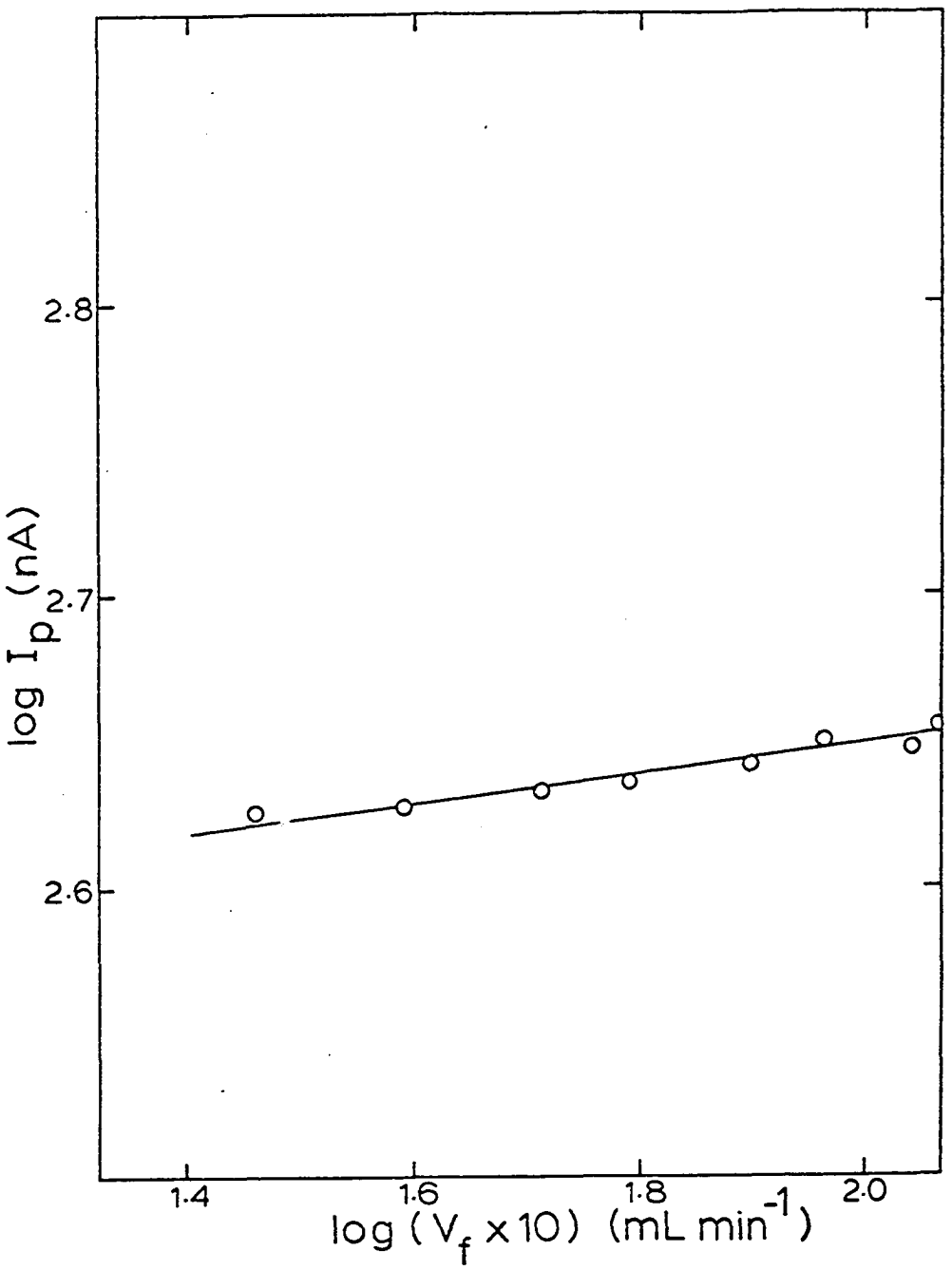
2·8
2·7
2·6
log I_p (nA)
1·4
1·6
1·8
2·0
log (V_f x 10) (mL min^{-1})

Table IV-4. Dependence of I_p on V_f for the SDME

V_f (mL min^{-1})	log (V_f x 10^2)	I_p (nA)	log I_p
1.17	2.07	249	2.396
1.12	2.05	248	2.395
1.02	2.01	243	2.386
0.92	1.96	236	2.373
0.79	1.90	211	2.324
0.71	1.85	186	2.268
0.62	1.80	160	2.203
0.52	1.72	129	2.111
0.39	1.59	96.5	1.985
0.29	1.46	68.5	1.836
0.21	1.32	54	1.73

Figure IV-7. Log I_p versus log V_f for the SDME

FIA

E_i - -1.20 V versus SSCE

E_f - +0.10 V versus SSCE

T - 2 sec

V_s - 0.206 mL

injections - 10^{-5} M Pb(II)

media - 0.3 M tartaric acid/0.04 M NaCl

at pH 3.30

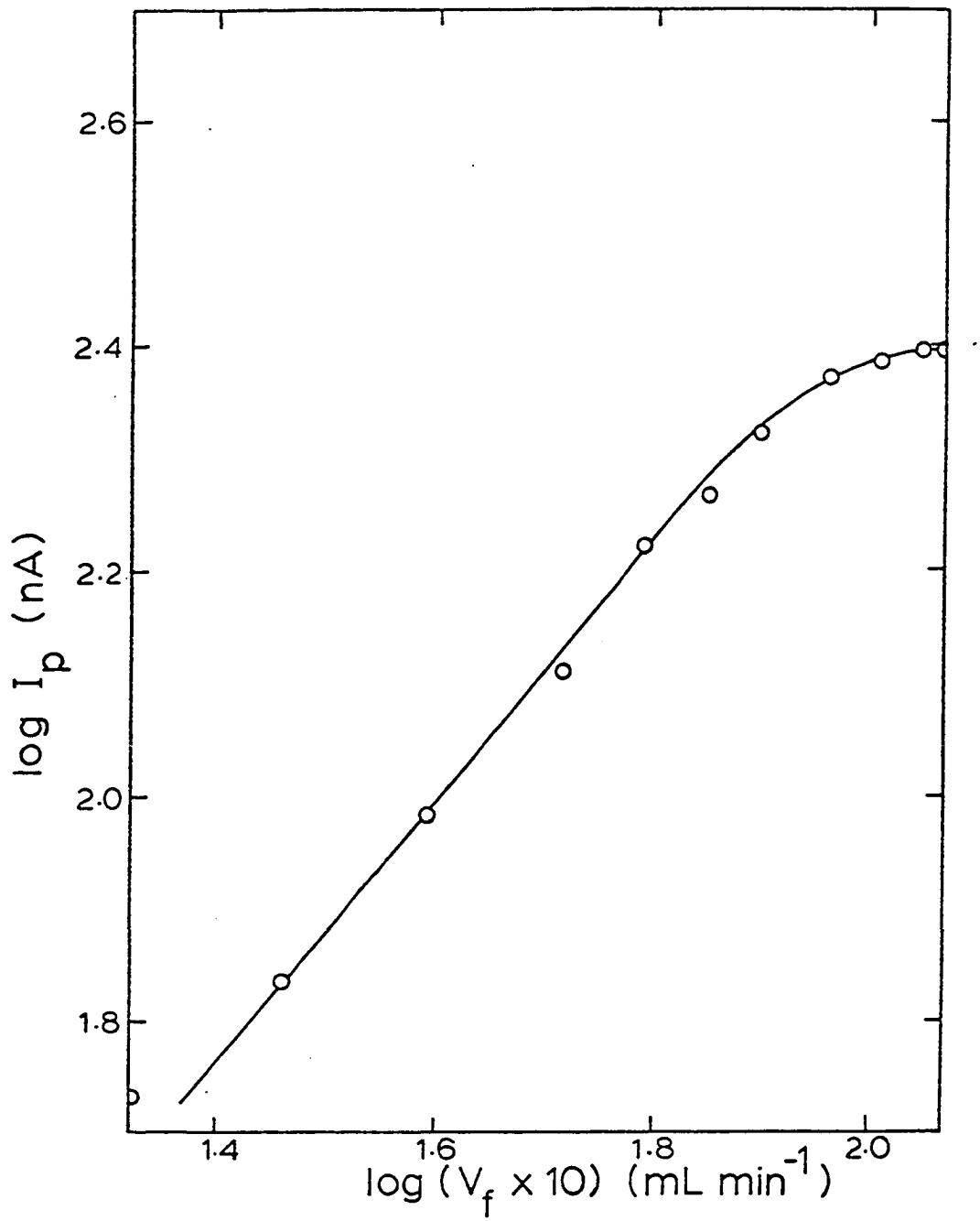
2·6
2·4
2·2
2·0
1·8
log I_p (nA)
1·4
1·6
1·8
2·0
log (V_f x 10) (mL min^{-1})

Table IV-5. Dependence of Q on V_f for the TFME

V_f (mL min^{-1})	log (V_f x 10)	Q (μcoul)	log Q
1.30	1.11	387	2.588
1.20	1.08	433	2.636
1.10	1.04	460	2.663
1.00	1.00	532	2.726
0.90	0.95	595	2.775
0.80	0.90	678	2.831
0.70	0.85	799	2.903
0.60	0.78	972	2.988
0.50	0.70	1230	3.090
0.40	0.60	1560	3.193
0.30	0.48	2210	3.344

Figure IV-8. Log Q versus log V_f for the TFME

FIA

E_i - -1.20 V versus SCE

E_f - 0.00 V versus SCE

T - 2 sec

V_s - 0.206 mL

injections - 10^{-5} M Pb(II)

media - 0.3 M tartaric acid/0.04 M NaCl

at pH 3.30

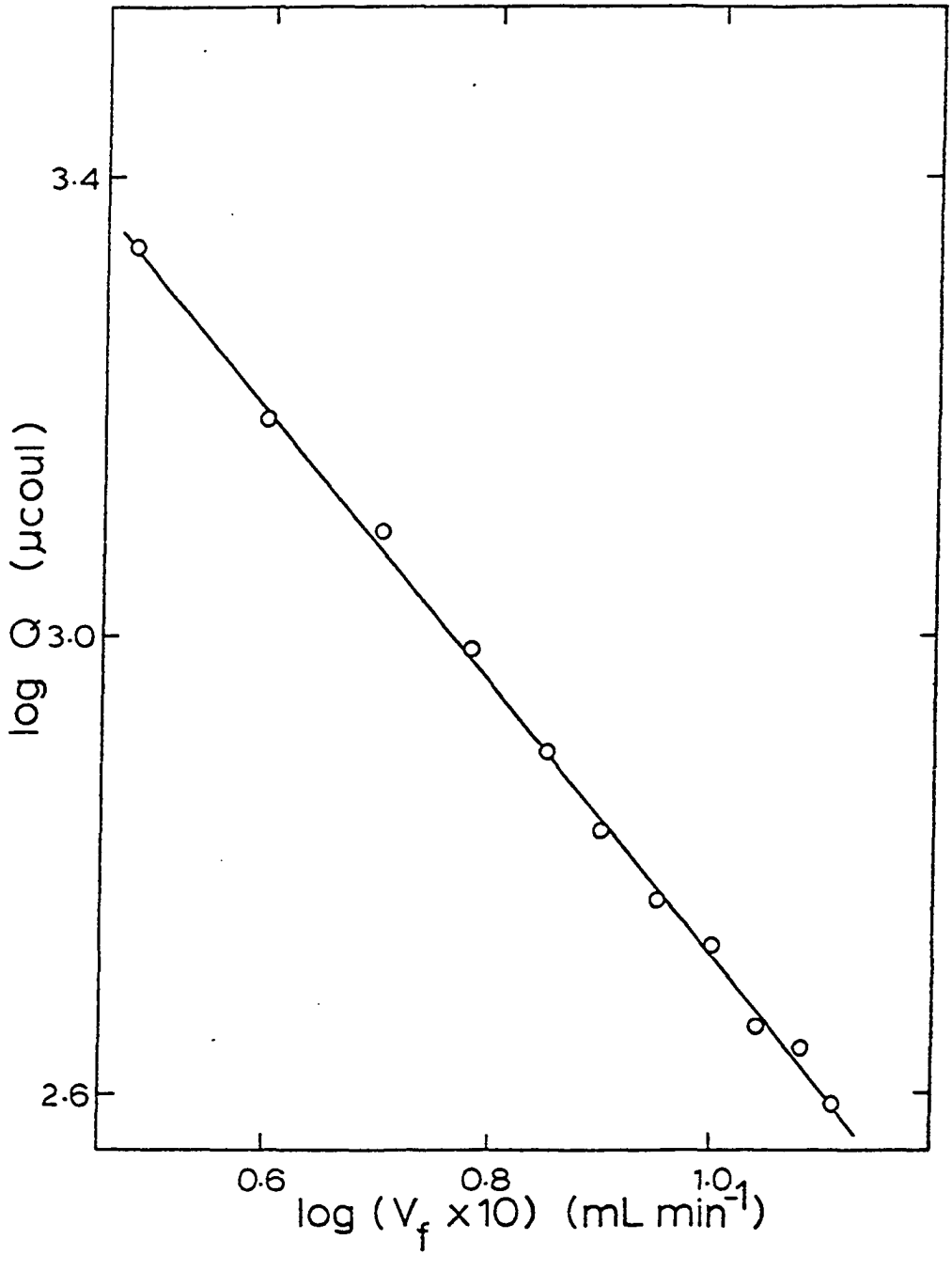
3·4
3·0
2·6
log Q (μcoul)
0·6
0·8
1·0
log (V_f x10) (mL min⁻¹)

Table IV-6. Dependence of Q on V_f for the HMDE

V_f (mL min^{-1})	log (V_f x 10^2)	Q (μcoul)	log Q
1.17	2.07	9.48	1.977
1.12	2.05	9.26	1.967
1.02	2.01	9.85	1.994
0.92	1.96	11.5	2.060
0.79	1.90	13.4	2.127
0.71	1.85	14.4	2.159
0.62	1.80	16.8	2.227
0.52	1.72	19.4	2.288
0.39	1.59	24.9	2.396
0.29	1.46	32.2	2.508
0.21	1.32	48.4	2.685

Figure IV-9. Log Q versus log V_f for the HMDE

FIA

E_i - -1.20 V versus SSCE

E_f - +0.10 V versus SSCE

T - 0.5 sec

V_s - 0.206 mL

injections - 10^{-5} M Pb(II)

media - 0.3 M tartaric acid/0.04 M NaCl at pH 3.30

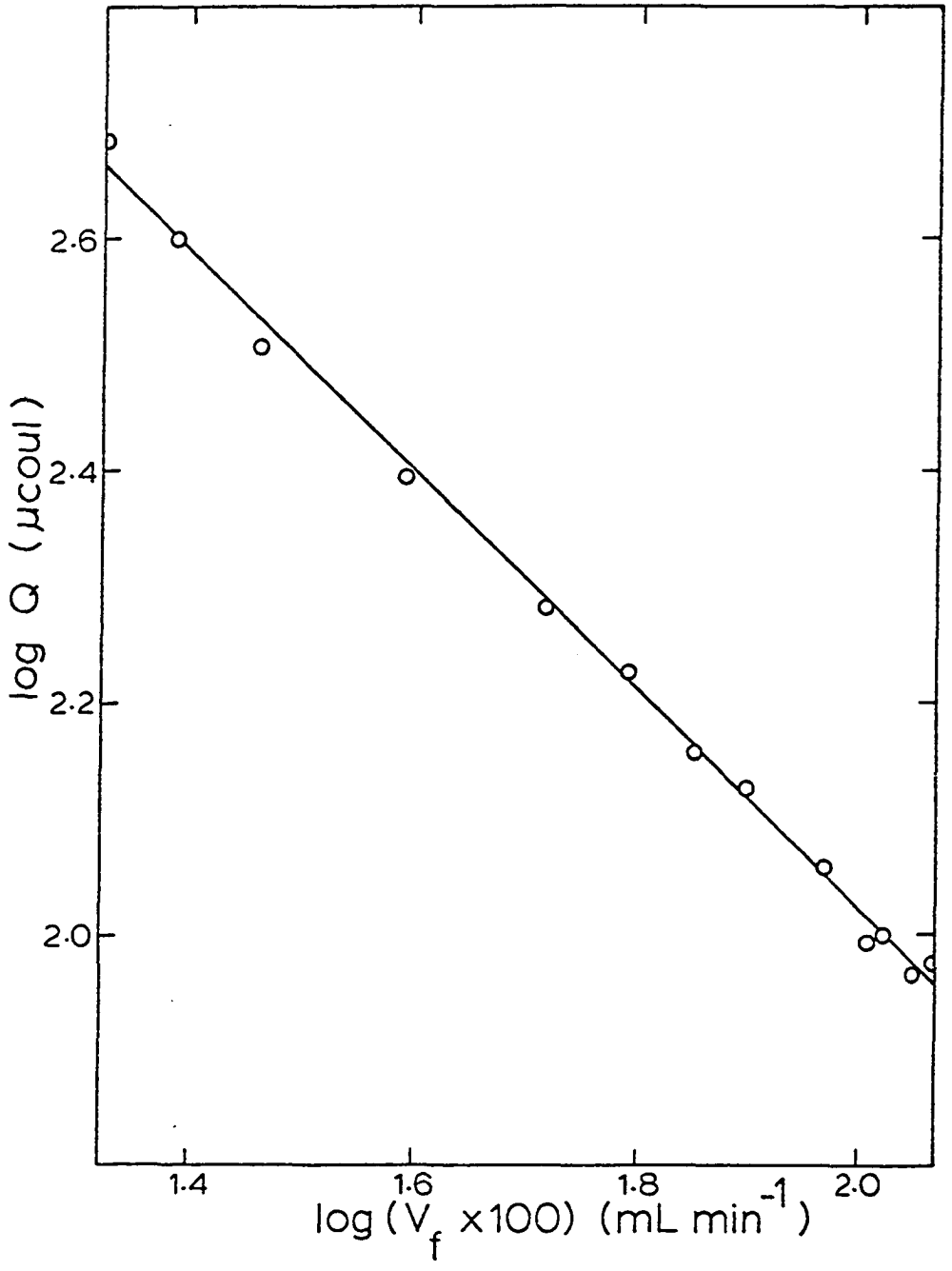
2·6
2·4
2·2
2·0
log Q (μcoul)
1·4
1·6
1·8
2·0
log (V_f x100) (mL min^-1)

Table IV-7. Dependence of Q on V_f for the SDME

V_f (mL min^{-1})	log (V_f x 10^2)	Q (μcoul)	log Q
1.17	2.07	2.99	1.476
1.12	2.05	3.11	1.492
1.02	2.01	3.38	1.529
0.92	1.96	3.54	1,550
0.79	1.90	3.40	1.531
0,71	1.85	3.22	1.508
0.62	1.80	3.34	1.523
0.52	1.72	3.13	1.496
0,39	1.59	3.15	1.499
0.29	1.46	3.13	1.496
0.21	1.32	3.54	1.548

Figure IV-10. Log Q versus log V_f for the SDME

FIA

E_i - -1.20 V versus SSCE

E_f - +0.10 V versus SSCE

T - 2 sec

V_s - 0.206 mL

injections - 10^{-5} M Pb(II)

media - 0.3 M tartaric acid/0.04 M NaCl at pH 3.30

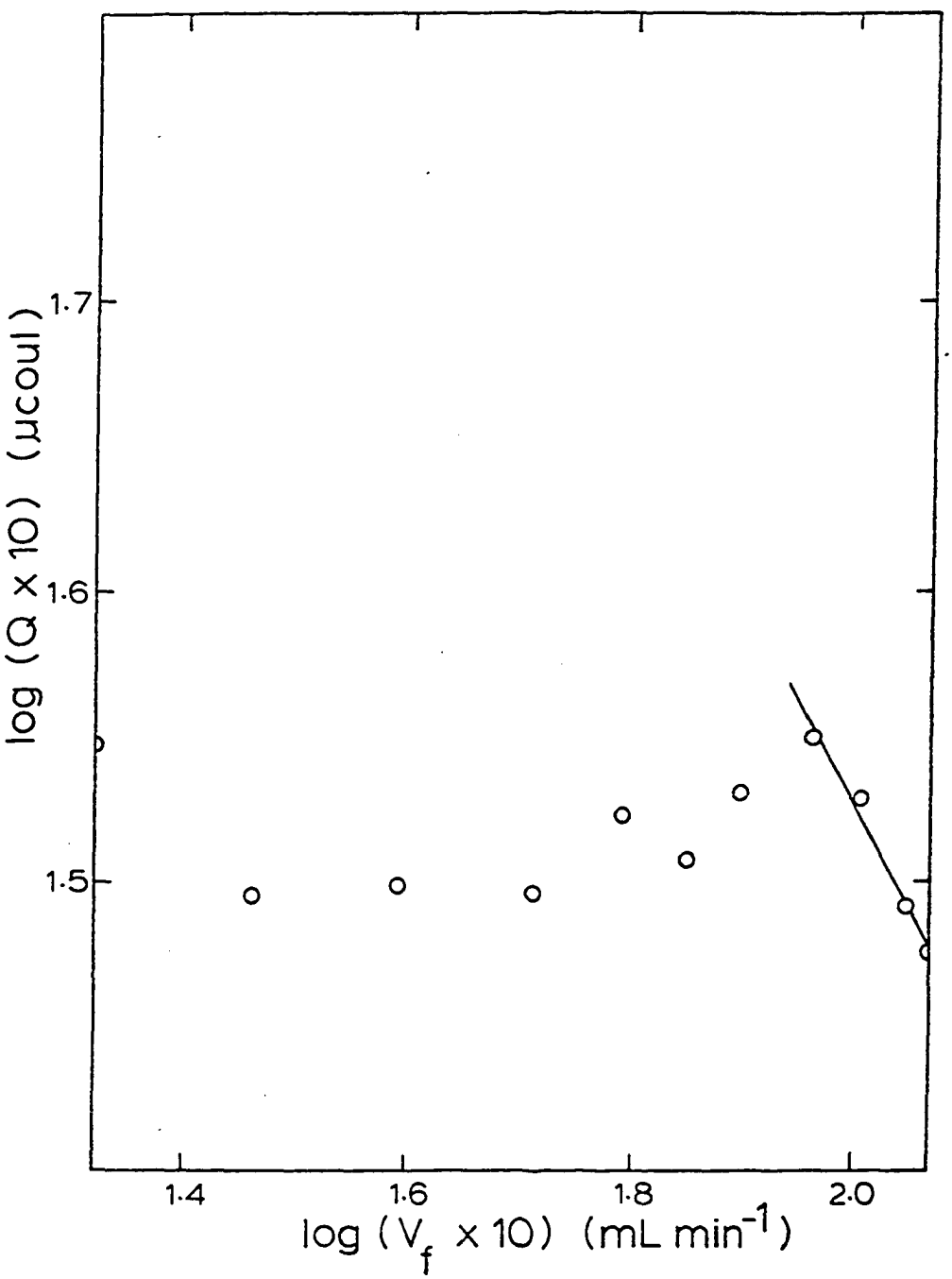
log (Q x 10) (μcoul)
1·7
1·6
1·5
1·4
1·6
1·8
2·0
log (V_f x 10) (mL min^-1)

Table IV-8. Slopes of log-log plots for I_p and Q versus V_f for the TFME, HMDE and SDME

	V_f (mL min^{-1})	TFME	HMDE	SDME
I_p	0.2 - 0.8	nℓ.[a]	0.05	1.05
	0.9 - 1.2	nℓ.	0.05	∿0
Q	0.2 - 0.8	-1.19	-0.95	i.d.[b]
	0.9 - 1.2	-1.19	-0.95	-0.72

[a] nℓ. = nonlinear.

[b] i.d. = ill-defined.

According to the results in Tables IV-3 and IV-6 and Figures IV-6 and IV-9, peak heights observed with the HMDE by FIA are almost independent of flow rate, whereas peak areas are nearly inversely proportional to flow rate. The possibility is suggested that the effect of dispersion on the distribution of analyte in the sample plug nearly offsets the effect of convection on the mass transport of the analyte to the electrode with the result that measurement of peak height is independent of flow rate under these experimental conditions. Therefore, Q is observed to be directly proportional to the residence time of the sample plug in the detector. Additionally, the data for the HMDE in Table IV-8 show the difference in the exponents of the flow rate terms for peak height and peak area is one as predicted by Equations III-24 and III-29. This difference is normally observed for the measurement of steady-state current rather than peak height as a function of flow rate as was explained in Section III.B.3. Further investigations of this interesting phenomena are obviously necessary for proper interpretation.

The flow rate dependence of the response for the SDME approaches that for the HMDE at flow rates greater than 0.9 mL min^{-1}. This is explained by considering the effect of the disruption of the diffusion layer at the electrode-solution interface for the SDME when the capillary is mechanically tapped to dislodge the Hg drops. At low flow rates, < 0.8 mL min^{-1}, the movement of the capillary, due to the mechanical action, disturbs the flow pattern of the solution at the inlet to the detector; and the drop lifetime, τ, is not long enough

to allow the diffusion layer to be re-established throughout the entire period of deposition. Therefore, the effective deposition period during the lifetime of each Hg drop is actually shorter than the applied deposition period for flow rates < 0.8 mL min^{-1}. At flow rates > 0.9 mL min^{-1}, the diffusion layer can be assumed to be rapidly re-established since the flow rate dependence of the response of the SDME agrees with that of the HMDE. Although the exponent of the flow rate for the peak area of the SDME, -0.72, does not equal that for the HMDE, -0.95, for flow rates > 0.9 mL min^{-1}, the value for the SDME was determined with only 4 data points (Figure IV-10). The collection of flow rate data for Q beyond 1.2 mL min^{-1} is expected to yield results which agree for both electrodes.

On the basis of the results of these experiments, it would be best to use the measurement of peak height for the HMDE to monitor fluid streams for Pb(II). The same is true for the SDME at flow rates > 0.9 mL min^{-1}. Both procedures provide a result which is virtually independent of flow rate. Although the measurement of peak area is independent of dispersion, it is dependent on flow rate for all of the electrodes tested, meticulous control of the flow rate is a necessity in the use of peak area as an analytical measurement of RPA.

4. Precision studies for Pb(II) by FIA

The precision of the response of the TFME, HMDE and SDME was determined by FIA. The relative standard deviation, σ_{rel}, of a set of peak heights observed for successive injections of Pb(II) was

calculated for each electrode and used as a measure of precision. The results are summarized in Table IV-9.

Typical anodic peaks for the detection of 15 μM Pb(II) by FIA are shown in Figure IV-11 for the SDME. Twenty successive injections were made containing 640 ng of Pb(II) per injection. The average value of the peak heights shown was 270 nA with a σ_{rel} of 2.6% (Table IV-9). The peak heights were observed to vary in a random manner. Similar results obtained with the TFME and the HMDE are not shown. Please refer to Figure IV-3 for a comparison of peak shapes observed by RPA for Pb(II) with these electrodes.

The electrode which was tested initially for RPA was the TFME. The TFME used during early studies was a film of about 500 Å of Hg on the GCTE. The result of the precision study performed with this electrode, shown in Table IV-9, had a value for σ_{rel} of 2.2%. However, peak heights gradually increased for successive injections of Pb(II) rather than varying in a random fashion. The data for the results given in Table IV-9 for the TFME are reported in Table IV-10 and illustrate the gradual increase in peak height for a TFME prepared without an intervening film of Au. Such problems of irreproducibility are also observed in ASV with a TFME. Workers such as Florence (40) and Stulikova (39) have solved this problem with the use of a well-polished, glassy carbon substrate and the deposition of the Hg in the form of fine droplets at potentials approaching -1.0 V versus SCE. These authors noticed that for deposition potentials of 0.0 - -0.2 V versus SCE, Hg was deposited as droplets with a relatively large

Table IV-9. Relative standard deviation of values for I_p for the detection of Pb(II) by FIA

Electrode	Number of injections	[Pb(II),M]	σ_{rel} (%)[a]
TFME a) Hg only	10	1×10^{-4}	2.2
b) Hg-Au	8	1×10^{-4}	1.1
HMDE	10	5×10^{-6}	3.0
SDME	20	1.5×10^{-5}	2.6

[a] $\sigma_{rel} = \frac{\sigma(100)}{\bar{x}}$

Figure IV-11. Peaks observed for 20 successive injections of 15 μM Pb(II) detected with the SDME

FIA

E_i - -1.20 V versus SSCE

E_f - +0.10 V versus SSCE

T - 2 sec

V_f - 1.0 mL min^{-1}

V_s - 0.206 mL

media - 0.3 M tartaric acid/0.04 M NaCl at pH 3.30

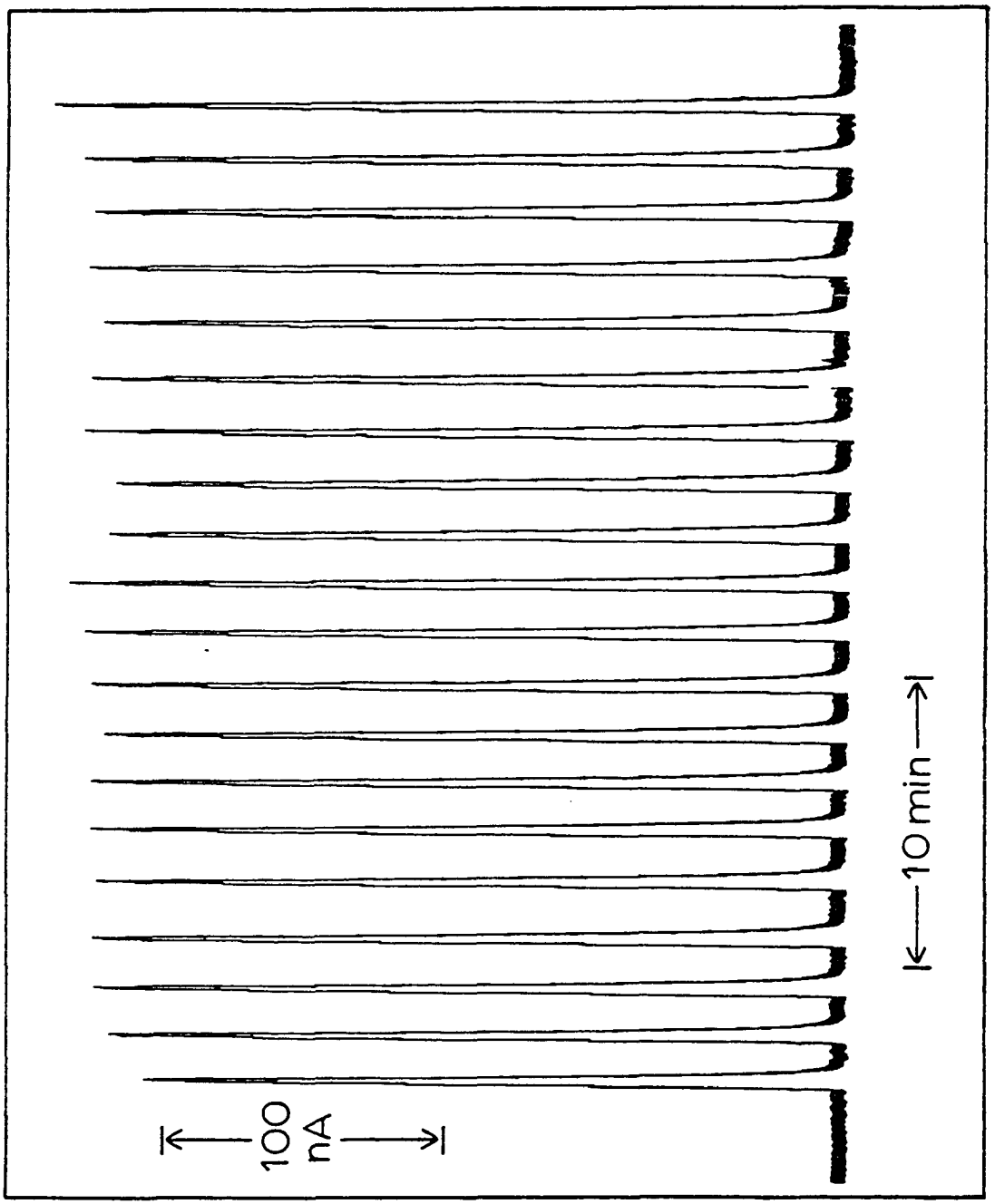
100 nA
10 min

Table IV-10. Values of I_p observed with the TFME for successive injections of Pb(II)

I_p (μA)[a]	I_p (μA)[b]
56.9	47.6
58.2	48.1
58.6	48.6
58.9	48.6
59.2	48.4
59.4	49.2
60.2	49.1
61.0	48.7
61.0	

[a]Hg film only on GCTE.

[b]Hg-Au film on GCTE.

diameter which coalesced with use and time resulting in a response with poor precision.

Deposition potentials from -0.3 - -1.0 V versus SCE, and Hg-film thicknesses of 0.05 - 1.0 μm, were used to prepare the Hg film in studies of precision for RPA. However, peak heights which increased with successive injections of Pb(II) were observed, possibly caused by the inability to efficiently polish the surface of the GCTE. Experimentally, a reproducible surface for the GCTE could not be prepared. Consequently, further research on the effect of the nature of the film on the response for RPA was inhibited.

Allen and Johnson (121) developed a technique called "stripping voltammetry with collection" where they used a Pt-ring, glassy carbon rotating-disk electrode for the determination of Hg(II). These workers observed that reproducible results for the determination of Hg(II) were obtained only when the Hg was deposited on a glassy carbon surface which had been plated with a few monolayers of Au. For RPA, when a film of Au is deposited on the GCTE followed by film of Hg, the peak heights no longer significantly increase for successive injections of Pb(II). The data in Table IV-10 illustrate the gradual increase in peak height in the absence of the Au substrate compared to the presence of the Au substrate for approximately equal thicknesses of the Hg films. The Hg-Au film used to obtain the results in Table IV-9 had a thickness of about 50 Å for Au and about 500 Å for Hg. These film thicknesses were observed experimentally to provide the optimum precision for the determination of Pb(II) by RPA. Apparently,

the Au substrate serves to immobilize the Hg film such that a stationary surface of Hg exists on the GCTE.

The results of this precision study show all three electrodes to be analytically useful. Although the response of the TFME with a Hg-Au film is more precise, the TFME requires at least 45 min for preparation of the film and stabilization of the baseline each day before use. Additionally, the film must be removed with a 10 min stripping period at the end of each day. The GCTE requires extra attention to ensure that there is no leakage of solution between the electrode body and the plastic assembly. Consequently, the added effort needed for the improvement in the precision of the response for the TFME is not warranted in most applications.

5. Calibration curves for Pb(II) by FIA

Equation III-23 predicts that I_{strip}, the analytical signal for RPA, is directly proportional to $C_M{}^{+m}{}^{b}$, the bulk concentration of M^{+m} in solution. Under controlled conditions of pulse period and flow rate, I_p and Q are also expected to be directly proportional to $C_M{}^{+m}{}^{b}$. Calibration curves for the detection of Pb(II) by FIA were obtained for TFME, HMDE and SDME. The measurement of I_p was chosen to prepare the calibration curves because peak heights are easily measured and were virtually independent of flow rate for the response of the HMDE and SDME (see Table IV-9). The results for the calibration curves based on I_p are given in Tables IV-11 to IV-13 and Figures IV-12 to IV-14 for the TFME, HMDE and SDME, respectively.

Table IV-11. Calibration curve for Pb(II) by FIA with the TFME

grams Pb(II) ($\times 10^9$)	log (ng Pb)	I_p ($A \times 10^9$)	log I_p
4.268×10^3	3.630	2.42×10^4	2.38
2.134×10^3	3.329	2.07×10^4	2.32
8.536×10^2	2.931	5.30×10^3	1.72
4.268×10^2	2.630	2.26×10^3	1.35
2.134×10^2	2.329	1.12×10^3	1.05
8.536×10^1	1.931	4.2×10^2	0.67
4.268×10^1	1.630	2.1×10^2	0.33
2.134×10^1	1.329	1.1×10^2	0.04

Figure IV-12. Calibration curve for Pb(II) with the TFME

FIA

E_i - -1.20 V versus SCE

E_f - 0.00 V versus SCE

T - 2 sec

V_f - 1.0 mL min^{-1}

V_s - 0.206 mL

media - 0.01 M H_2SO_4/0.05 M Na_2SO_4

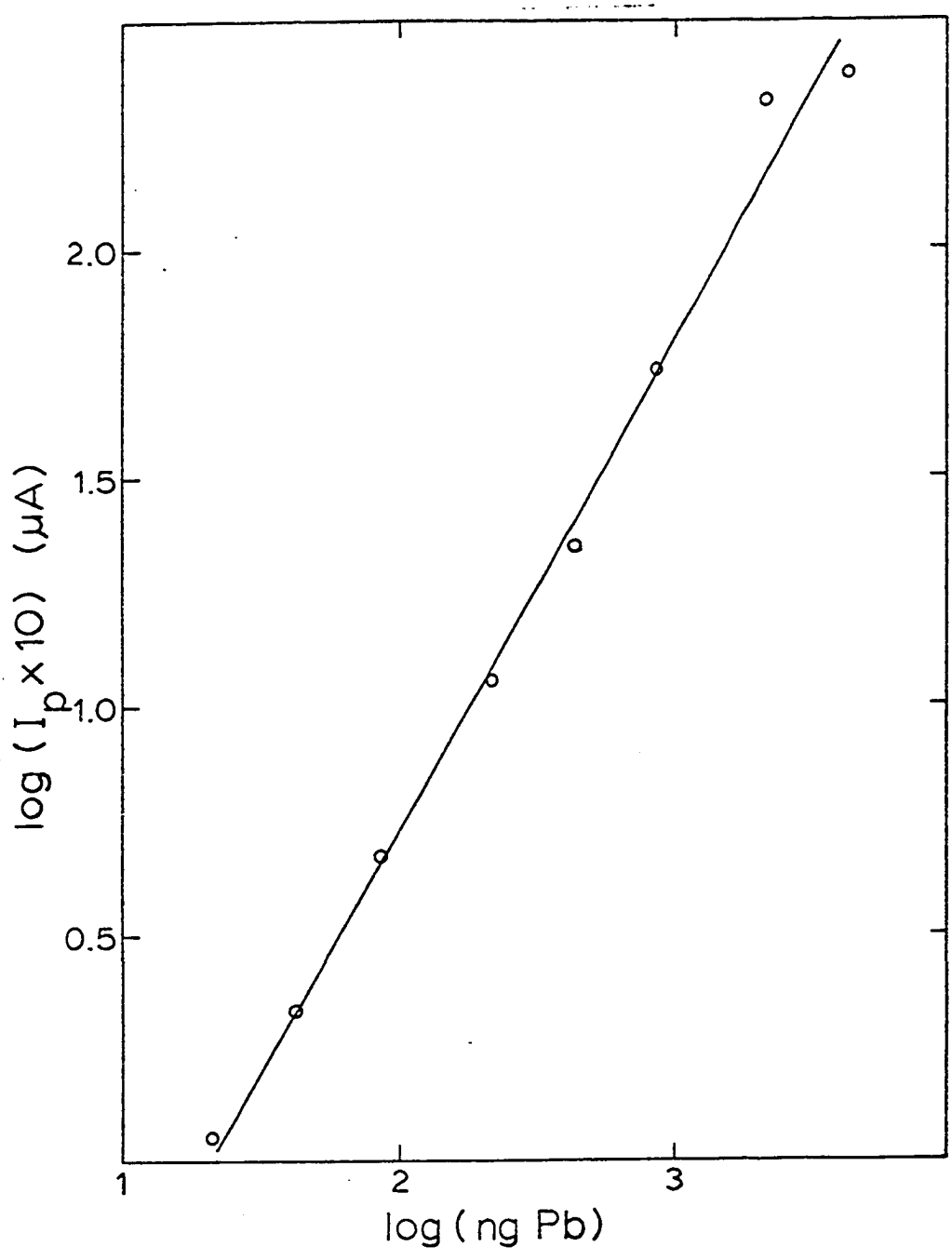
2.0
1.5
1.0
0.5
log (I_p x 10) (μA)
1
2
3
log (ng Pb)

Table IV-12. Calibration curve for Pb(II) by FIA with the HMDE

grams Pb(II) ($\times 10^9$)	log (ng Pb)	I_p (A $\times 10^9$)	log I_p
2.134×10^4	4.329	2.52×10^4	4.401
4.268×10^3	3.630	4.86×10^3	3.687
2.134×10^3	3.329	2.22×10^3	3.347
4.268×10^2	2.630	4.85×10^2	2.686
2.134×10^2	2.329	2.50×10^2	2.397
4.268×10^1	1.630	5.13×10^1	1.710
2.134×10^1	1.329	2.40×10^1	1.379
4.268	0.630	7.80	0.890
2.134	0.329	6.25	0.796

Figure IV-13. Calibration curve for Pb(II) with the HMDE

FIA

E_i - -1.20 V versus SSCE

E_f - +0.10 V versus SSCE

T - 0.5 sec

V_f - 1.0 mL min^{-1}

V_s - 0.206 mL

media - 0.3 M tartaric acid/0.04 M NaCl at pH 3.30

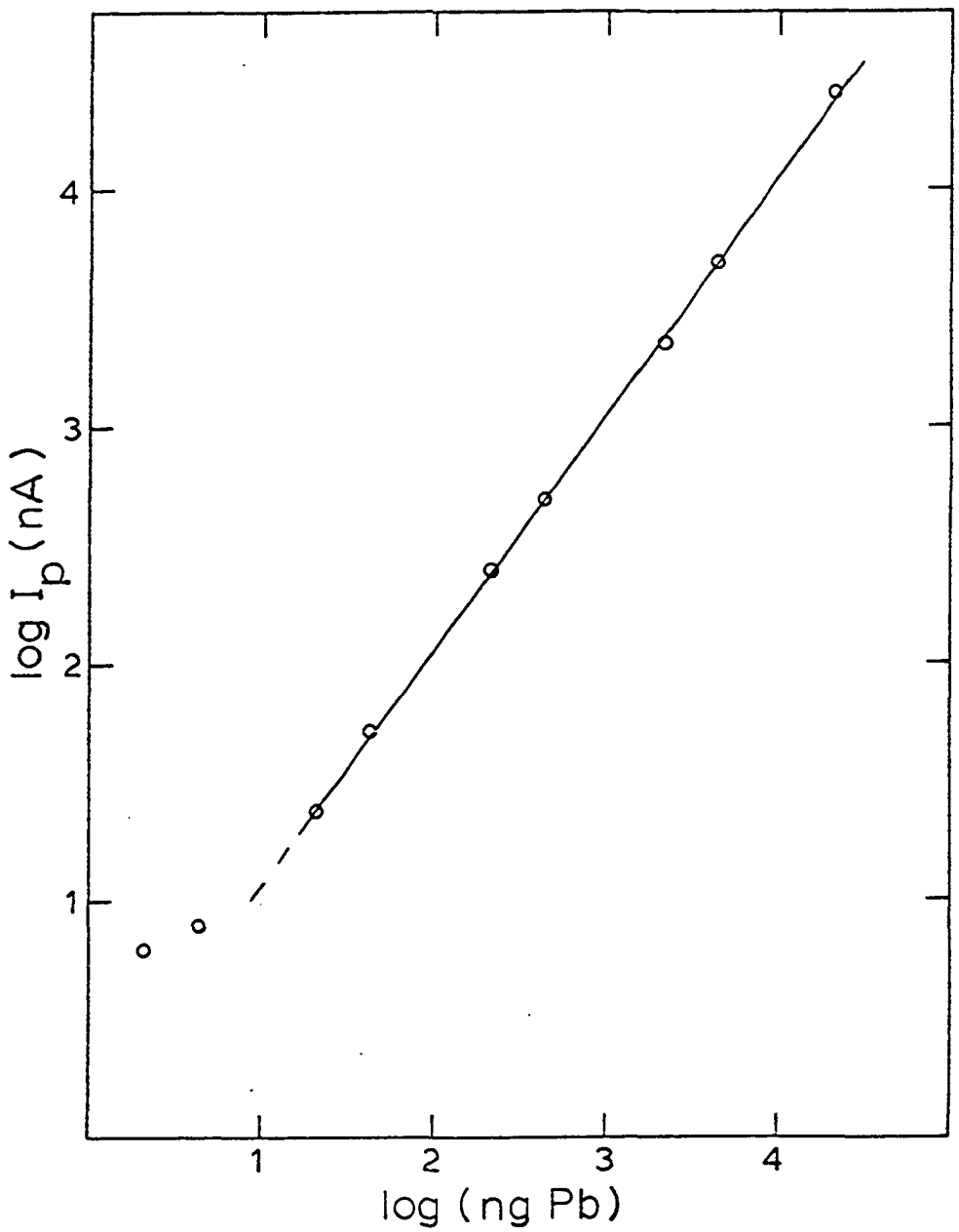
log I_p (nA)
4
3
2
1
1
2
3
4
log (ng Pb)

Table IV-13. Calibration curve for Pb(II) by FIA with the SDME

grams Pb(II) ($\times 10^9$)	log (ng Pb)	I_p (A $\times 10^9$)	log I_p
4.268×10^4	4.630	1.63×10^4	4.213
2.134×10^4	4.329	8.75×10^3	3.942
8.536×10^3	3.931	3.75×10^3	3.574
4.268×10^3	3.630	1.89×10^3	3.277
2.134×10^3	3.329	9.93×10^2	2.997
8.536×10^2	2.931	3.88×10^2	2.589
4.268×10^2	2.630	1.91×10^2	2.282
2.134×10^2	2.329	9.47×10^1	1.976
8.536×10^1	1.931	3.37×10^1	1.527
4.268×10^1	1.630	1.47×10^1	1.166
2.134×10^1	1.329	5.5	0.740

Figure IV-14. Calibration curve for Pb(II) with the SDME

FIA

E_i - -1.20 V versus SSCE

E_f - +0.10 V versus SSCE

T - 2 sec

V_f - 1.0 mL min^{-1}

V_s - 0.206 mL

media - 0.3 M tartaric acid/0.04 M NaCl at pH 3.30

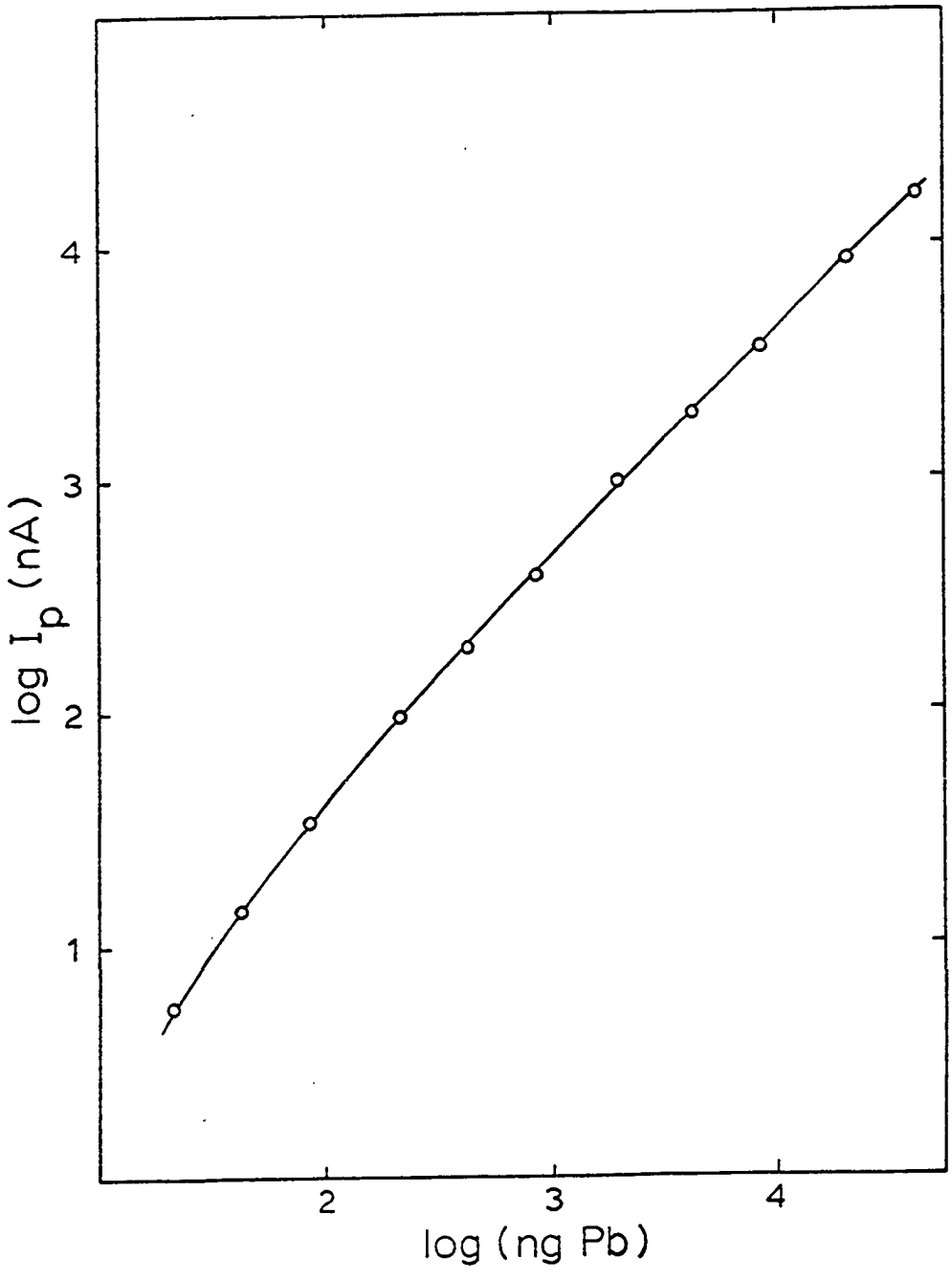
log I_p (nA)
1
2
3
4
2
3
4
log (ng Pb)

The calibration curve obtained by FIA with the TFME (Figure IV-12) corresponds to injections of Pb(II) in the range 64 ng - 4.3 μg for a 0.206 mL injection of sample; this concentration range is equivalent to 1.5 μM - 0.1 mM Pb(II). The line shown was determined by a calculation of linear least squares. The correlation coefficient for the data is 0.997. The calibration curve is linear for greater than two orders of magnitude. The detection limit for Pb(II) is estimated as 25 ng (0.12 ppm). The detection limit is not limited by the noise of the electronics but by the noise in the background current which is attributed to an incomplete coverage of the GCTE with the Hg film. The detection limit was also very sensitive to leaks of solution around the GCTE.

Figure IV-13 shows the calibration curve for Pb(II) taken by FIA with the HMDE. Injections of 0.206 mL containing 2.1 ng - 21 μg Pb(II) were made; this concentration range is equivalent to 50 nM - 0.5 mM Pb(II). The curve is linear, excluding the two data taken at lowest concentration, for approximately three orders of magnitude with a correlation coefficient of 0.9998. The detection limit is represented by the lowest point in Figure IV-8 and corresponds to 2.1 ng Pb(II) (0.01 ppm).

Finally, the calibration curve obtained with the SDME is shown in Figure IV-14 for Pb(II) in the range 20 ng - 42 μg for the 0.206-mL injection, which corresponds approximately to 0.5 mM - 1 mM. The detection limit is estimated to be 13 ng (0 06 ppm). Although slightly curved, the calibration curve is useful for quantitative analysis

provided the standards are close in value to the concentration of the unknown. The nonlinearity of the plot in Figure IV-14 cannot be explained at this time.

The detection limit for Pb(II) observed with the HMDE and SDME was not controlled by the chemical or physical nature of these electrodes but by the electronic noise from the pulse polarograph. The background noise observed under various conditions is shown in Figure IV-15. The presence of dissolved oxygen had no effect on the background noise for the HMDE and SDME as observed by comparing response A to B and D to E. The convection of the fluid stream had no influence on the background noise as illustrated by comparing response A to C and response D to F. Finally, the effect of the mechanical drop-knocker was negligible as can be seen by making any comparison of the response of the HMDE to that of the SDME. The baseline drift observed with the HMDE was a characteristic of the response of a stationary electrode soon after the application of the applied potential and typically this baseline drift stabilized in < 15 min. The background noise may be caused by transients produced by the switch of the sample-and-hold circuit in the pulse polarograph. Superior sample-and-hold circuitry may considerably improve the detection limits obtainable with both electrodes.

The results of the calibration experiments make a clear distinction in the quantitative performance of the TFME, HMDE and SDME for RPA. The performance of the HMDE is superior. The HMDE produced the largest range of linear response with excellent linearity and with the

Figure IV-15. Background noise observed with the HMDE and SDME

E_i - -1.20 V versus SSCE

E_f - +0.10 V versus SSCE

T - HMDE = 0.5 sec

SDME = 2 sec

media - 0.3 M tartaric acid/0.04 M NaCl

at pH 3.30

HMDE: A - air-saturated, quiescent

B - O_2-free, quiescent

C - air-saturated, fluid stream, V_f - 1.0 mL min^{-1}

SDME: D - air-saturated, quiescent

E - O_2-free, quiescent

F - air-saturated, fluid stream, V_f - 1.0 mL min^{-1}

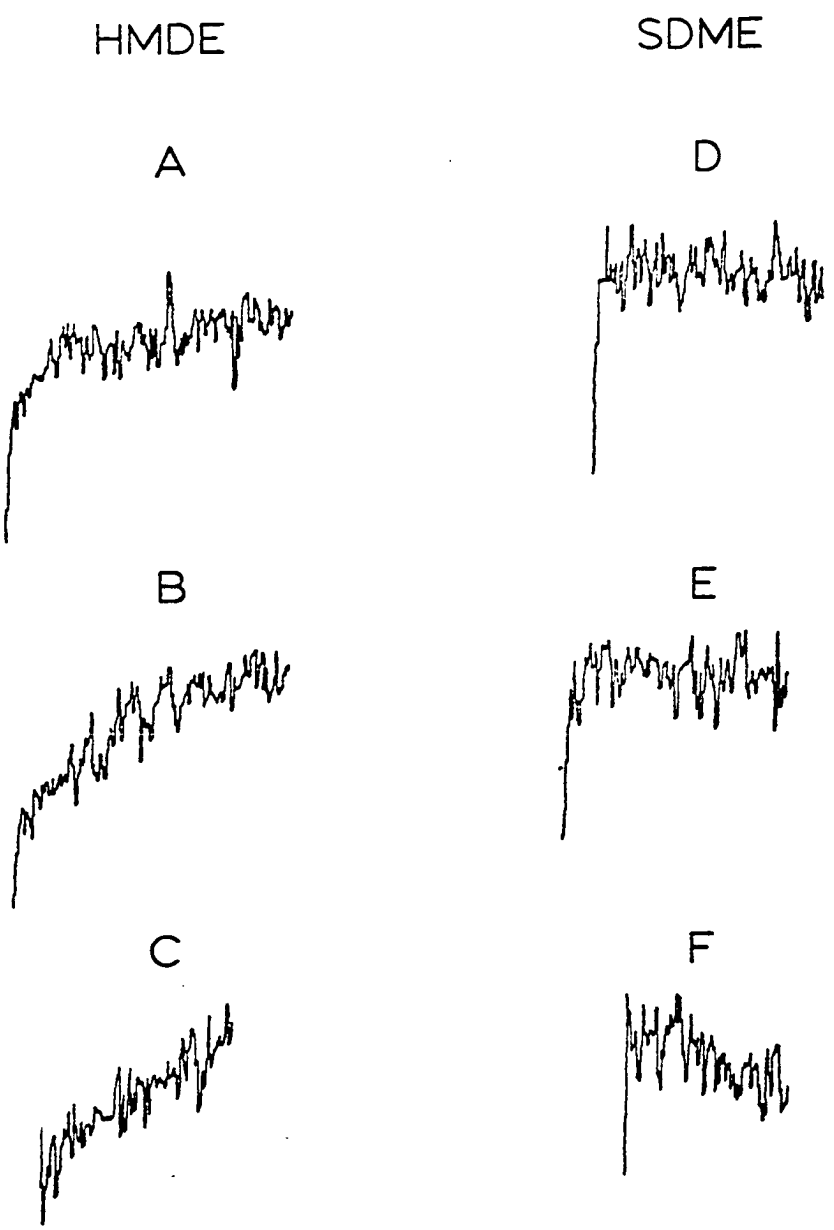
HMDE
SDME
A
D
B
E
C
F

lowest detection limit for the detection of Pb(II). The SDME produced a calibration curve which is nonlinear at low concentration. Application of the SDME is preferable only in situations where electrode fouling (passivation) is a problem. The response of the TFME is reasonably linear but over a smaller concentration range than for the HMDE. The detection limit for Pb(II) is higher for the TFME than for the HMDE. However, the TFME does have great promise in application to RPA. The use of a TFME is theoretically the most efficient way to affect a maximum electrode response for RPA. The large area-to-volume ratio of the TFME enables the metal to efficiently concentrate in the film during deposition and to readily diffuse to the electrode surface during the measurement of the anodic current. Peak tailing with a TFME is minimal. Figure IV-3 illustrates the enhanced analytical signal obtained with the TFME relative to the HMDE and SDME in spite of an electrode area that is one-tenth of that for the HMDE and SDME. The detection limit may be drastically lowered through the use of an electrode design which would make it possible to easily polish the glassy carbon substrate and to deposit a uniform film of Hg and Au. These considerations surely justify further study of the TFME.

6. Compatibility with cation-exchange liquid chromatography

The selectivity of RPA as applied with a Hg indicating electrode may be adequate to justify that no preliminary separations are necessary in some cases, e.g., the determination of Cu(II) in the presence of Pb(II) and Zn(II) mentioned in Section III.D.4.

Practically speaking, however, the analysis of a complex sample for one or more components requires some separation method prior to detection. The EC detector is compatible with methods of LC which use a mobile phase of high conductivity. For the determination of metal ions, ion-exchange liquid chromatography is the method of choice. Cation-exchange liquid chromatography (CELC) was selected rather than anion-exchange liquid chromatography. The separation of metal ions by anion-exchange liquid chromatography with a full-capacity resin utilizes eluents which commonly consist of halides or chelating agents at high concentration. Such reagents will interfere with the detection process of RPA by decreasing the potential region available for a current measurement which is free from electrochemical interference of dissolved oxygen. For example, the $E_{1/2}$ value for the anodic polarographic wave for 1 M Cl^- is 0.03 V versus SCE; hence, an interference-free potential region is unavailable for RPA in a medium which contains 1 M Cl^-.

The chromatographic facilities of CELC were limited. Pumps for LC which were capable of delivering eluents at high pressure were unavailable during the preliminary chromatographic experiments. Even if such a pump had been available, cation-exchange resins capable of producing separations of high efficiency were not. As a result, the application of the Hg indicating electrodes with RPA to HPLC could not be achieved. Nonetheless, good separations were obtained with a peristaltic pump and cation-exchange resins of approximately 40-50 μm in diameter.

In anticipation of the determination of one or more metals in a standard sample of orchard leaves, separation methods using CELC were sought which could separate metal ions such as Cu(II), Zn(II), Pb(II) and Cd(II). The response of the TFME, HMDE and SDME with RPA was also of interest to determine if the response accurately defined the concentration profiles of the metal ions eluted from the chromatographic column. Thus, separation methods for metal ions were developed for synthetic samples using two types of cation-exchange resins, a low-capacity, surface-sulfonated resin and a full-capacity, sulfonated resin.

Chromatograms are shown in Figures IV-16 and IV-17 for the separation of Tl(I), Cd(II) and Pb(II) with a column of low-capacity resin (45-53 μm). Figure IV-16 was taken with the TFME and Figure IV-17 was taken with the SDME. The baseline separations were achieved within 15 min for the isocratic elution with 0.01 M H_2SO_4 containing 0.05 M Na_2SO_4. The effective eluting agent of the cation-exchange process in this eluent was Na^+. The acid was present to provide additional conductivity for the EC detector. The results show that EC detectors are useful with eluents of low ionic strength and chromatographic columns with resin of low capacity. The peaks defined by the SDME were symmetrical for these metal ions, whereas the peaks observed with the TFME were symmetrical with the exception of that for Cd(II). The unsymmetrical peak for Cd(II) is an artifact of the TFME which was observed also by FIA for films of Hg only and of the Hg-Au composite. Therefore, the formation of an intermetallic

Figure IV-16. Chromatographic separation of Tl(I), Cd(II) and Pb(II) with detection by the TFME

E_i - -1.20 V versus SCE

E_f - 0.00 V versus SCE

T - 2 sec

V_f - 1.0 mL min^{-1}

V_s - 0.206 mL

injection - 10^{-5} M in each metal ion

eluent - 0.01 M H_2SO_4/0.05 M Na_2SO_4

column - low capacity, cation-exchange resin (45 - 53 μm), 4 mm-i.d. x 100 mm

peaks - A = Tl(I)

B - Cd(II)

C - Pb(II)

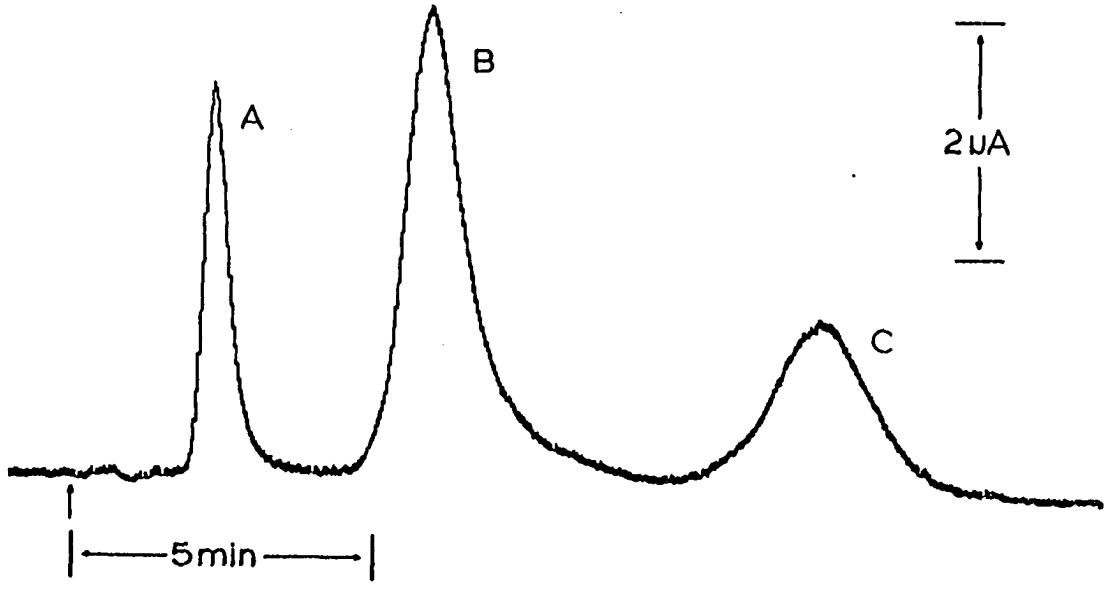
A
B
C
2μA
5min

Figure IV-17. Chromatographic separation of Tl(I), Cd(II) and Pb(II) with detection by the SDME

E_i - -1.20 V versus SSCE

E_f - +0.10 V versus SSCE

T - 2 sec

V_f - 1.0 mL min^{-1}

V_s - 0.206 mL

injection - 10^{-5} M in each metal ion

eluent - 0.01 M H_2SO_4/0.05 M Na_2SO_4

column - low capacity, cation-exchange resin (45 - 53 μm), 4 mm-i.d. x 100 mm

peaks - A = Tl(I)

B = Cd(II)

C = Pb(II)

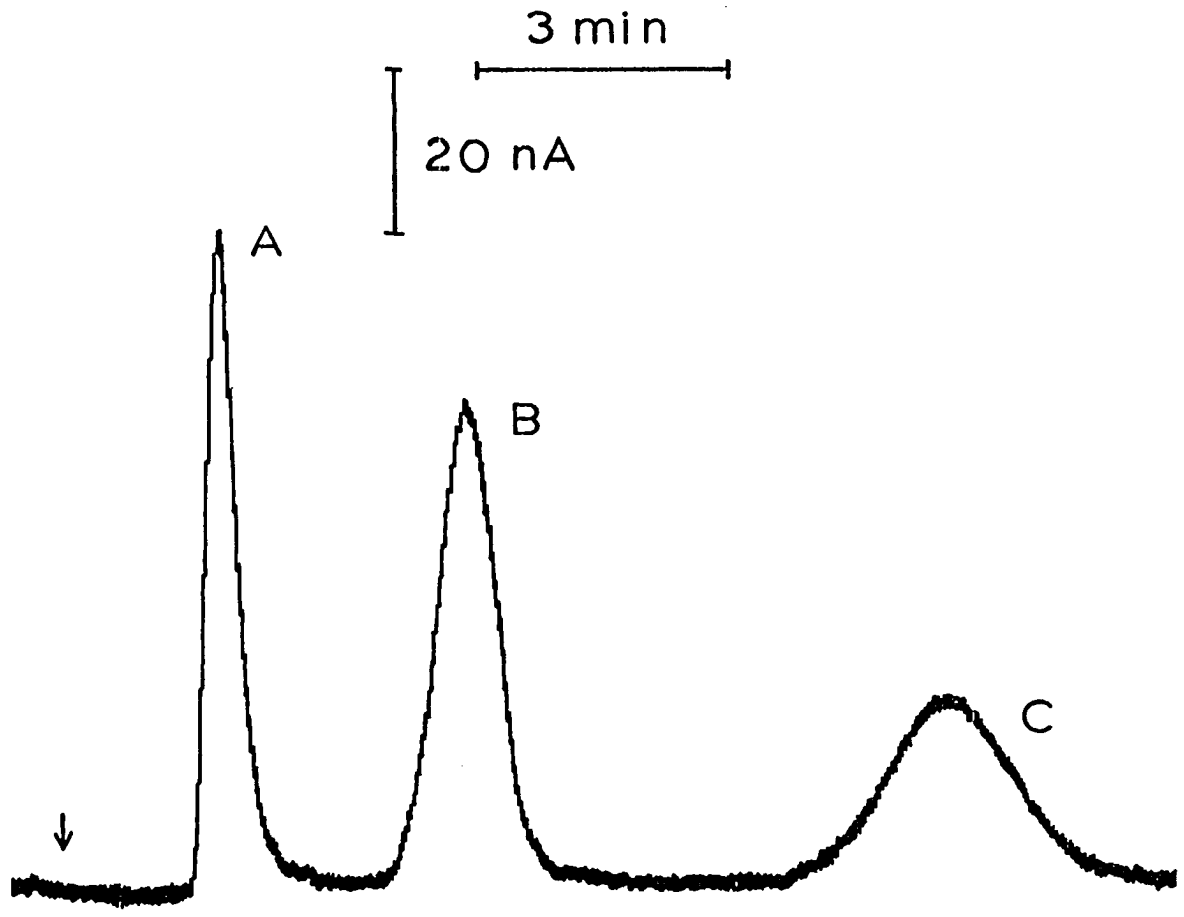
3 min
20 nA
A
B
C

compound of Cd with Au in the film is not an explanation for peak tailing. When Cu(II) and Zn(II) were included in the sample, they were eluted simultaneously with Cd(II). An alternate approach was needed for the separation of these three metal ions.

Figures IV-18 and IV-19 present the chromatographic separations of Cu(II), Zn(II), Pb(II) and Cd(II) obtained with a column of AG 50W X 8 (37 - 44 μm), a cation-exchange resin of full capacity. Figure IV-18 was obtained with the HMDE and Figure IV-19 was obtained with the SDME. The baseline separations were achieved within 30 min for the isocratic elution with 0.3 M tartaric acid/ 0.02 M NaCl at pH 3.30. This chromatographic method was adapted from similar methods by Takata and Muto (101), and Girard (102). An increase in the concentration of tartaric acid or an increase of the pH of the eluent decreased the retention times of Cu(II), Zn(II) and Pb(II) with little effect on that for Cd(II). Cu(II) was only slightly retained under these conditions. The retention time for Cd(II) was decreased by increasing the concentration of Cl^- in the eluent. Good separations were obtained within a reasonable period of time. Again, peak definition in the response of the SDME was only slightly better than the stationary electrode, the HMDE. The most significant difference in peak widths was for the peaks of Cd(II) which appeared at the end of the chromatograms.

The chromatographic experiments illustrated that the TFME, HMDE and SDME with detection by RPA are compatible for use with CELC. The stationary Hg electrodes, the TFME and the HMDE, produce chromatographic

Figure IV-18. Chromatographic separation of Cu(II), Zn(II), Pb(II) and Cd(II) with detection by the HMDE

E_i - -1.20 V versus SSCE

E_f - +0.10 V versus SSCE

T - 0.5 sec

V_f - 1.0 mL min^{-1}

V_s - 0.206 mL

injection - 10^{-4} M in each metal ion

eluent - 0.3 M tartaric acid/0.02 M NaCl at pH 3.30

column - AG 50W X 8, cation-exchange resin (37 - 44 μm), 4-mm i.d. x 100 mm

peaks - A = Cu(II)

B = Zn(II)

C = Pb(II)

D = Cd(II)

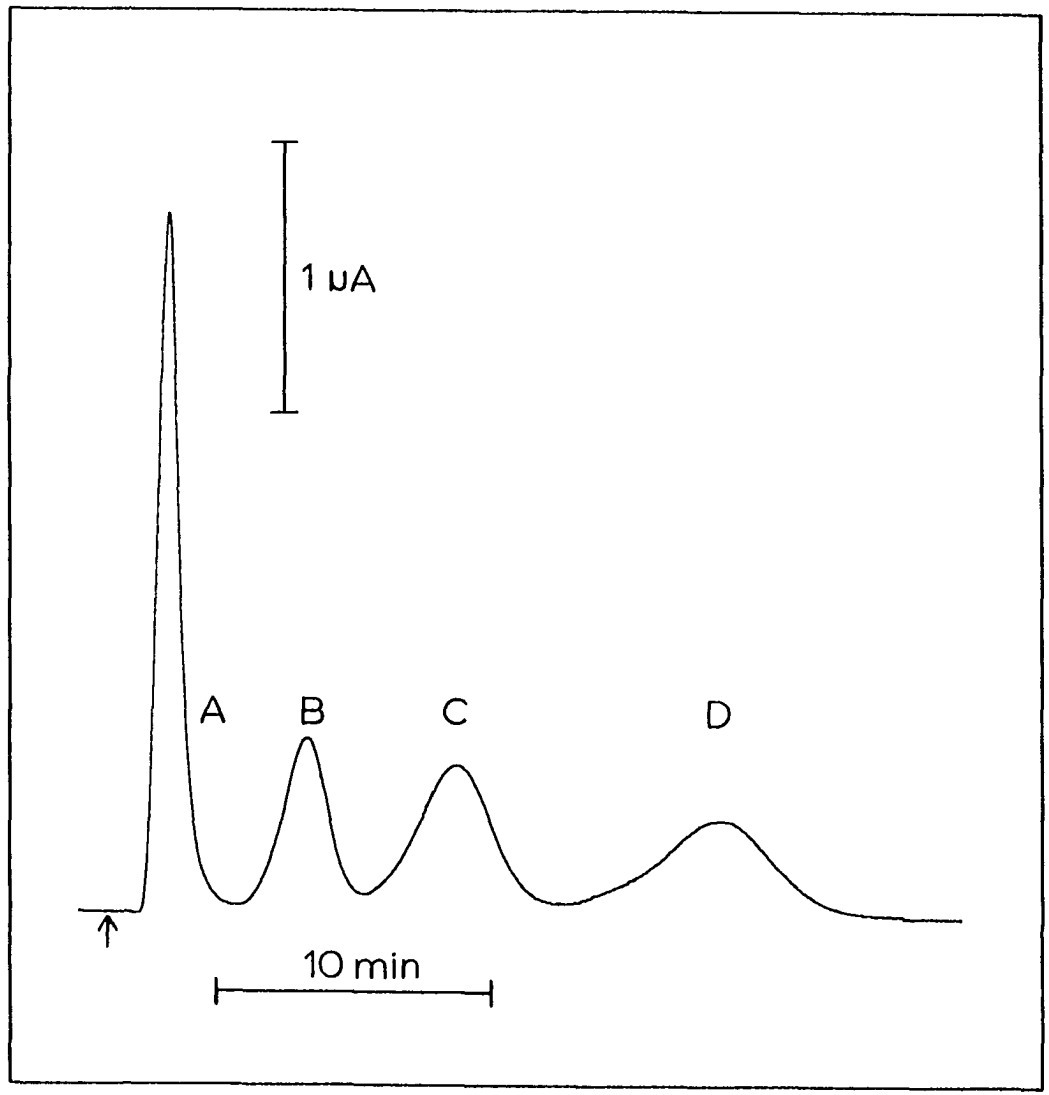
1 µA
A
B
C
D
10 min

Figure IV-19. Chromatographic separation of Cu(II), Zn(II), Pb(II) and Cd(II) with detection by the SDME

E_i - -1.20 V versus SSCE

E_f - +0.10 V versus SSCE

T - 2 sec

V_f - 1.0 mL min^{-1}

V_s - 0.206 mL

injection - 10^{-4} M in each metal ion

eluent - 0.3 M tartaric acid/0.02 M NaCl at pH 3.30

column - AG 50W X 8, cation-exchange resin (37 - 44 μm), 4 mm-i.d. x 100 mm

peaks - A = Cu(II)

B = Zn(II)

C = Pb(II)

D = Cd(II)

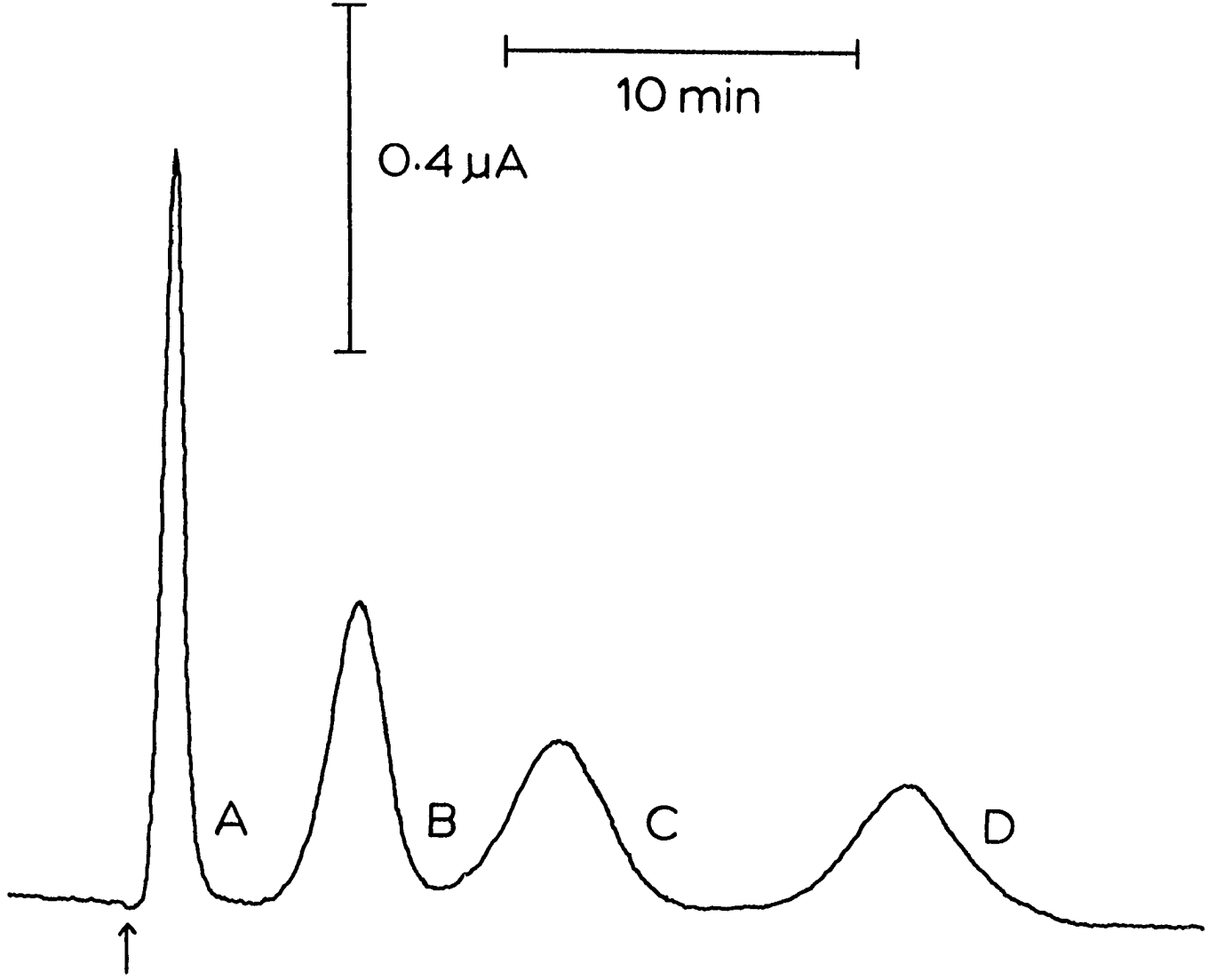
10 min
0·4 µA
A
B
C
D

peaks which have slightly more tailing than those observed with the SDME, as is expected. Excessive peak tailing observed for the detection of Cd(II) with the TFME is not well-understood. The selection of either the HMDE or SDME is justified for analytical applications with CELC.

7. Conclusions

The TFME, HMDE and SDME were evaluated as indicating electrodes of EC detectors for RPA. The response of these electrodes was comparable in terms of peak definition, precision and compatibility for use with CELC. When using peak height as the analytical measurement, the response of the HMDE was virtually independent of flow rate. Peak heights were also independent of flow rate for the SDME at flow rates > 0.9 mL min^{-1}. However, the HMDE has a large range of linear response with excellent linearity, and also a low detection limit compared to the TFME and SDME. Therefore, the HMDE was used with the EC detector for the analysis of a "real" sample, as is presented in Section V.

V. DETERMINATION OF Pb IN ORCHARD LEAVES BY REVERSE PULSE AMPEROMETRY

A. Introduction

The ultimate appraisal of any technique proposed for chemical analysis can come only after the application of the technique to the analysis of a "real" sample. A "real" sample presents a challenge to the analyst in that methods of sample dissolution and analyte isolation often must be devised to produce a sample solution with a matrix which is compatible with the experimental conditions for the determination of the analyte(s) by the new technique. The quantitative result of the determination must be accurate and reproducible in order to confirm that the technique is practical for application to chemical analysis.

A sample of orchard leaves was chosen to be analyzed by RPA. Orchard leaves is one of several biological matrices which are Certified Standard Reference Materials for trace metals available from the National Bureau of Standards. A list of the constituents of the orchard leaves (NBS SRM 1571) is given in Table V-1. The sample of orchard leaves was considered to provide a good test for the application of RPA because dissolution of the sample and separation of the metal ions were necessary to prepare the sample for final analysis. The orchard leaves were dissolved by wet digestion with an acid mixture of HNO_3, $HClO_4$ and H_2SO_4. The metal ions, Cu(II), Zn(II) and Pb(II), were separated with a chromatographic column of AG 50W X 8 cation-exchange resin. The metal ions were isocratically eluted with

Table V-1. Constituents present in the orchard leaves

Constituent	Concentration
Nitrogen	2.76 ± 0.05%
Calcium	2.09 ± 0.03%
Potassium	1.47 ± 0.03%
Magnesium	0.62 ± 0.02%
Phosphorus	0.21 ± 0.01%
Iron	300 ± 20 ppm
Manganese	91 ± 4
Sodium	82 ± 6
Lead	45 ± 3
Boron	33 ± 3
Zinc	25 ± 3
Arsenic	14 ± 2
Copper	12 ± 1
Rubidium	12 ± 1
Nickel	1.3 ± 0.2
Mercury	0.155 ± 0.015
Cadmium	0.11 ± 0.02
Selenium	0.08 ± 0.01
Uranium	0.029 ± 0.005

0.17 M tartaric acid containing 0.01 M NaCl at pH 3.30. The method of standard addition was used to quantitatively determine Pb in the orchard leaves.

B. Experimental

1. Instrumentation

The flow-analyzer used for this work was a modified version of that described in Section III.C.1. During the development of the procedure for the analysis of the orchard leaves, a pump normally used for HPLC, and capable of delivering eluents at high pressure, was available. The pump was a Milton-Roy dual piston pump (Model CK) which was used with an LDC Pulse Dampener to produce eluent flow through the ion-exchange column at a pressure of about 400 psi. This pump is described in detail in Reference 122. A glass column of dimensions 2-mm i.d. x 125 mm was packed with 37 - 44 μm, AG 50W-X 8, cation-exchange resin and utilized for the separation of the metal ions. The detector was the Model 310 Polarographic LC Detector from EG&G Princeton Applied Research.

2. Chemicals

All chemicals were Analytical Reagent Grade except where noted. The sample of NBS Standard Reference Material 1571 (orchard leaves) was dated April 10, 1979, and was stored according to the instructions included with the sample. The orchard leaves were analyzed during December 1979. All water was triply distilled. Demineralization

occurred after the first distillation and the second distillation was from an alkaline permanganate solution (0.01 M $KMnO_4$/0.1 M NaOH).

3. Procedures

The compound $Pb(NO_3)_2$ was used as the standard for Pb(II) as recommended by Smith and Parsons (123). The $Pb(NO_3)_2$ was dried for 6 hr at 110 °C and stored in a desiccator with $CaSO_4$ as the desiccant. Standard solutions of Pb(II) were prepared by weighing the appropriate amount of $Pb(NO_3)_2$ to produce a solution of 1.000×10^{-2} M Pb(II) in a 100-mL volumetric flask. The diluent was 0.01 M HNO_3.

The orchard leaves were dried for 6 hr at 67 °C and stored alone in a desiccator with $CaSO_4$ as the desiccant. The desiccator was stored in a dark, dry cabinet.

Samples of orchard leaves weighing approximately 1.5 g were weighed accurately for analysis. The sample was transferred to a 250-mL Erlenmeyer flask. The mixture of the concentrated acids added to the sample was 10 mL HNO_3, 10 mL $HClO_4$ and 3 mL H_2SO_4. A reflux condenser was placed on top of the flask and the flask was heated on a hot plate. The temperature was steadily raised until reddish-brown fumes from the oxides of nitrogen were observed and then gradually raised to 203 °C as determined with a thermometer. The $HClO_4$ was completely volatilized. The wet digestion was complete only when fumes of H_2SO_4 were evolved, i.e., at a temperature greater than 203 °C. The sample was allowed to cool slightly and then transferred to a 50-mL volumetric flask. On reaching room temperature, the sample

solution was diluted to the mark with triply distilled water. The acid content of the sample solution, as a result of the dissolution procedure, was 0.53 M H_2SO_4.

The dissolution procedure did not completely dissolve the sample. A small amount of residual silica was present in the sample and some silica was carried over in every transfer.

C. Results and Discussion

1. Preliminary investigations for the analysis of the orchard leaves

The SDME was tested as an indicating electrode for the analysis of the orchard leaves with CELC in spite of the observation of a non-linear calibration curve for Pb(II) with this electrode in FIA. The use of the SDME has the advantage of a renewable and reproducible electrode surface. Therefore, any possible contamination of the electrode surface by the sample solution can be avoided. The response of the SDME to an injection of the sample is shown in Figure V-1. The large fluctuations in the background current relative to the analytical signal, as observed at such a high setting of the current sensitivity, made the use of the SDME impractical. Thus, the SDME was not applied in this analysis. The remainder of the analytical work was performed with the HMDE as the indicating electrode.

A blank determination was obtained with the HMDE for pure water using the identical procedure described for analysis of the orchard leaves. The result is shown in Figure V-2. A detector response is observed at Point A with the HMDE and corresponds to a nonzero blank

Figure V-1. Analysis of the orchard leaves with the SDME

E_i - -1.20 V versus SSCE

E_f - +0.10 V versus SSCE

T - 2 sec

V_f - 1.0 mL min^{-1}

V_s - 0.206 mL

media - 0.17 M tartaric acid/0.01 M NaCl at pH 3.30

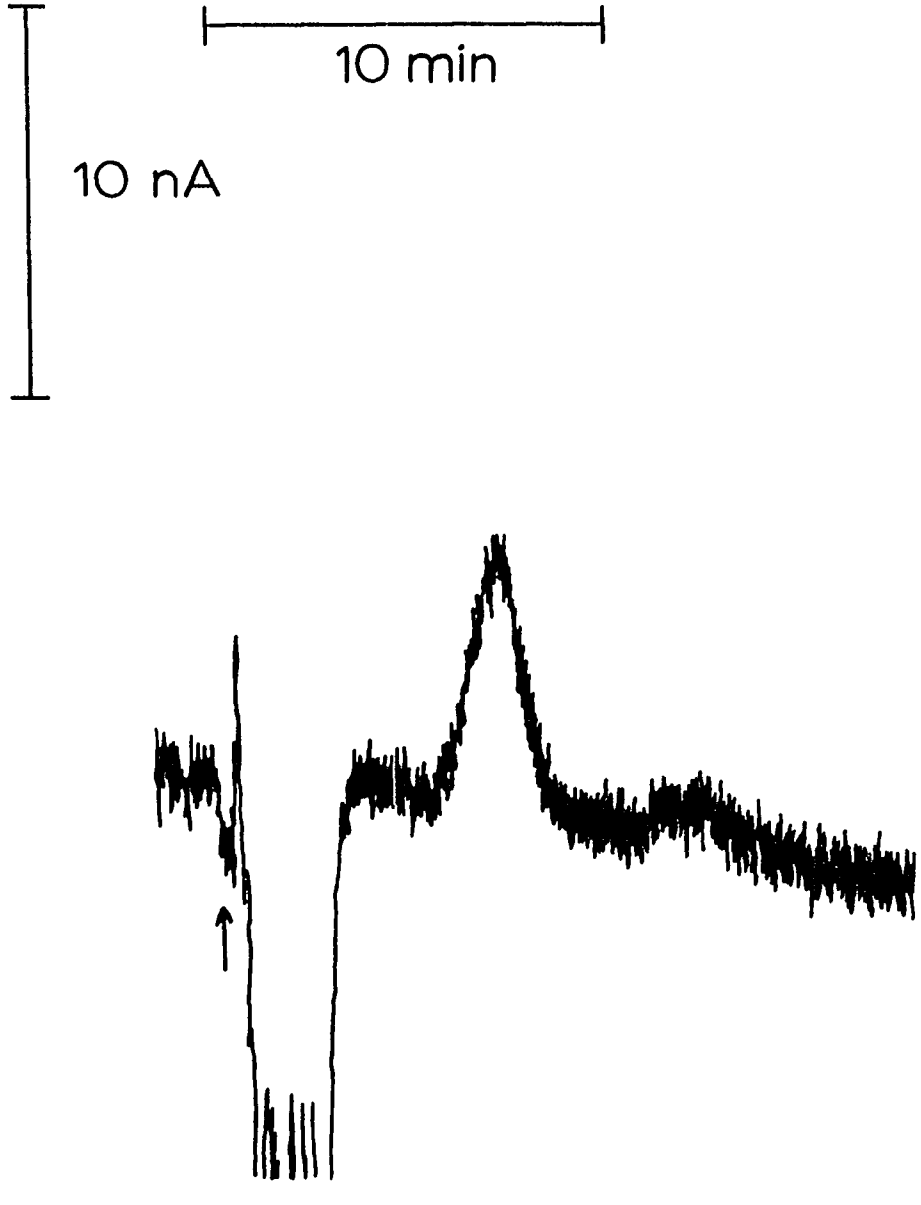
10 min
10 nA

Figure V-2. Determination of the blank with the HMDE

E_i - -1.20 V versus SSCE

E_f - +0.10 V versus SSCE

T - 0.5 sec

V_f - 1.0 mL min^{-1}

V_s - 0.206 mL

media - 0.17 M tartaric acid/0.01 M NaCl at pH 3.30

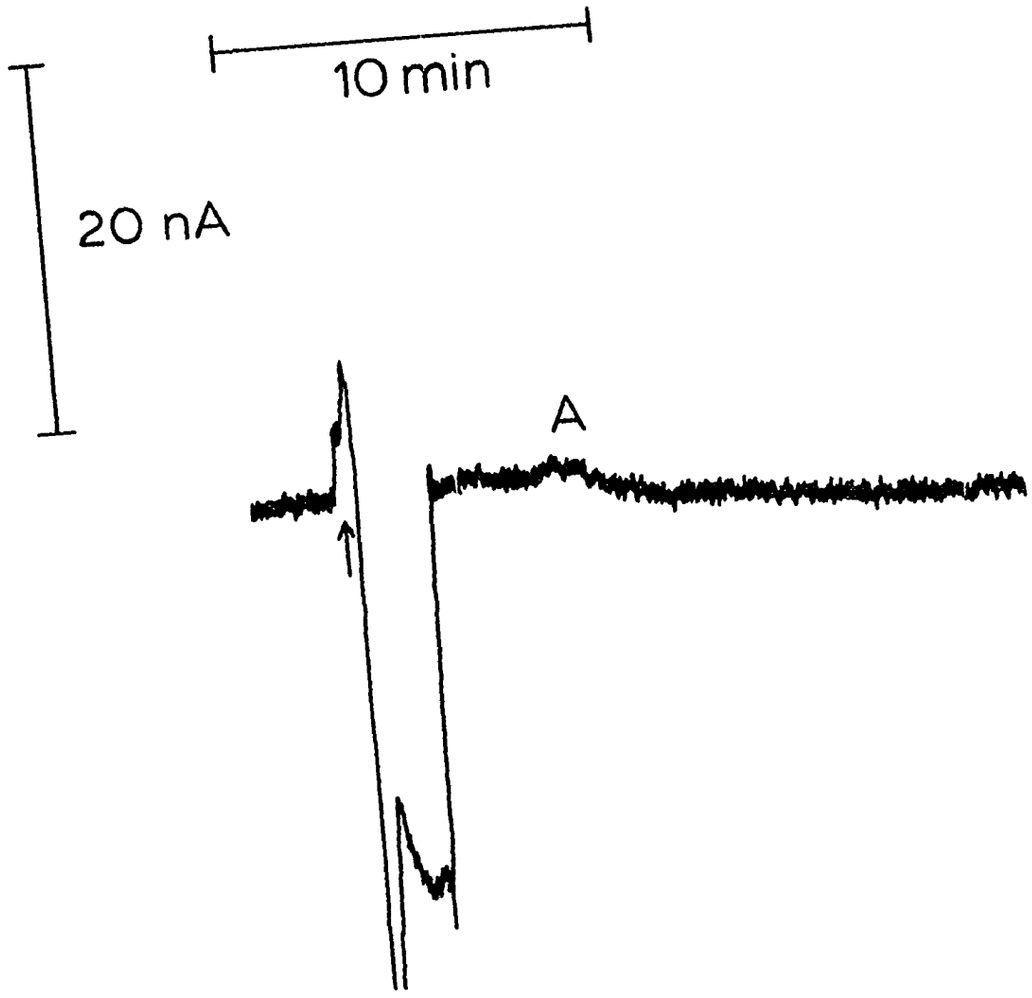
10 min
20 nA
A

for Zn(II). The amount of Zn(II) in the blank was significant compared to the amount in the sample and the quantitative determination of Zn in the orchard leaves was, therefore, not attempted. No Pb(II) was detected in the blank.

The precision of the response for Pb(II) by RPA with the HMDE was evaluated for 6 x 10^{-6} M Pb(II) in 0.53 M H_2SO_4. The cation-exchange column was present in the flow-analyzer. The eluent was 0.17 M tartaric acid containing 0.01 M NaCl at pH 3.30. The concentration of Pb(II) was within the range used for the method of standard addition and the supporting electrolyte of 0.53 M H_2SO_4, approximated the matrix of the sample solution for the analysis of the orchard leaves. A relative standard deviation of 4.0% for the measurement of peak area was determined for 7 injections of the Pb(II) solution under the experimental conditions of the analysis. The precision was concluded to be acceptable.

2. Determination of Pb by the method of standard addition

The determination of Pb in the orchard leaves was performed in duplicate by the method of standard addition. The selection of the method of standard addition was justified because of the possible difficulty in reproducing the matrix of the sample solution in a standard sample, and the fact that Pb(II) was not detected in the blank.

The preparation of the standard solution for Pb(II) and the sample solution of the orchard leaves is described in Section V.B.3.

A standard stock solution of 6.00×10^{-5} M Pd(II) was prepared. A 5-mL aliquot of the sample solution was transferred to each of a series of 10-mL volumetric flasks. Aliquots of the standard solution with volumes of 0 mL, 0.5 mL, 1.0 mL, etc., were then added to the successive flasks. Dilutions were made with triply distilled water. Injections of 0.206 mL were made for each solution. Determinations for each solution were obtained in duplicate.

Figure V-3 illustrates the chromatograms observed for injections of sample solutions with standard additions of Pb(II). The baseline shift following each injection is the response of the detector to the H_2SO_4 in the sample plug. Peaks a, b and c are for Cu(II), Zn(II) and Pb(II), respectively. Peak areas rather than peak height were used as a quantitative measurement of Pb(II). Figure V-3 also illustrates the graphical procedure used to define the peaks for Pb(II) which were then integrated with a planimeter. The results of the two determinations are given in Table V-2. The plots of peak area, Q, versus μg Pb added are shown in Figure V-4. The lines through the data, as well as the intercept with the x-axis, were determined by a least-squares calculation. The average value of the two results for the determination of Pb in the orchard leaves is 45.4 μg g^{-1}. The orchard leaves have a certified value of 45 ± 3 μg g^{-1} for Pb as determined by isotopic dilution spark source mass spectroscopy, photon activation analysis and polarography. The certificate for analysis also gives an uncertified value of 44 μg g^{-1} for Pb for a sample of orchard leaves which was dissolved with a mixture of HNO_3 and $HClO_4$. The results of the

Figure V-3. Determination of Pb in the orchard leaves by RPA with the HMDE and the method of standard addition

E_i - -1.20 V versus SSCE

E_f - +0.10 V versus SSCE

T - 0.5 sec

V_f - 1.0 mL min^{-1}

V_s - 0.206 mL

media - 0.17 M tartaric acid/0.01 M NaCl at pH 3.30

Determination I - A = 0 µg Pb added

B = 6.22 µg Pb added

C = 12.4 µg Pb added

a - Cu(II)

b - Zn(II)

c - Pb(II)

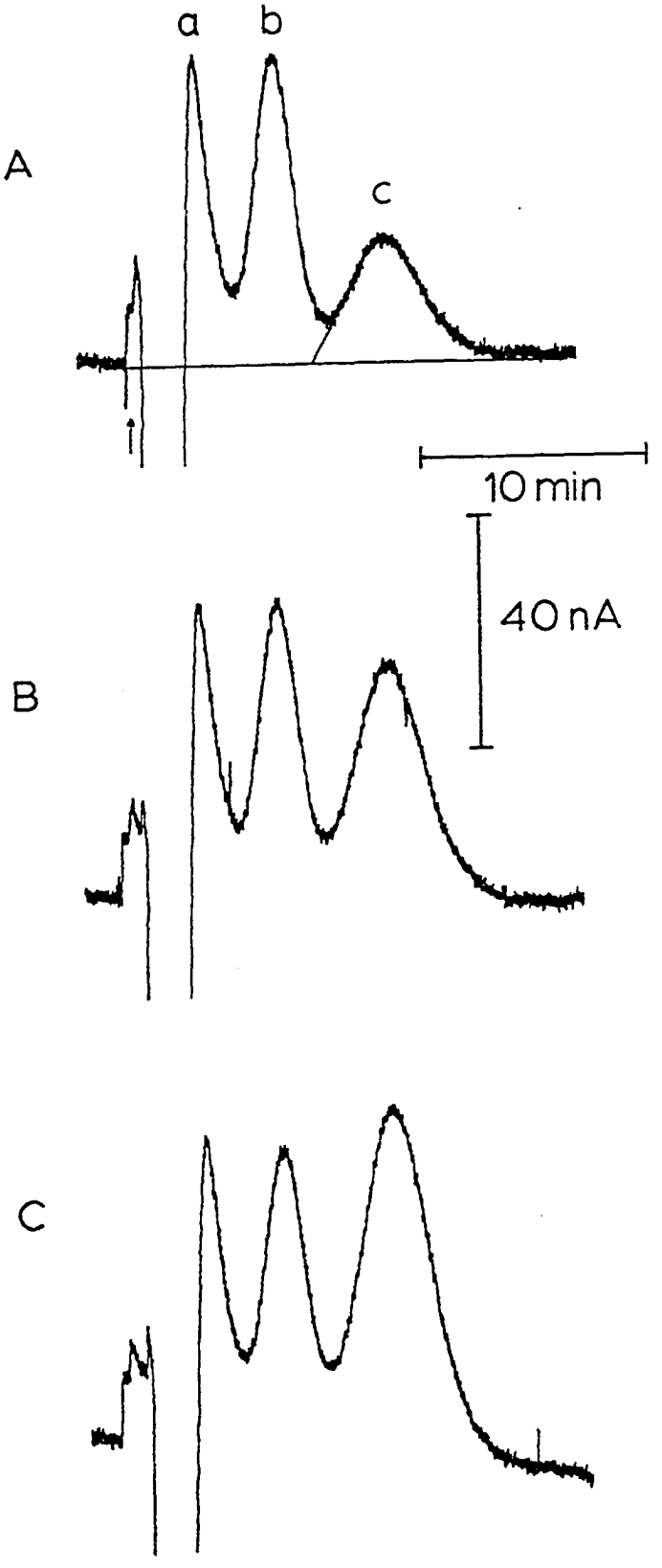
a
b
c
A
10 min
40 nA
B
C

Table V-2. Determination of Pb in the orchard leaves by the method of standard addition

Determination I. 44.7 μg Pb g^{-1}		
Sample	μg Pb added	Q (μcoul)
1	0	4.62
2	6.22	9.59
3	12.4	13.5

Determination II. 46.2 μg Pb g^{-1}		
Sample	μg Pb added	Q (μcoul)
1	0	4.54
2	6.22	7.75
3	12 4	11.2
4	18.7	15.4
5	24.9	19.4

Figure V-4. Q versus μg Pb added for the determination of Pb in the orchard leaves

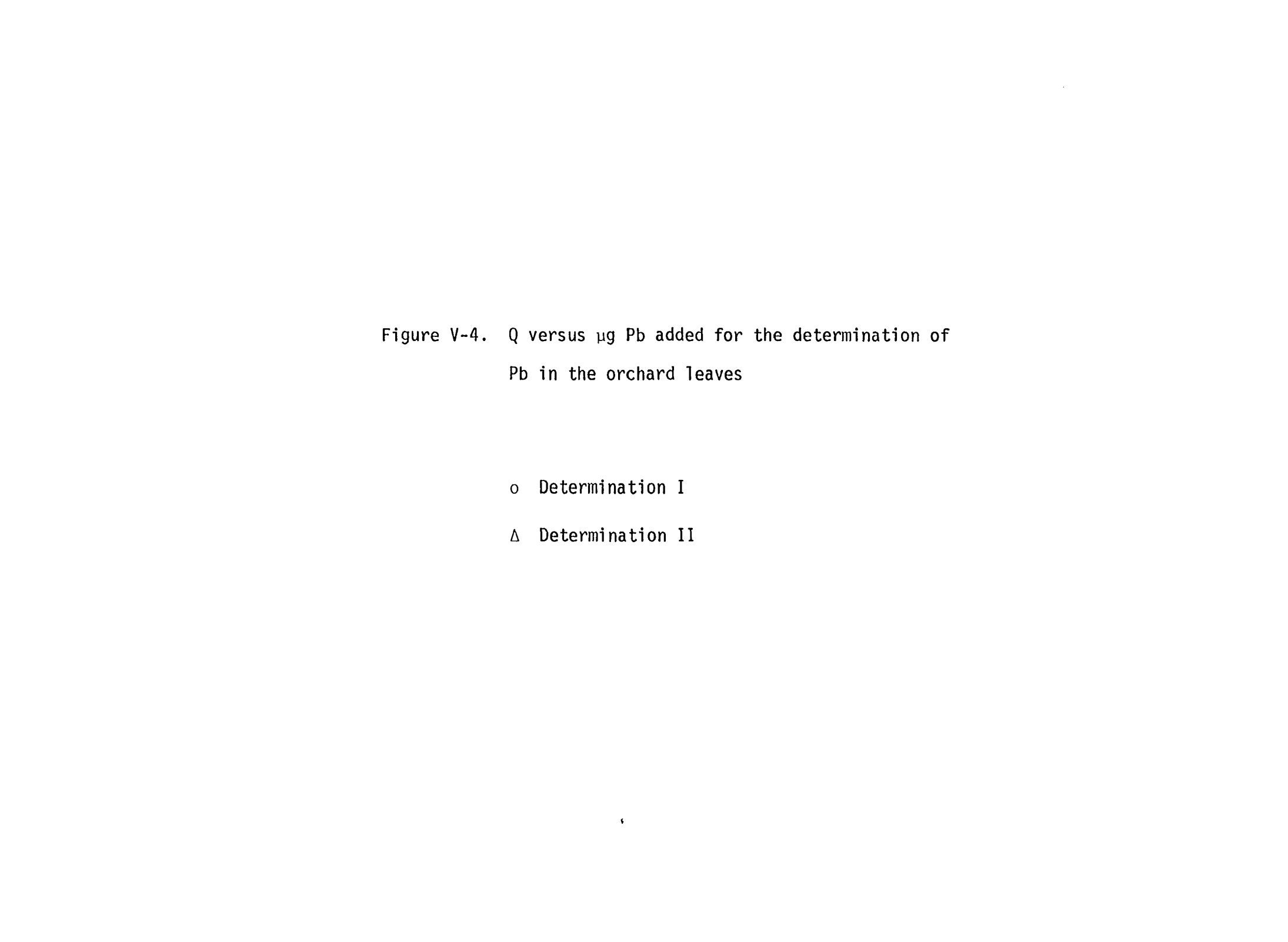

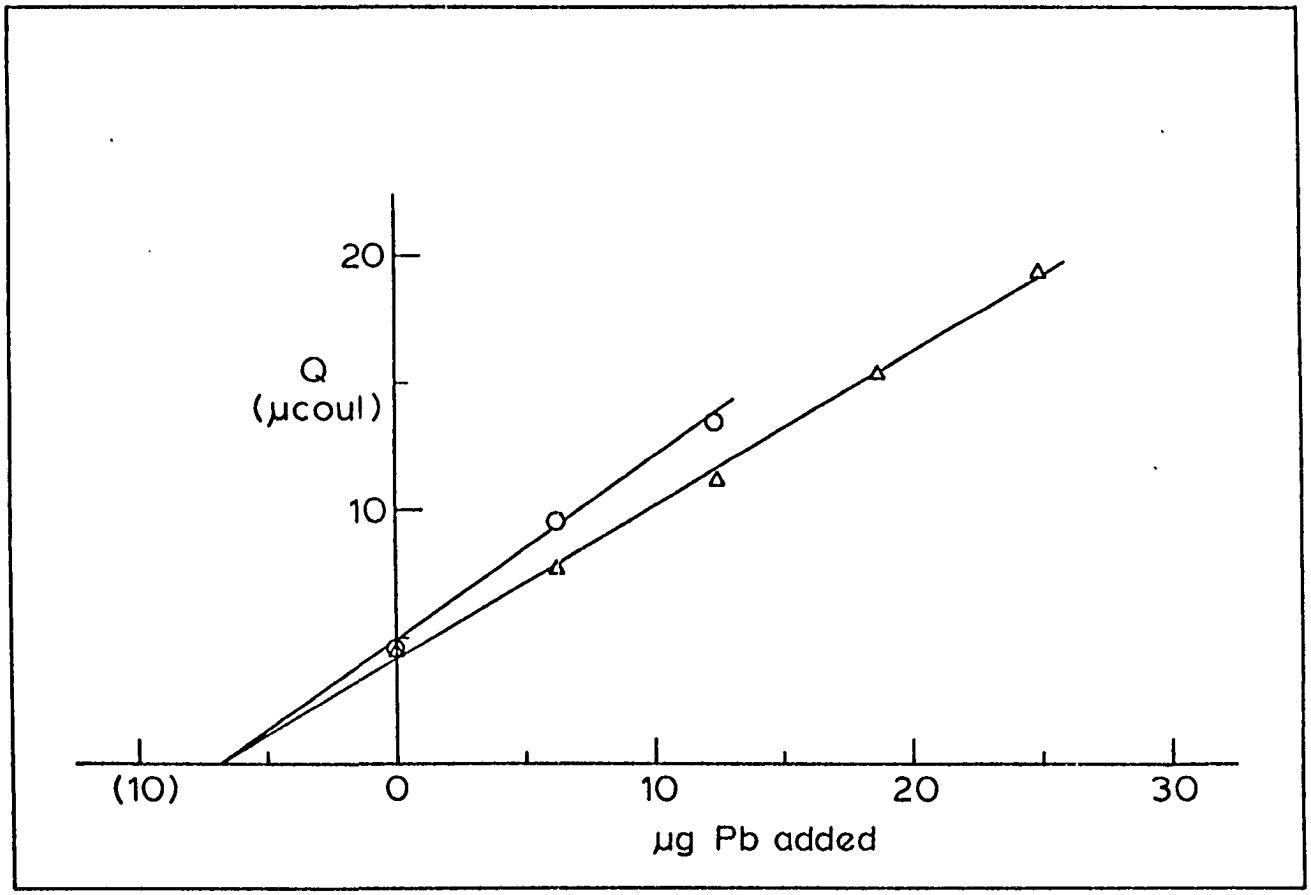
20
Q
(µcoul)
10
(10)
0
10
20
30
µg Pb added

determination described in this dissertation agree well with the value which is certified.

3. Conclusions

The method of RPA was applied with a HMDE and CELC to determine Pb in a standard reference material (NBS SRM 1571) of orchard leaves. The orchard leaves were prepared for analysis by wet digestion with an acid mixture of HNO_3, $HClO_4$ and H_2SO_4. The standard-addition method was used to quantitatively determine the Pb content of the orchard leaves. The results agreed very well with the value certified by the National Bureau of Standards.

VI. SUMMARY

Reverse pulse amperometry has been proposed as an electroanalytical technique which, when applied at a Hg indicating electrode, is capable of routinely monitoring fluid streams for metal ions without the requirement of deaeration. RPA is based on the application of an unsymmetrical pulsed-potential waveform to produce an electroanalytical signal which is proportional to the concentration of metal ion and is measured at a potential where dissolved oxygen does not undergo an electrochemical reaction. Neither dissolved oxygen nor hydrogen peroxide were found to interfere with the quantitative determination of several metal ions tested. A large variety of metal ions, including Pb(II), Tl(I), Fe(III), Sb(III), Ni(III) and VO_3^-, were found to be detectable by RPA despite the difference in the nature of their electrochemical reactions on Hg.

An approximate mathematical derivation was presented to describe the response of RPA. Equations derived were useful in explaining qualitative differences in the response observed as a function of several experimental variables.

RPA was applied with the thin-film mercury electrode (TFME), hanging mercury-drop electrode (HMDE) and "static" dropping mercury electrode (SDME) and the response of these electrodes was compared for the detection of Pb(II). Comparison was based on peak definition, dependence of the peak on pulse period and flow rate, precision of analytical results, linear dynamic range, detection limit and

compatibility for use with cation-exchange liquid chromatography. The HMDE was found to provide the largest range of response with excellent linearity. The lowest detection limit for Pb(II) was also found for use of the HMDE. Peak height as the analytical measurement with the HMDE was found to be virtually independent of flow rate.

RPA was applied with a HMDE and cation-exchange liquid chromatography to determine Pb in a standard reference material from the National Bureau of Standards (NBS SRM 1571, orchard leaves). The method of standard addition was used to quantitatively determine the Pb content. The results obtained agreed well with the certified value for Pb.

VII. SUGGESTIONS FOR FUTURE RESEARCH

The technique of RPA has been introduced in this dissertation and some of the most important questions concerning the application of RPA to chemical analysis have been answered. A considerable amount of work is yet to be done if all of the capabilities RPA has to offer for chemical analysis are to be determined. Several suggestions for future research are included here.

Electronic circuitry can be modified to improve the detection limits for metal ions when using the 174A Polarographic Analyzer for RPA. The use of sample-and-hold circuits which can reduce the electronic noise observed with the present circuitry should significantly improve the signal-to-noise ratio. In addition, the 174A Polarographic Analyzer does not have RC circuitry which is conveniently capable of varying t_i, t_p and T over a large range of values suitable for RPA. For instance, if t_p could be shortened to provide a current measurement 20 msec after application of the anodic pulse rather than 57 msec, a substantial increase in the analytical signal should be observed. The capability of being able to conveniently vary t_i, t_p and T would facilitate the optimization of these parameters for RPA as applied in chemical analysis. The RC circuitry for the Model 303 SMDE should also be modified in order to produce a Hg drop with a continuously variable size to optimize the area-to-volume ratio of the Hg drop.

The TFME used in this work deserves further study. As previously mentioned, the TFME appears to be the most suitable Hg electrode for

application to RPA because of its large area-to-volume ratio. A glassy-carbon disk electrode is available from EG&G Princeton Applied Research which can be directly applied with the Model 303 SMDE and also used with the Model 310 Polarographic LC Detector. The glassy carbon disk is designed so that the glassy carbon surface can be easily polished; and, therefore, it should be possible to electrodeposit a strongly adherent film of Hg, or Hg and Au, on this electrode. The electrode design makes it possible to easily disassemble the EC detector for surface analysis of the deposited film. The design circumvents the problems of electrode leakage which are a characteristic of the tubular electrode. The application of RPA with a TFME which produces a relatively low noise in the background current should result in detection limits for metal ions at sub-ppb levels; especially with the modification of the electronic circuitry suggested above.

Methods of HPLC are available for the ion-exchange separation of the metal ions of Cu, Zn, Cd, Pb, Ni and Mn (95,100,101,102). The time necessary for a complete separation of these species has been shown to be less than 8 min. RPA has been shown to be compatible with CELC and the combination of these techniques has been used to analyze orchard leaves. RPA should be applied with high-performance, CELC in order to evaluate the full impact this technique has on routine chemical analysis. Indeed, this application appears to be very promising.

The technique of NPA can be used for the detection of anions which form slightly dissociated compounds with Hg(I,II). A value for E_f can be chosen to coincide with the mass transport-limited oxidation

of Hg(I,II) because of the presence of the anion; and, a value for E_i can be chosen to clean the Hg electrode of any film which is formed at E_f. Preliminary work of this nature demonstrated that Cl^-, Br^-, I^- and SCN^- could be detected in a fluid stream following a separation by anion-exchange liquid chromatography with a low-capacity resin. This approach will be useful in those cases where the added selectivity provided by an EC detector is necessary.

VIII. BIBLIOGRAPHY

1. Browning, E. "Toxicity of Industrial Metals", 2nd ed.; Butterworths: London, England, 1969.

2. Morgan, G. B.; Bretthauer, E. W. Anal. Chem. 1977, 49, 1210A.

3. Luckey, L. D.; Venugopal, B.; Hutcheson, D. "Heavy Metal Toxicity, Safety and Hormology"; Academic Press: New York, New York, 1975; Chapters 1, 4.

4. Di Cyan, E. "Vitamins in your Life"; Simon and Schuster: New York, New York, 1974; Chapter 11.

5. Wolf, W. R. Anal. Chem. 1978, 50, 190A.

6. Sunderman, F. W., Jr. In "Toxicology of Trace Elements", Goyer, R. A.; Mehlman, M. A., Eds.; "Advances in Modern Toxicology"; John Wiley & Sons: New York, New York, 1977; Volume 2, Chapter 9.

7. Betteridge, D. Anal. Chem. 1978, 50, 832A.

8. Ruzicka, J.; Hansen, E. H.; Mosbaek, H. Anal. Chim. Acta 1977, 92, 235.

9. Kissinger, P. T. Anal. Chem. 1977, 49, 447A.

10. Michel, L.; Zatka, A. Anal. Chim. Acta 1979, 105, 109.

11. Pinta, M. "Modern Methods for Trace Element Analysis"; Ann Arbor Sciences: Ann Arbor, Michigan, 1978; Chapters 4, 6.

12. Sturgeon, R. E. Anal. Chem. 1977, 49, 1255A.

13. Pinta. M. "Modern Methods for Trace Element Analysis"; Ann Arbor Science: Ann Arbor, Michigan, 1978; Chapters 5, 6.

14. Dulka, J. J.; Risby, T. H. Anal. Chem. 1976, 48, 640A.

15. Fassel, V. A.; Kniseley, R. N. Anal. Chem. 1974, 46, 1110A.

16. Fassel, V. A. Science 1978, 202, 183.

17. Fassel, V. A. Anal. Chem. 1979, 51, 1291A.

18. Pinta, M. "Modern Methods for Trace Element Analysis"; Ann Arbor Science: Ann Arbor, Michigan, 1978; Chapter 9.

19. Wang, C. H.; Willis, D. L.; Loveland, W. D. "Radiotracer Methodology in the Biological, Environmental and Physical Sciences"; Prentice-Hall: Englewood Cliffs, New Jersey, 1975; Chapter 17.

20. Roboz, J. In "Trace Analysis - Physical Methods", Morrison, G. H., Ed.; Interscience: New York, New York, 1965; Chapter 11.

21. Prescott, S. R.; Campana, J. E.; Jurs, P. C.; Risby, T. H.; Yergey, A. T. Anal. Chem. 1976, 48, 829.

22. Pinta, M. "Modern Methods for Trace Element Analysis"; Ann Arbor Science: Ann Arbor, Michigan, 1978; Chapter 8.

23. Guiochon, G.; Pommier. C. "Gas Chromatography in Inorganics and Organometallics"; Ann Arbor Science: Ann Arbor, Michigan, 1973; Chapter VIII.

24. Meites, L. "Polarographic Techniques"; Interscience: New York, New York, 1955.

25. Parry, E. P.; Osteryoung, R. A. Anal. Chem. 1965, 37, 1634.

26. Turner, J. A.; Abel, R. H.; Osteryoung, R. A. Anal. Chem. 1975, 47, 1343.

27. Canterford, D. R. J. Electroanal. Chem. 1974, 52, 144.

28. Osteryoung, J. G.; Christie, J. H.; Osteryoung, R. A. Bull. Soc. Chim. Belges 1975, 84, 647.

29. Klein, N.; Yarnitsky, Ch. J. Electroanal. Chem. 1975, 61, 1.

30. Christie, J. H.; Osteryoung, R. A. J. Electroanal. Chem. 1974, 49, 301.

31. Oldham, K. B.; Parry, E. P. Anal. Chem. 1966, 38, 867.

32. Osteryoung, J. G.; Osteryoung, R. A. Amer. Lab. 1972, 44, 8.

33. Brooks, M. A.; de Silva, J. A. F.; Hackman, M. R. Amer. Lab. Dec., 1973.

34. Vydra, F.; Stulik, K.; Julakova, E. "Electrochemical Stripping Analysis"; John Wiley & Sons: New York, New York, 1976.

35. Brainina, Kh. Z. "Stripping Voltammetry in Chemical Analysis"; John Wiley & Sons: New York, New York, 1974.

36. Copeland, T. R.; Skogerboe, R. K. Anal. Chem. 1974, 46, 1257A.

37. Allen, H. E.; Matson, W. R.; Mancy, K. H. J. Water Pollut. Contr. Fed. 1970, 42, 573.

38. Roe, D. K.; Toni, J. E. A. Anal. Chem. 1965, 37, 1503.

39. Stulikova, M. J. Electroanal. Chem. 1973, 48, 33.

40. Florence, T. M. J. Electroanal. Chem. 1970, 27, 273.

41. Hume, D. N.; Carter, J. N. Chem. Anal. (Warsaw) 1972, 17, 747.

42. Florence, T. M.; Farrar, Y. J. J. Electroanal. Chem. 1974, 51, 191.

43. Florence, T. M. J. Electroanal. Chem. 1974, 49, 255.

44. Nurnberg, H. W. Electrochim. Acta 1977, 22, 935.

45. Christian, G. D. J. Electroanal. Chem. 1969, 23, 1.

46. Valenta, P.; Mart, L.; Rutzel, H. J. Electroanal. Chem. 1977, 82, 327.

47. Batley, G. E.; Florence, T. M. J. Electroanal. Chem. 1974, 23, 55.

48. De Angelis, T. P.; Heineman, W. R. Anal. Chem. 1976, 48, 2262.

49. Siegerman, H.; O'Dom, G. Amer. Lab. 1972, 4, 59.

50. Lund, W.; Eriksen, R. Anal. Chim. Acta 1979, 107, 37.

51. Copeland, T. R.; Christie, J. H.; Osteryoung, R. A.; Skogerboe, R. K. Anal. Chem. 1973, 45, 2171.

52. Swartzfager, D. G. Anal. Chem. 1976, 48, 2189.

53. MacDonald, A.; Duke, P. D. J. Chromatogr. 1973, 83, 331.

54. Stulik, K.; Hora, V. J. Electroanal. Chem. 1976, 70, 253.

55. Meschi, P. L. Chemistry Dept., Iowa State University, Ames, Iowa, Sept. 1978; private communication.

56. Wang, J.; Ouziel, E.; Yarnitsky, Ch.; Ariel, M. Anal. Chim. Acta 1978, 102, 99.

57. Drake, B. Acta Chem. Scand. 1950, 4, 554.

58. Kemula, W. Rocz. Chem. 1952, 26, 281; Chem. Abstr. 1950, 44, 8408g.

59. Lewis, J. A.; Overton, K. C. Analyst (London) 1954, 79, 293.

60. Wilson, L. D.; Smith, R. J. Anal. Chem. 1953, 25, 218.

61. Mann, C. K. Anal. Chem. 1957, 29, 1385.

62. Tustanowskii, S. J. Chromatogr. 1967, 31, 266.

63. Rebertus, R. L.; Capell, R. L.; Bond, G. W. Anal. Chem. 1958, 30, 1825.

64. Blaedel, W. J.; Todd, J. W. Anal. Chem. 1958, 30, 1821.

65. Blaedel, W. J.; Strohl, J. H. Anal. Chem. 1961, 33, 1631.

66. Blaedel, W. J.; Strohl, J. H. Anal. Chem. 1964, 36, 445.

67. Hartmann, H.; Budan, G. Chem. Ztg. 1950, 74, 606.

68. Mairanovskii, S. G.; Barashkova, N. V.; Vol'kenshtein, B. Elektrokhimiya 1965, 1, 72.

69. Scarano, E.; Bonicelli, M. G.; Forina, M. Anal. Chem. 1970, 42, 1470.

70. Wasa, T.; Musha, S. Bull. Chem. Soc. Jap. 1975, 48, 2176.

71. Koen, J. G.; Huber, J. F. K.; Poppe, H.; den Boef, G. J. Chromatogr. Sci. 1970, 8, 192.

72. Stillman, R.; Ma, T. S. Mikrochim. Acta 1973, 32, 491.

73. Fleet, B.; Little, C. J. J. Chromatogr. Sci. 1974, 12, 747.

74. Application Note AN-108, EG&G Princeton Applied Research Corporation, Princeton, New Jersey, 1974.

75. Bond, A. M. Talanta 1973, 20, 1139.

76. Florence, T. M.; Farrar, Y. J. J. Electroanal. Chem. 1973, 41, 127.

77. Kikuchi, S.; Honda, K.; Kim, S. Bull. Chem. Soc. Jap. 1954, 27, 65.

78. Israel, Y.; Vromen, A.; Paschkes, B. Talanta 1967, 14, 925.

79. Benesch, R. E.; Benesch, R. Science 1953, 118, 447.

80. Yarnitsky, C.; Ouziel, E. Anal. Chem. 1976, 48, 2024.

81. Kraus, K. A.; Nelson, F. "Proc. of First U. N. International Conf. on Peaceful Uses of At. Energy" 1956, 7, 113.

82. Strelow, F. W. E. Anal. Chem. 1960, 32, 1185.

83. Strelow, F. W. E.; Sondorp, H. Talanta 1972, 19, 1113.

84. Strelow, F. W. E.; Rethmeyer, R.; Bothma, C. J. C. Anal. Chem. 1965, 37, 106.

85. Pitstick, G. F.; Sweet, T. R.; Morie, G. P. Anal. Chem. 1963, 35, 995.

86. Dadone, A.; Baffi, F.; Trache, R. Talanta 1976, 23, 593.

87. Seymour, M. D.; Sickafoose, J. P.; Fritz, J. S. Anal. Chem. 1971, 43, 1734.

88. Kawazu, K.; Fritz, J. S. J. Chromatogr. 1973, 77, 397.

89. Kawazu, K.; Shibata, M.; Kakiyama, H. J. Chromatogr. 1975, 115, 543.

90. Kawazu, K. J. Chromatogr. 1976, 120, 171.

91. Fritz, J. S.; Story, J. N. Anal. Chem. 1974, 46, 825.

92. Fritz, J. S.; Story, J. N. J. Chromatogr. 1974, 90, 267.

93. Lieser, K. H. Radiochem. Radioanal. Lett. 1974, 18, 323.

94. Small, H.; Stevens, T. A.; Bauman, W. C. Anal. Chem. 1975, 47, 1801.

95. Yamabe, T. J. Chromatogr. 1973, 83, 59.

96. Hayashi, T.; Miwa, Y.; Yamabe, T. J. Chromatogr. 1974, 94, 271.

97. Yamabe, T.; Hayashi, T. J. Chromatogr. 1974, 102, 273.

98. Miwa, Y.; Hayashi, T.; Yamabe, T. J. Chromatogr. 1975, 108, 323.

99. Miwa, Y.; Yamabe, T. J. Chromatogr. 1975, 115, 276.

100. Takata, Y.; Fujita, K. J. Chromatogr. 1975, 108, 255.

101. Takata, Y.; Muto, G. Anal. Chem. 1973, 45, 1864.

102. Girard, J. E. Anal. Chem. 1979, 51, 836.

103. Kalousek, M. Collect. Czech. Chem. Commun. 1948, 13, 105; Chem. Listy 1946, 40, 149.

104. Kalousek, M.; Ralek, M. Collect. Czech. Chem. Commun. 1954, 19, 1099.

105. Kambara, T. Bull. Chem. Soc. Jap. 1958, 27, 523, 527, 529.

106. Oldham, K. B.; Parry, E. P. Anal. Chem. 1970, 42, 229.

107. Opekar, F.; Stulik, K. J. Electroanal. Chem. 1977, 85, 207.

108. Kirowa-Eisner, E.; Osteryoung, J. Anal. Chem. 1978, 50, 1062.

109. Saito, A.; Himeno, S. J. Electroanal. Chem. 1979, 101, 257.

110. Osteryoung, J.; Kirowa-Eisner, E. Anal. Chem. 1980, 52, 62.

111. Schwarz, W. M.; Shain, I. J. Phys. Chem. 1965, 69, 30.

112. Meschi, P. L.; Johnson, D. C. Chemistry Dept., Iowa State University, Ames, Iowa; unpublished data

113. Petersen, W. M. Amer. Lab. 1979, 11, 69.

114. Morris, V. L. M.S. Thesis, Iowa State University, Ames, Iowa, 1976.

115. Andrews, R. W. Chemistry Dept., University of Alabama, Birmingham, Alabama, 1979; private communication.

116. Johnson, D. C. "Introduction to Electrochemical Methods of Analysis"; University Bookstore: Ames, Iowa, 1977; Chapter IV.

117. Meites, L. "Polarographic Techniques"; Interscience: New York, New York, 1955; Appendix B.

118. Diehl. H. "Quantitative Analysis: Elementary Principles and Practice"; Oakland Street Science Press: Ames, Iowa, 1974; Chapter 12.

119. Lindstrom, T. R.; Johnson, D. C. Chemistry Dept., Iowa State University, Ames, Iowa; unpublished data.

120. Yoshimori, T.; Arakawa, M.; Takeuchi, T. Talanta 1965, 12, 147.

121. Allen, R. E.; Johnson, D. C. Talanta 1973, 20, 799.

122. Koile, R. C. Ph.D. Dissertation, Iowa State University, Ames, Iowa, 1979.

123. Smith, B. W.; Parsons, M. L. J. Chem. Educ. 1973, 50, 679.

IX. ACKNOWLEDGEMENTS

I wish to thank Dr. Dennis C. Johnson for his multi-faceted help and support. Thanks also goes to the members of his research group who, in many ways, made my graduate experience educational, and always interesting.

Financial support from grants GP-40646X and CHE 76-17826 from the National Science Foundation and a grant from Dionex Corporation is gratefully acknowledged.

Credit goes to Eldon E. Ness, George W. Steininger and John L. Sauke for their invaluable mechanical skills which were used to produce various apparatus applied in this research.

I thank my Mom, and Dad and Lena, for their never-ending support throughout my education, and for the "care" packages they sent which were heartily welcomed.

Special thanks to my wife, Julie, for her encouragement and understanding throughout my graduate career.